

GEOLOGICA ULTRAIECTINA

MEDEDELINGEN VAN DE  
FACULTEIT GEOWETENSCHAPPEN  
UNIVERSITEIT UTRECHT

No. 259

**Surface chemistry and acid-base activity of *Shewanella putrefaciens*:  
Cell wall charging and metal binding to bacterial cell walls**

**Jacqueline Claessens**

Promotor: Prof. dr. P. Van Cappellen  
Department of Earth Sciences - Geochemistry  
Faculty of Geosciences, Utrecht University

Co-promotor: Dr. A.M. Laverman  
Department of Earth Sciences - Geochemistry  
Faculty of Geosciences, Utrecht University

Members of dissertation committee:

Dr. L.G. Benning	Leeds University
Dr. C. Koretsky	Western Michigan University
Prof. dr. G.J. de Lange	Utrecht University
Prof. dr. J. Middelburg	NIOO-KNAW, Yerseke; Utrecht University
Prof. dr. W.H. van Riemsdijk	Wageningen University
Prof. dr. J.P.M. Tommassen	Utrecht University

**Surface chemistry and acid-base activity of *Shewanella putrefaciens*:  
Cell wall charging and metal binding to bacterial cell walls**

Oppervlaktechemie en zuur-base activiteit van *Shewanella putrefaciens*:

Celwandlading en metaalbinding aan bacteriële celwanden

(met een samenvatting in het Nederlands)

PROEFSCHRIFT

ter verkrijging van de graad van doctor aan de Universiteit Utrecht  
op gezag van de Rector Magnificus, Prof. dr. W.H. van Gispén, ingevolge  
het besluit van het College voor Promoties in het openbaar te verdedigen  
op maandag 10 april 2006 des middags te 12.45 uur

door

**Jacqueline Wilhelmién Claessens**

geboren op 19 januari 1976 te Geldrop

This research was conducted at the Department of Earth Sciences-Geochemistry, Faculty of Geosciences, Utrecht University, The Netherlands.

This work was financially supported by the Netherlands Organization for Scientific Research (NWO-Pionier Award).

Cover design: Ellen Fest; cover illustration: Yellow Stone National Park

Printing: Grafisch bedrijf Ponsen & Looijen, Wageningen

ISBN-10: 90-5744-123-3

ISBN-13: 978-90-5744-123-3

**Table of contents**

Chapter 1	Surface chemistry of microorganisms	1
Chapter 2	What do acid-base titrations of live bacteria tell us? A preliminary assessment	13
Chapter 3	Acid-base activity of live bacteria: Implications for quantifying cell wall charge	31
Chapter 4	Response of <i>Shewanella putrefaciens</i> to pH stress and possible geochemical implications	55
Chapter 5	Competitive binding of $\text{Cu}^{2+}$ and $\text{Zn}^{2+}$ to cells of <i>Shewanella</i> <i>putrefaciens</i>	77
References		103
Summary		111
Samenvatting		115
Dankwoord		119
Curriculum Vitae		121

---

---

---

---

# **Chapter 1**

## **Surface chemistry of microorganisms**

---

## 1.1 Scope

Microorganisms are found in almost every natural environment due to their extremely high genetic and physiological diversity (Newman and Banfield, 2002). The high microbial diversity is expressed by variations in cell size and morphology, metabolic strategies and adaptation to environmental conditions. Apart from their existence in practically every natural habitat, the microbial biomass significantly contributes to the total biomass of an ecosystem. For instance, in a grassland, a microbial biomass of 30.4 g carbon m<sup>-2</sup> is estimated, whereas the above ground green biomass is only slightly more, that is, 43.0 g carbon m<sup>-2</sup> (Prescott et al., 1996).

Microbial activity in environmental systems affects the chemistry and physical properties of the environment. Microorganisms convert nutrients to forms that are bioavailable for plants in soils and water, and in that way microbial activity plays an important role in the functioning of ecosystems. In marine ecosystems, for example, microorganisms contribute significantly to global primary productivity and occupy a key position at the base of the marine food chain (Scanlan and West, 2002). Furthermore, microorganisms are also used to clean up contaminated environments and water bodies. Nutrients and electron acceptors are supplied to enhance microbial activity in bioremediation studies (Kim et al., 2005; Bento et al., 2005). In the treatment of wastewaters, activated sludges, aerobic and anaerobic cultures are used (Gurbuz et al., 2004; Tziotziou et al., 2005; Quesnel et al., 2005).

Chemical exchanges at the solid-solution interface play a key role in the chemical speciation of environmental fluids. Bacteria are relatively small and as a consequence have a large specific surface area compared to mineral surfaces. Therefore, microbial surfaces may significantly contribute to chemical exchanges that occur in the system solid-biomass-solution. At most environmental pHs bacterial cell walls are negatively charged and thus have a high affinity for metal cations (e.g., Plette et al., 1996; Fein et al., 1997; Daughney et al., 2001). As a result, microbial surfaces have a major impact on metal ion mobility in environmental systems. Furthermore, metals complexed in the cell wall may serve as nucleation sites for mineral precipitation via counter adsorption of anions (Schultze-Lam et al., 1996).

The physical-chemical interactions between bacterial cells and mineral surfaces also regulate adhesion processes. Mineral surfaces are often colonized by bacterial cells and cell-mineral adhesion plays a key role in the mobility and retention of microorganisms in environmental systems. In drinking water systems the adhesion of bacterial cells to pipes and growth of biofilms can deteriorate water quality (Donlan et al., 1994; Appenzeller et al., 2002). In biotechnological applications, however, cells bound to surfaces are used in wastewater treatments (Tziotziou et al., 2005). The main advantages of using these immobilized cells are retention of the cells in the reactor and prevention of suspended bacterial biomass in the effluent.

## 1.2 Natural surfaces

### 1.2.1 Metal (hydr)oxide surfaces, microbial surfaces and humic substances

The surface chemistry of metal (hydr)oxides has been studied extensively (Dzombak and Morel, 1990). Metal (hydr)oxide surfaces are characterized by a variety of potential binding sites (Fig. 1.1). The reactivity of the oxygen atoms at the mineral surface is determined by the coordination chemistry of the bonds with the metal atoms in the underlying crystal. The charge of the oxygen groups can be calculated from the oxygen-metal coordination, according to the Pauling bond valence rules. Commonly, the surface chemistry of metal (hydr)oxides is simplified by considering only one type of oxygen atom at a two-dimensional surface (Fig. 1.2).

These surface oxygen groups are protonated or deprotonated, depending on the pH of the solution



where S represents the metal atom. The charge of the mineral surface is compensated by electrolyte ions in the diffuse double layer. The charging of metal (hydr)oxide surfaces is highly dependent on the electrolyte concentration. At high electrolyte concentrations the electrostatic interactions at the surface decrease, because the surface charge is better shielded.

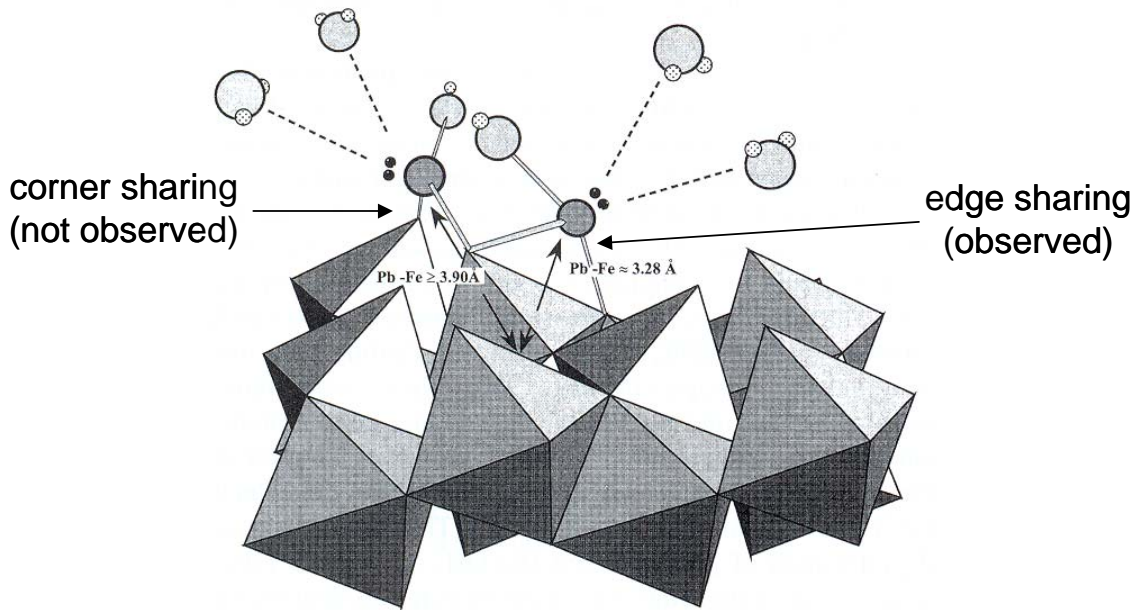


**Figure 1.1:** Binding of lead to hematite or goethite surfaces (Bargar et al., 1997). Lead binds in an inner-sphere manner to at least two surface functional groups. The observed sorption complexes are edge sharing, whereas corner sharing is not observed.

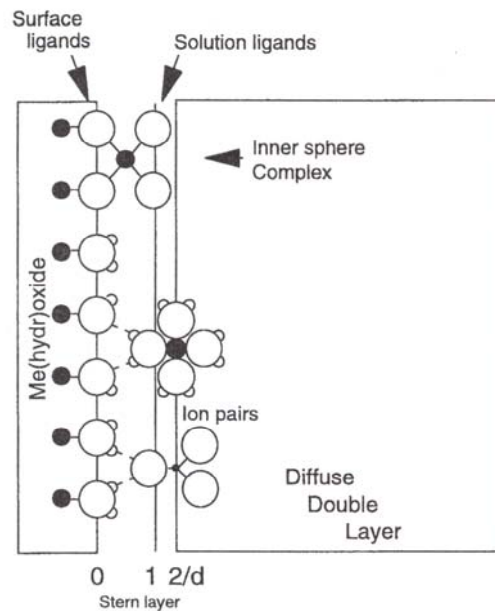


**Figure 1.2:** Schematic representation of the metal (hydr)oxide surface, showing planes associated with surface hydroxyl groups, inner-sphere complexes, outer-sphere complexes and the diffuse layer (Hiemstra and van Riemsdijk, 1996).

Cell walls of bacteria are even more complex than mineral surfaces (Fig. 1.3). Based on differences in their cell wall structure, bacteria are divided in two groups: Gram-positive and Gram-negative bacteria. Gram-positive bacteria have a plasma membrane consisting of a phospholipid bilayer. A thick peptidoglycan layer, made of cross-linked amino acids and sugars, surrounds the plasma membrane. Gram-negative bacteria also have a plasma membrane but a thin peptidoglycan layer, and an additional outer membrane. The outer membrane consists of phospholipids and lipopolysaccharides (LPS). The lipopolysaccharides are the outermost layer of the cell walls of Gram-negative bacteria. These macromolecules contain carboxylate, phosphate and amino groups (e.g., Beveridge and Murray, 1980; Plette et al., 1995). In analogy with mineral surfaces, bacterial cell walls are often represented as a two-dimensional array of carboxylate, phosphate and amino groups that are protonated or deprotonated, depending on the pH of the outside solution (Fig. 1.4).

One major difference between metal (hydr)oxide surfaces and bacterial cell walls is the mechanism by which electrolyte ions compensate the surface charge. In bacteria, electrolyte ions can enter the cell walls in such a way that the charge is at least partly compensated within the macromolecular structure. Therefore, bacterial cell walls are unlikely to develop a diffuse double layer like metal (hydr)oxide surfaces. Instead, microbial cell walls more likely show properties similar to humic substances. Humic acids are also negatively charged at most environmental pHs and are considered to be gel like structures permeable for electrolyte ions (Benedetti et al., 1995; Avena et al., 1999). The charging of humic acids and isolated cell walls of Gram-positive bacteria depends weakly on the electrolyte concentration, implying a relatively minor role of electrostatic interactions in this process (Plette et al., 1995; Avena et al., 1999).

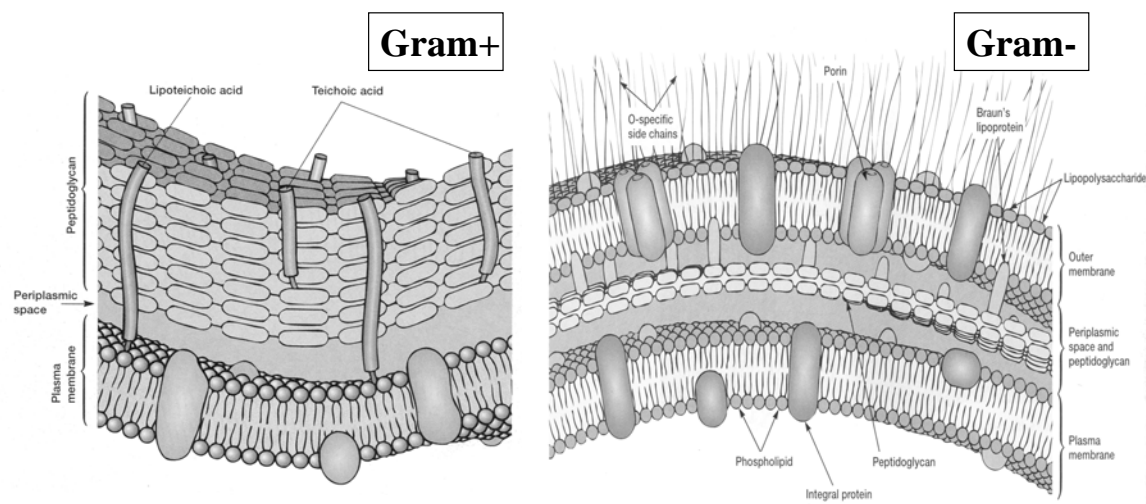


**Figure 1.3:** Cell wall structures of Gram-positive and Gram-negative bacteria (Prescott et al., 1996).

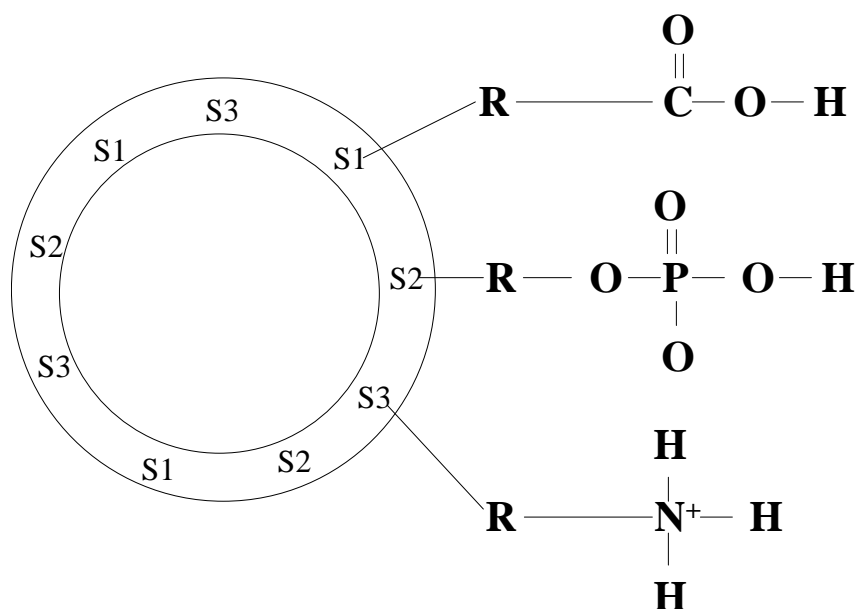


**Figure 1.4:** Schematic representation of the surface chemistry of a bacterial cell wall. R represents the macromolecules to which the functional groups are attached. S1, S2 and S3 are carboxylate, phosphate and amino groups, respectively.

### 1.2.2 Acid-base titrations and metal binding experiments

Acid-base titrations have been used widely to study the mineral-aqueous solution interface and to quantify the protonation and deprotonation reactions of mineral surface functional groups (Dzombak and Morel, 1990). The acid-base properties of humic acids have also been investigated with acid-base titrations (Avena et al., 1999). More recently, acid-base

titrations have been used for characterizing the acid-base properties of cell wall functional groups. Initially, titrations were carried out mainly with dead bacterial cells or isolated cell walls (Goncalves et al., 1987; Plette et al., 1995; van der Wal et al., 1997a). A number of recent acid-base titration studies have now been performed with live cells of Gram-positive (Daughney and Fein, 1998; Daughney et al., 2001; Borrok and Fein, 2005) and Gram-negative bacteria (Haas, 2004).

The acid-base properties of functional groups play a crucial role in metal binding to natural surfaces. Metal binding to minerals and humic substances has been studied extensively (Weng et al., 2002; Gustafsson et al., 2003; Toner et al., 2006). More limited metal binding experiments have been carried out with isolated cell walls (Plette et al., 1996), dead cells (Agraz et al., 1994) and live cells of Gram-positive (Fein et al., 1997) and Gram-negative bacteria (Haas et al., 2001). Nonetheless, binding of metals to microorganisms is crucial for the understanding of metal mobility and toxicity in the environment as well as detoxification mechanisms, by which microorganisms convert toxic components into non-toxic products (Gurbuz et al., 2004).

### **1.2.3 Surface complexation models**

Different electrostatic models have been developed to derive intrinsic affinity constants for proton and metal binding to metal (hydr)oxide surfaces. The models differ in the characterization of the diffuse double layer and in the number of protonation reactions of the surface sites. Surface sites have one or two protonation reactions in 1 and 2 p*K* models, respectively. In the simplest models, the compensating charge in solution is purely diffuse, whereas in the more complex models, one or two charge-free layers are defined close to the surface, followed by a diffuse layer further out (Fig. 1.2). All models, however, show common properties, that is, the electrostatic nature of the interactions and the discrete protonation constants for the surface sites.

The models that simulate the charging behavior and metal binding to humic acids not only take into account the electrostatic interactions but also the chemical heterogeneity of the material (Kinniburgh et al., 1996). Instead of using discrete protonation constants, these models are characterized by a continuous distribution of affinity constants. In the Donnan models, the humic acids are treated as distinct electrically neutral phases permeable for

electrolyte ions, where the charge is compensated within the molecule rather than in the diffuse layer.

The weak dependence of cell wall charging on the electrolyte concentration implies a low electrostatic interaction in bacterial cell walls (Plette et al., 1995). Instead, the gradual change in surface charge with pH observed for bacterial cell walls has been explained by a distribution of proton affinity constants of the functional groups. Charging of bacterial cell walls and binding of metal cations to cell wall functional groups, however, have also been modeled using surface complexation models that include electrostatic correction terms (e.g., Fein et al. 1997; Daughney et al., 2001; Haas et al., 2001).

### **1.3 Microbial activity**

In contrast to abiotic surfaces, the metabolic activity of live cells promotes the exchange of chemical components with the environment. Reactions mediated by microorganisms may change the chemical properties of the ambient conditions by consuming chemical substrates and releasing waste products. In particular, the release of metabolically produced acids complicates the interpretation of acid-base titrations of live organisms.

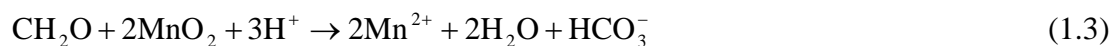
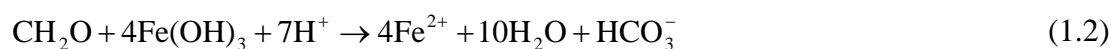
Microbial reactions are extremely diverse and to a large extent depend on the chemical conditions of the surrounding environment. In most natural systems, the variability in reduction potential regulates the succession of different microbial metabolic pathways by the availability of electron acceptors. Under oxic conditions, O<sub>2</sub> is used as terminal electron acceptor for cell respiration. With decreasing reduction potential, microorganisms using nitrate, manganese, iron, sulfate and CO<sub>2</sub> as terminal electron acceptors compete for energy substrates (Thullner et al., 2005). Furthermore, fermentation reactions using oxidized organic compounds as electron acceptors may become significant in the absence of external electron acceptors.

In the presence of a terminal electron acceptor, most microorganisms convert sugars, e.g. glucose, to pyruvate in the glycolytic pathway, which is then metabolized in respiration reactions during the tricarboxylic acid (TCA) cycle. The complete oxidation of pyruvate in the TCA cycle results in the release of CO<sub>2</sub> although succinate can also be released as intermediate product (Lin et al., 2005). In the absence of a terminal electron acceptor, pyruvate is metabolized instead by fermentation reactions, which produce organic acids, such

as acetate, succinate, formate and lactate (Clark, 1989; Sanchez et al., 2005). Facultative anaerobic bacteria can grow either by respiration reactions or by using sugars as sole carbon and energy source in fermentation reactions when external electron acceptors are not available (Clark, 1989).

The CO<sub>2</sub> released by microorganisms dissolves in water to form carbonic acid, a major weathering agent for minerals (Andrews and Schlesinger, 2001). Other metabolic products, such as protons and organic acids, may build up to concentrations in the extracellular environment that affect the solubility reactions of minerals (Hiebert and Bennett, 1992; Bennett et al., 2001). Mineral dissolution reactions are therefore to a large extent regulated by the availability of acids and organic ligands in the solution.

Depending on the metabolic pathways, reduction reactions can also increase the pH of the solution. For instance, reduction of iron or manganese oxides by metal reducing bacteria, such as *Shewanella putrefaciens* (DiChristina, 1989), results in consumption of protons according to the simplified stoichiometry



Iron and manganese reduction reactions, coupled to organic matter oxidation, locally increases pH in aquatic sediments (Van Cappellen and Wang, 1996; Jourabchi et al., 2005) and stratified water columns (Van Cappellen et al., 1998). The release of Fe (II) and Mn (II) in the solution due to metal reduction reactions may also result in the precipitation of secondary minerals (Bell et al., 1987).

## 1.4 Objectives

The general aim of this study is to gain insight into the surface chemistry of live cells, by characterizing the acid-base properties of functional groups in the cell walls of live microorganisms as well as their affinities for metal cations. A major goal is to determine if models and techniques, such as surface complexation models and acid-base titrations, that were originally developed to characterize the reactivity of mineral surfaces can be used to study the surface chemistry of live bacteria, particularly in view of the complex

macromolecular structure of the cell wall and the possible effects of cell metabolism. The latter requires to gain insight into the release of metabolic products, including protons and organic acids, to solution, and to determine the effects that these metabolic products may have on biogeochemical processes and metal binding to the cells.

## 1.5 Outline of the thesis

In this study *Shewanella putrefaciens*, a Gram-negative facultative anaerobe bacterium, is used. Due to its extremely high metabolic versatility, *S. putrefaciens* is often used as a model organism. *S. putrefaciens* has been detected in a variety of aquatic and subsurface environments (Venkateswaran et al., 1999). In natural environments, *S. putrefaciens* utilizes iron and manganese (hydr)oxides as terminal electron acceptors (DiChristina, 1989). *S. putrefaciens* can also reduce a variety of other electron acceptors including nitrate, nitrite, tetrathionite, glycine, fumarate, trimethylamine-N-oxide, thiosulfate, sulfite, chromate and U (VI) (Obuekwe and Westlake, 1982; Semple and Westlake, 1987; Lovley et al., 1991).

In **chapter 2**, the results of continuous acid-base titrations of live cells of *S. putrefaciens* are presented. These show that processes other than protonation-deprotonation reactions of functional groups in cell walls affect the acid-base behavior of the bacterial cells. Therefore, to constrain the role of these processes, pH stat experiments with live cell suspensions were performed. We measured acid or base consumption as a function of time, as well as the changes in buffering capacity, DOC (dissolved organic carbon) and cation concentrations of the aqueous medium. In addition, the electrophoretic mobility and the viability of the cells, and the release of macromolecules to solution were monitored. This chapter yields information on the response of microorganisms to changes in the pH and electrolyte composition of their environment.

In **chapter 3**, time dependent acid or base consumption curves of cell suspensions are used to separate the contributions of protonation and deprotonation of functional groups from those of other processes affecting the acid-base behavior of the live cells. Series of pH stat experiments with live cells, intact dead cells and disrupted cells of *S. putrefaciens* were performed. In the experiments with live cells, the solutions were screened for the build-up of products indicative of metabolic activity, especially organic acids. In addition, we determined

the buffering capacity of lipopolysaccharides, a major constituent of the cell wall of Gram-negative bacteria, and we compared the acid-base behavior of *S. putrefaciens* to that of the Gram-positive bacterium *Bacillus subtilis*. From these results the cell wall charges of *S. putrefaciens* and *B. subtilis* were calculated as a function of pH.

In **chapter 4** we elaborate on the release of metabolic products by *S. putrefaciens* in pH stat experiments. The rates of release of protons and organic acids in metabolic reactions and their dependence on redox conditions, pH and temperature were quantified. Mass balances were made that relate CO<sub>2</sub> and organic acid release to that of proton release in respiration and fermentation reactions. The chapter further discusses the possible implications of the experimental results for metal reduction and mineral dissolution reactions in environmental systems.

**Chapter 5** follows up on the results of the acid-base properties of cell wall functional groups obtained in chapter 3, by determining the binding of Cu<sup>2+</sup> and Zn<sup>2+</sup> to functional groups in cell walls of live cells of *S. putrefaciens* in one- and two-metal systems. The experiments were performed over a wide range of metal concentrations and at different pH values. The affinity constants for binding of Cu<sup>2+</sup> and Zn<sup>2+</sup> to bacterial cells were derived using a simple cell wall complexation model. In order to understand the mechanisms of metal binding, we compared one- and two-site binding models. Furthermore, the effects of electrostatic corrections and the presence of organic ligands in solution were investigated.

---

---

## **Chapter 2**

### **What do acid-base titrations of live bacteria tell us? A preliminary assessment**

Jacqueline Claessens, Thilo Behrends and Philippe Van Cappellen (2004) *Aquatic Sciences*, 66, 19-26.

---

## Abstract

To gain insight into the non-equilibrium processes that affect the titration curves of bacteria, we performed pH stat experiments with suspensions of live cells of the Gram-negative bacterium *Shewanella putrefaciens*. The experiments lasted for 5 hours, during which acid or base addition was monitored. Periodically, the electrophoretic mobility of the cells, as well as the buffering capacity and the concentrations of cations and dissolved organic carbon (DOC) of the solution, were measured. At the end of the experiments, the viability of the cells was determined. In a limited number of cases, final solutions were screened for the presence of cell-wall constituents using gel electrophoresis. The results showed a very different behavior of the cell suspensions under acid and alkaline conditions. At pH 4, acid addition ceased after 20 minutes. The cells remained intact but were no longer viable at the end of the experiment, while little change in the buffering capacity of the solution was observed. The data at pH 4 were consistent with protonation of cell wall functional groups. At pH 8 and 10, base addition continued during the entire duration of the experiments. The cells remained viable, and the buffering capacity and DOC concentration of the solutions increased with time. Gel electrophoresis indicated that proteins and lipopolysaccharides had been released to solution at pH 10. In contrast to pH 4, the buffering capacity of the bacterial cells under alkaline conditions did not appear to be limited by the initial availability of ionisable functional groups in the cell wall. This preliminary study shows that a complex set of processes, including active metabolic responses, control the acid-base activity of live cell suspensions.

## 2.1 Introduction

Many geochemical processes, including precipitation and dissolution of minerals, are microbially mediated. These processes involve reactions between the cell walls of living microorganisms and mineral surfaces or aqueous solutions. In the last decade, the nature of these interactions has been probed using techniques and models developed to investigate the chemical structure and reactivity of mineral-aqueous solution interfaces. Some researchers have performed acid-base titrations and metal adsorption studies on isolated bacterial cell walls (Plette et al., 1995; Plette et al., 1996; Van der Wal et al., 1997a), while others have used suspensions of live cells (Daughney et al., 1998; Daughney and Fein, 1998; Cox et al., 1999; Fowle and Fein, 1999; Fowle et al., 2000; Fowle and Fein, 2000; Mirimanoff and Wilkinson, 2000; Daughney et al., 2001; Haas et al., 2001; Yee and Fein, 2001). These studies have highlighted the important role of cell wall functional groups, including carboxylate, phosphate, hydroxyl and amino groups, in controlling the surface chemistry of microorganisms.

Microbial cell walls differ fundamentally from mineral surfaces, however. They are truly three-dimensional macromolecular structures, rather than two-dimensional arrays of functional groups. The cell wall of Gram-positive bacteria consists of a phospholipid bilayer, the cytoplasmic membrane, surrounded by a rather thick peptidoglycan layer. The latter is composed of sugars and amino acids and its rigidity gives strength and shape to the cell. Gram-negative bacteria have an even more complex structure. The peptidoglycan layer is surrounded by an outer membrane, consisting of phospholipids and lipopolysaccharides in which other cell wall components, for example porins, are imbedded.

Furthermore, bacteria are living organisms: their cell walls are designed to obtain nutrients from the environment, and to protect the organism from harmful chemical changes in the surrounding medium. As a consequence, the function and structure of the cell wall of a living cell may change during acid-base titrations or metal adsorption experiments, due to passive and active (energy consuming) processes. Some of the processes that may regulate the acid-base activity of live bacterial suspensions are illustrated in Figure 2.1 and Table 2.1. Specific metabolic responses or leakage of cell constituents into the aqueous medium are obviously not encountered when dealing with mineral-water systems.

In this paper, we present a preliminary study of the acid-base activity of live bacteria. We used the facultative anaerobic Gram-negative bacterium *Shewanella putrefaciens*. Both acid-base titrations and pH stat experiments were performed. In the latter, we measured acid or base consumption as a function of time, as well as the changes in buffering capacity, DOC (dissolved organic carbon) and cation concentrations of the aqueous medium. In addition, the electrophoretic mobility and the viability of the cells, plus the release of macromolecules to solution were monitored. The study yields information on the response of microorganisms to changes in the pH and electrolyte composition of their environment.

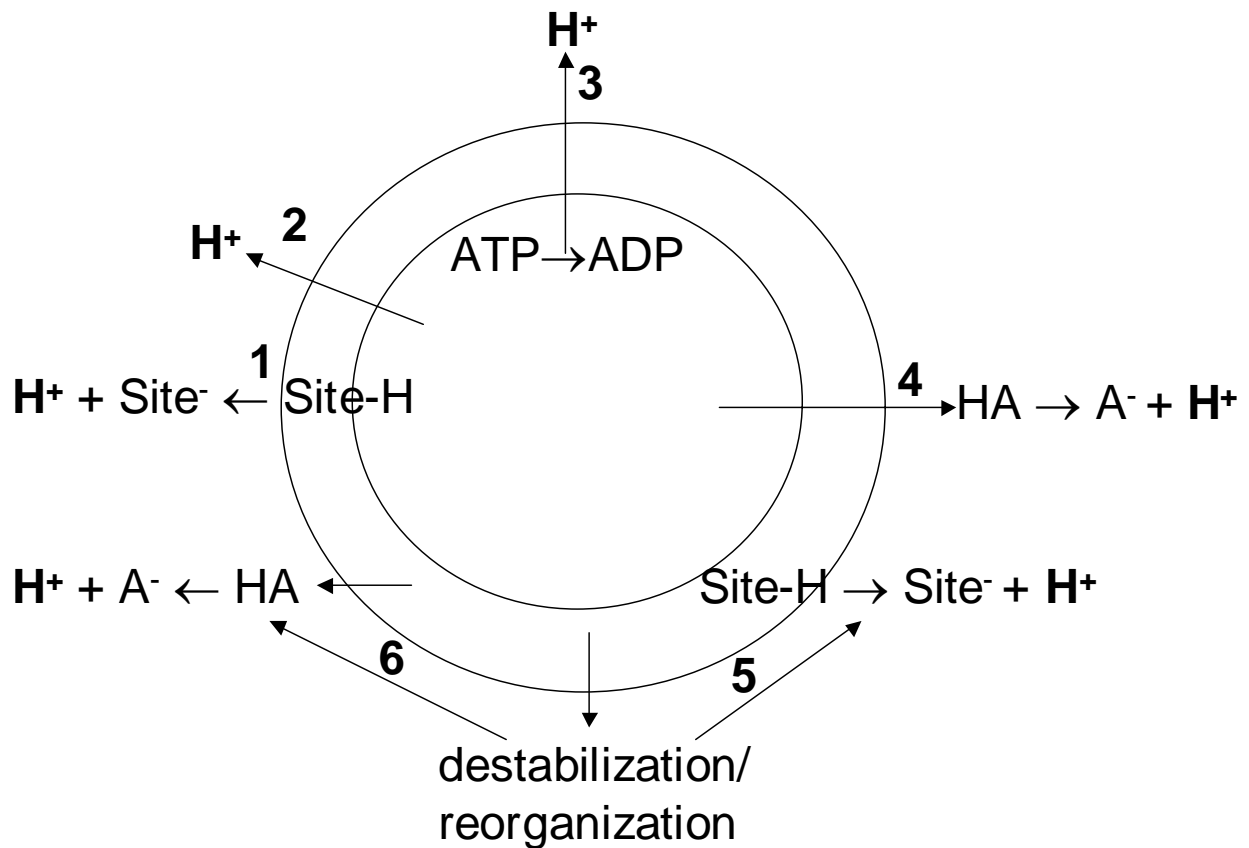


**Figure 2.1:** Schematic representation of the acid-base activity of a live cell at high pH. See Table 2.1 for details on the various base-neutralizing processes.

**Table 2.1:** Possible passive and active responses of a live bacterium exposed to high pH. The numbering of the processes corresponds to that in Figure 2.1. The list is not exhaustive.

---

<b>Chemical processes</b>	
1. Deprotonation of functional groups	Macromolecules of the cell wall contain exposed ionisable functional groups that protonate or deprotonate, according to their acid dissociation constant and the pH of the medium.
2. Proton leakage	At high pH, hydrogen ions diffuse out of the cell as a result of the proton concentration gradient across the cell wall.
<hr/>	
<b>Metabolic responses</b>	
3. Proton pumping	Living cells can counter leakage by actively transporting protons against the concentration gradient, using ATP as the energy provider.
4. Exudation of organic acids	By producing and subsequently releasing organic acids, bacteria may attempt to buffer the pH increase of the external medium.
<hr/>	
<b>Cell wall destabilization</b>	
5. Electrostatic destabilization	Electrical charging of the cell wall may lead to a destabilization of its three dimensional structure, and may expose previously inaccessible functional groups, which may then deprotonate.
6. Release of cell wall components	Electrostatic repulsion may potentially also cause the detachment of weakly-bound acidic cell wall components.

---

## 2.2 Materials and Methods

### 2.2.1 Bacterial cultures

*Shewanella putrefaciens* strain 200R cells were grown at room temperature in liquid Luria Bertani (LB) medium (5 g yeast extract, 10 g trypton and 10 g NaCl in 1 liter) or in a 0.01 M NaCl medium (5 g yeast extract, 1.3 g trypton and 0.6 g NaCl in 1 liter). Bacterial growth was monitored by measuring the optical density (OD) of the cell suspensions at 660 nm wavelength. The bacteria were harvested in mid-logarithmic or end-logarithmic stage, at a cell density of  $10^{12}$  cells L<sup>-1</sup>. Harvested cells were pelletized by centrifugation (15000 g for 20

min or 2600 g for 30 min). The supernatant was discarded and the pelletized cells were resuspended in either 0.15 M or 0.01 M NaCl solution. The washing procedure was repeated one more time. The cell densities of the final bacterial stock suspensions were determined by measuring the OD, or by epifluorescence microscopy, using the acridine orange direct count (AODC) method (Lovley and Phillips, 1988).

### **2.2.2 Acid-base titrations**

Acid-base titrations of *S. putrefaciens* suspensions were performed in an automated titrator (Metrohm 716S controlled by Metrohm Tinet 2.4) at room temperature. Suspensions of  $10^{11}$  cells  $L^{-1}$  were prepared by diluting 0.01 M NaCl stock cell suspensions in 0.01 M NaCl. Cell suspensions were titrated with freshly prepared 0.01 M NaOH and 0.01 M HCl solutions in a polypropylene vessel. The pH was initially brought to 4 with 0.01 M HCl. The suspension was purged with argon for 1 hour to remove  $CO_2$  before initiating base titration from pH 4 to 10, followed by acid titration from pH 10 to 4. Each titration was performed in 20 steps, with equilibration times of 2 or 5 min between successive additions of base or acid. The suspensions were continuously purged with argon. Titrants were added in minimum volumes of 10  $\mu$ l HCl and 20  $\mu$ l NaOH.

### **2.2.3 pH stat experiments**

Experiments were performed in an automated titrator (Metrohm 716S controlled by Metrohm Tinet 2.4) at room temperature. Bacterial suspensions (150 ml) were prepared from the stock cell suspensions grown in LB-medium or 0.01 M NaCl medium, and diluted to  $10^{11}$  cells  $L^{-1}$  with either 0.15 M or 0.01 M NaCl. The initial pH of the bacterial suspensions was measured. The pH of the suspensions was brought to the desired value of 4, 6.5, 8 or 10 by addition of 0.01 M HCl or 0.01 M NaOH. The pH was kept constant for 5 hours and the consumption of HCl or NaOH by the bacterial suspension was recorded.

In one series of pH stat experiments, OD was measured periodically on aliquots of the suspension. In addition, just after the initial pH adjustment ( $t = 0$ ) and at the end of each experiment, a live count was performed: 1 ml of the bacterial suspension was diluted 10 times in series to a final dilution of  $10^{-6}$ . Dilutions  $10^{-4}$ ,  $10^{-5}$  and  $10^{-6}$  were used for live counts: 100  $\mu$ l were spread on solid medium in triplicate and grown for three days before scoring for colony formation.

In a separate series of pH stat experiments, which were continuously purged with N<sub>2</sub>, aliquots were collected periodically and filtered successively through a glass fiber filter (Whatman), a 0.45 μm pore size filter (acrodisc PVDF) and finally a 0.2 μm pore size filter (acrodisc PVDF), in order to separate the bacteria from the solution. The filtrate was immediately purged with N<sub>2</sub> and titrated back to the initial suspension pH. The amount of acid or base required to titrate the suspension back to the initial pH value was defined as the buffering capacity (later referred to as bc). The DOC (dissolved organic carbon) concentration of the filtrate was measured with a Shimadzu TOC analyzer 5050, the concentrations of major cations (K, Ca, Mg) were measured by ICP-MS (inductively coupled plasma-mass spectroscopy). The electrophoretic mobility of the cells was determined by directly injecting unfiltered aliquots in a Coulter Delsa 440sx.

Two additional pH 10 experiments were run. In the first one, the 0.01 M NaCl background electrolyte was replaced by 0.003 M MgCl<sub>2</sub>. In the second one, a suspension of heat-killed cells was used. The cell suspension was prepared by diluting a stock suspension grown in LB-medium to 10<sup>11</sup> cells L<sup>-1</sup>. The suspension was brought to 100 °C for 30 min, then left to cool to room temperature. After readjusting the volume to the initial value by adding deionized water, the pH stat experiment was started.

#### **2.2.4 Gel electrophoresis**

At the end of a number of pH stat experiments performed at pH 7 and 10, the suspension was centrifuged for 20 minutes at 15000 g in order to pelletize the cells. The cell pellet was resuspended in 1 ml of a pH 8.5 buffer (0.05 M Tris, 0.002 M EDTA). The suspensions were ultrasonicated for 1.5 min till a clear solution was obtained. The cell envelopes were pelletized by centrifugation for 2 h at 100000 g and the supernatant was discarded.

The supernatant obtained initially after centrifugation at 15000 g for 20 minutes was centrifuged further for 2 h at 100000 g to pelletize any remaining cell wall fragments. The resulting supernatant was assumed to contain only truly dissolved constituents, which were precipitated with 10 % TCA (trichloric acetic acid) overnight at 4 °C. The TCA samples were centrifuged for 20 min at 5000 g, washed with acetone and resuspended. The washing procedure was repeated one more time.

The TCA-precipitates were analyzed with SDS-PAGE (sodium dodecyl sulfate-polyacrylamide gel electrophoresis), using an 11 % polyacrylamide gel and Ag staining of the proteins (Leammi, 1970). The cell envelopes and cell wall fragments were also analyzed with SDS-PAGE, using a 15 % polyacrylamide gel and Ag staining for the lipopolysaccharides, or LPS (Tsai and Frasch, 1982).

## 2.3 Results

### 2.3.1 Acid-base titrations

Hysteresis was observed between forward (from pH 4 to 10) and backward (from pH 10 to 4) titrations of the bacterial cell suspensions (Fig. 2.2). The titration curves were time-dependent: increasing the time steps between titrant additions from 2 to 5 min resulted in more acid and base consumption by the suspensions. These results indicated that reversible protonation-deprotonation reactions alone could not account for the observed acid-base activity of the cell suspensions.

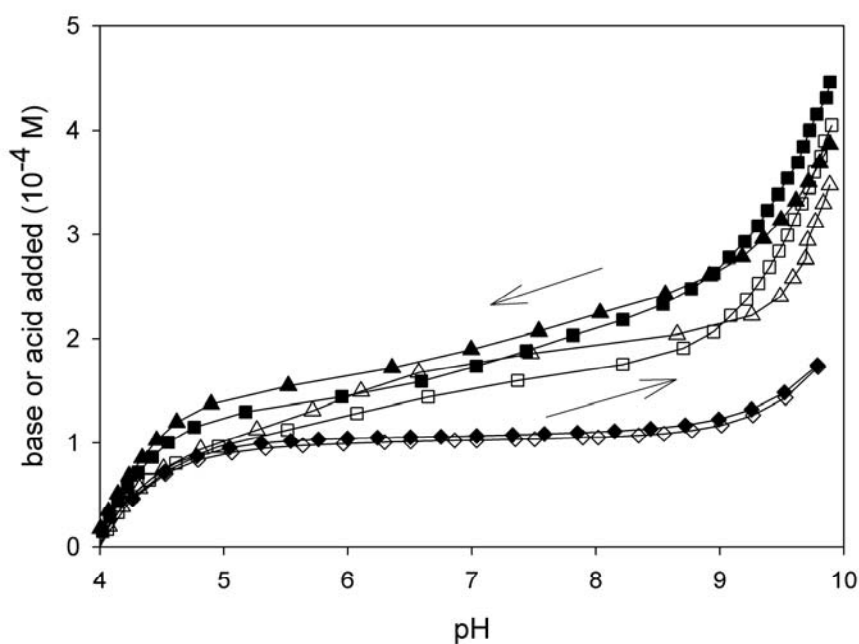


**Figure 2.2:** Continuous titrations of *S. putrefaciens* cell suspensions in 0.01 M NaCl (150 ml total volume,  $10^{11}$  cells  $L^{-1}$ ): equilibration times of 2 min ( $\blacktriangle$ ) and 5 min ( $\blacksquare$ ). Open symbols correspond to the forward base titration, closed symbols to the backward acid titration. The two lower curves correspond to duplicate titrations of the background electrolyte.

### 2.3.2 Acid and base consumption in pH stat experiments

In the pH stat experiments, the amount of acid or base required to maintain the bacterial cell suspensions at a constant pH was measured as a function of time (Figs. 2.3A and B). No acid or base had to be added to keep the pH constant at 6.5. At pH 4, acid consumption ceased after a rapid initial addition during the first 20 minutes. In contrast, at pH 8 and 10, base addition continued over the entire duration of the experiments. More base was needed at pH 10 than at pH 8, particularly during the first hour. Similar observations were made in experiments carried out in 0.15 and 0.01 M NaCl background electrolyte (Figs. 2.3A and B).

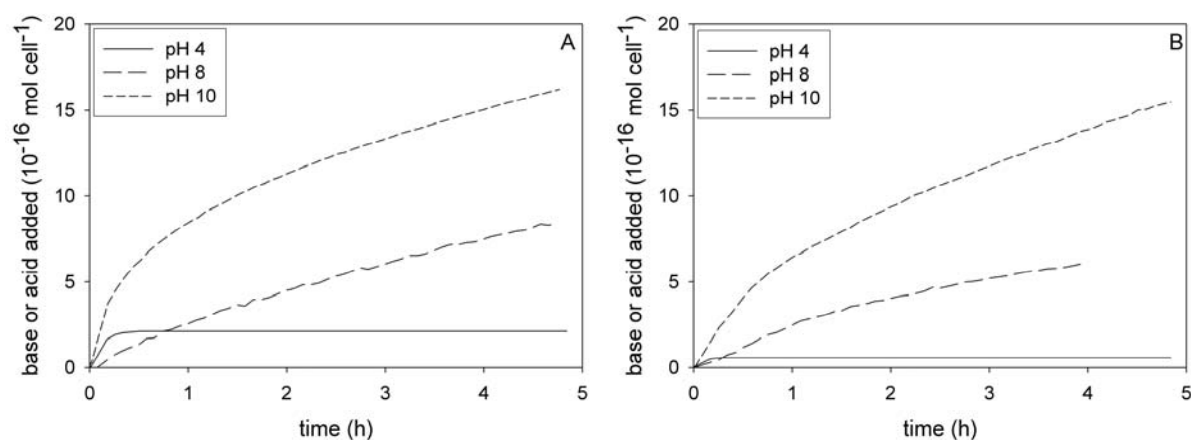


**Figure 2.3:** Acid or base consumption in pH stat experiments with *S. putrefaciens* cell suspensions at pH 4, 8 and 10, in 0.15 M (A) and 0.01 M NaCl (B) (150 ml total volume,  $10^{11}$  cells  $L^{-1}$ ). Cells were cultured in LB-medium. The origin of time corresponds to the moment the pH was adjusted to the desired value. The acid or base consumption of the background electrolyte is subtracted from the measured total consumption by the bacterial cell suspension.

Base consumption at pH 10 by suspensions of cells killed by boiling deviated from that of live cells (Fig. 2.4). In particular, a continuous base addition during the entire duration of the experiment was not observed for the heat-killed cell suspensions. In the latter, base consumption ceased after about 30 minutes, but the amount of base consumed during this time exceeded that of the live suspension. These results also showed an initially higher buffering capacity of the heat-killed cells, which could have been caused by (1) release of internal buffering capacity associated with the cells' cytoplasm, or (2) unsheltering of proton active sites in the cell wall structure. The continued base addition after the first hour implied an active (metabolic) response of the live cells to the alkaline conditions.

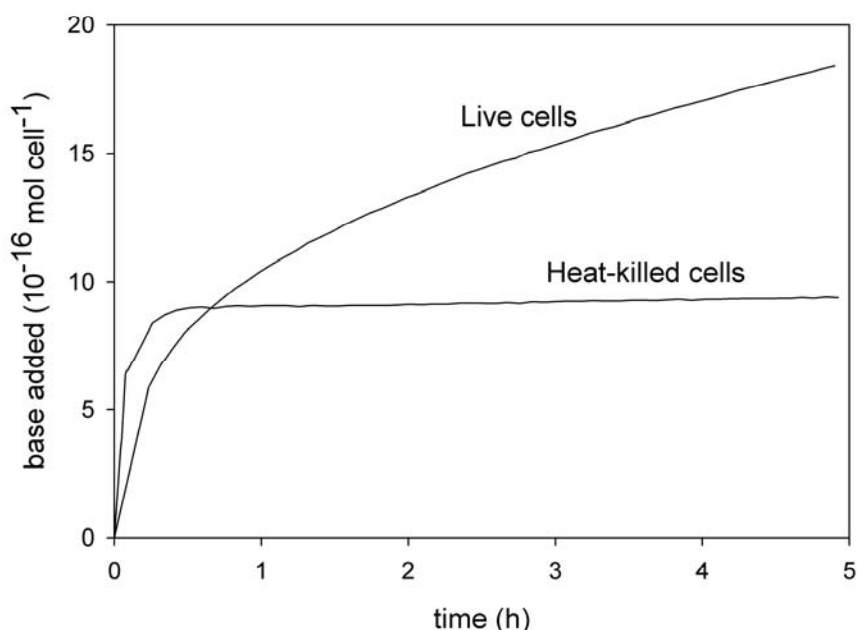


**Figure 2.4:** Base consumption in pH stat experiments with suspensions of live cells and dead, heat-killed cells at pH 10, in 0.15 M NaCl (150 ml total volume,  $10^{11}$  cells  $L^{-1}$ ). Cells were cultured in LB-medium. The base consumption of the background electrolyte is subtracted from the measured total consumption by the bacterial cell suspension.

### 2.3.3 Cell viability

The optical density (OD) measurements showed that at least 75 % of the cells were intact at the end of the pH stat experiments with suspensions of live bacteria, at all pH values tested. However, live counts indicated that the cells were no longer viable after exposure to pH 4 for 5 hours. At the other pH values (6.5, 8 and 10), the viability of the cells did not significantly change between the beginning and end of the experiments.

### 2.3.4 Cell electrophoretic mobility and solution chemistry

Figures 2.5-2.7 compare, for pH 4, 8 and 10, the time evolution of the solution chemistry and the electrophoretic mobility of the bacteria in 0.01 M NaCl, while Figure 2.8 shows the results obtained in 0.003 M  $MgCl_2$  at pH 10. As can be seen, there were major differences among the experiments.

At pH 4, the electrophoretic mobility of the cells underwent a dramatic shift during the first 20 minutes, followed by a much more gradual change during the remainder of the

experiment (Fig. 2.5). At the end of the experiment, the electrophoretic mobility differed significantly from the initial mobility of cultured bacteria. The concentration of DOC and the buffering capacity of the filtered solution showed relatively minor variations. The total concentration of the dissolved cations K, Ca and Mg, expressed in equivalents per unit volume, however, increased systematically with time. This was mainly due to an increase of K and was more pronounced than in the pH stat experiment at 6.5 (result not shown); the concentrations of Ca and Mg did not vary significantly.

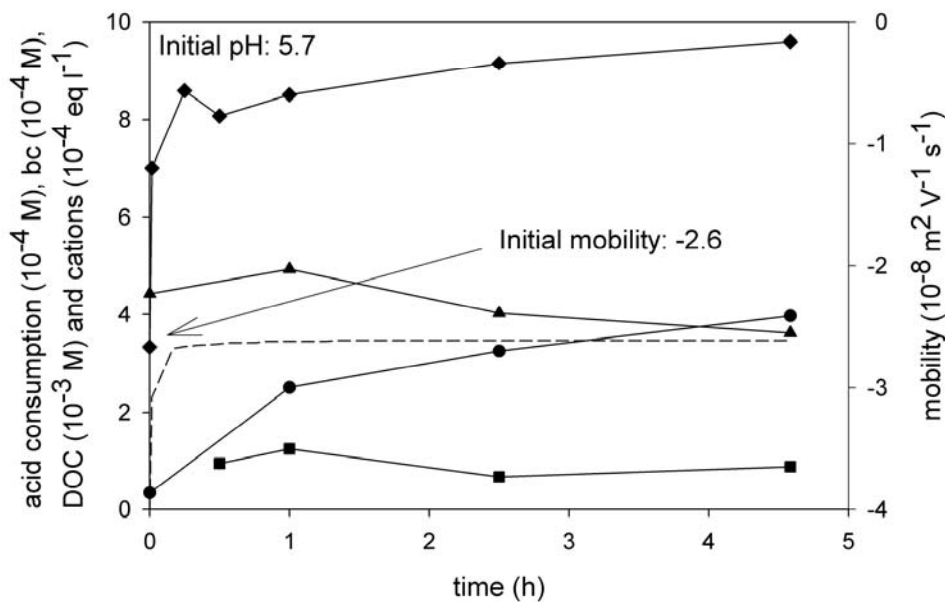


**Figure 2.5:** Acid consumption (dashed line), solution chemistry (buffering capacity (■) DOC (▲) and cation concentration (●)) and electrophoretic cell mobility (◆) as function of time at pH 4, in 0.01 M NaCl (150 ml total volume,  $10^{11}$  cells  $L^{-1}$ ). Cells were cultured in LB-medium. The buffering capacity of the solution is identified as bc. The cation concentration is the sum of the concentrations of K, Mg and Ca expressed in equivalence per liter.

At pH 8, base consumption occurred over the entire duration of the experiment (Fig. 2.6). As inferred from the electrophoretic mobility measurements, the cells initially experienced a rapid drop to a more negative surface charge, followed by a recovery. After the first hour, the electrophoretic mobility remained nearly constant, within the range of values measured prior to the initial pH adjustment. No significant change in the buffering capacity of the solution was measured, but the DOC concentration approximately doubled during the

experiment. The total concentration of K, Ca plus Mg increased. In addition to an increase of the K concentration in solution, as observed in the pH 4 experiment, a decrease of the concentrations of Ca and Mg was noted.

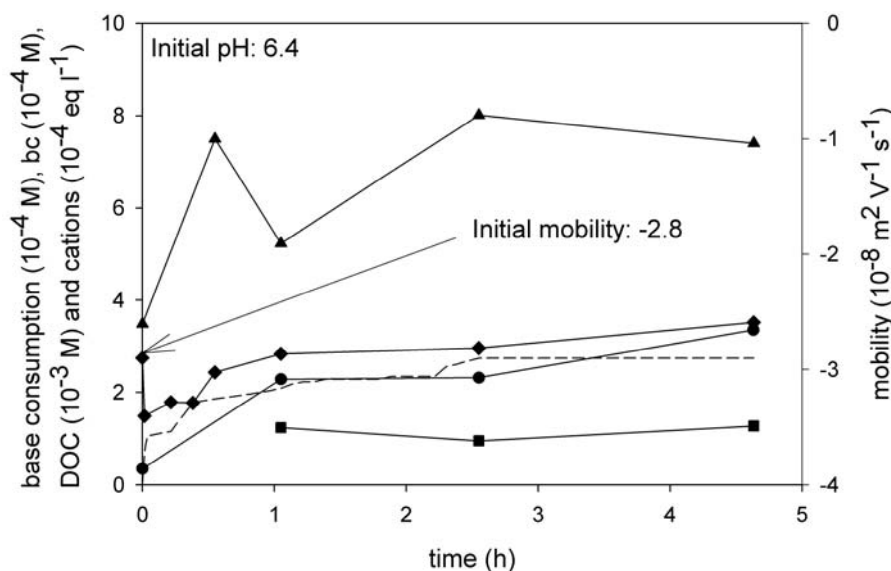


**Figure 2.6:** Base consumption (dashed line), solution chemistry and electrophoretic cell mobility as function of time at pH 8, in 0.01 M NaCl (150 ml total volume,  $10^{11}$  cells  $\text{L}^{-1}$ ). Cells were cultured in LB-medium. See Figure caption 2.5 for additional details.

When the cells were exposed to pH 10 in 0.01 M NaCl, the electrophoretic mobility instantaneously dropped to a more negative value (Fig. 2.7). As for the experiment at pH 8, the electrophoretic mobility progressively returned to values similar to those observed prior to pH adjustment. The buffering capacity, the DOC concentration and the total concentration of K, Ca plus Mg increased with time. The latter was due to an increase of the K concentration, as both the concentrations of Ca and Mg decreased. With the exception of the change in buffering capacity of the solution, the observed temporal changes at pH 10 were similar to those at pH 8.

The initial electrophoretic mobility of cells in 0.003 M  $\text{MgCl}_2$  background electrolyte was more positive than observed in NaCl solutions (Fig. 2.8). Furthermore, at pH 10, no significant changes in electrophoretic mobility were noted over the course of the pH stat experiment (Fig. 2.8). As for the pH 10 experiment in 0.01 M NaCl, the concentration of DOC increased with time. The total concentration of Na, K and Ca also increased, primarily

because of increasing concentrations of Na and K. The buffering capacity of the solution, however, did not show the large increase observed in 0.01 M NaCl solution.

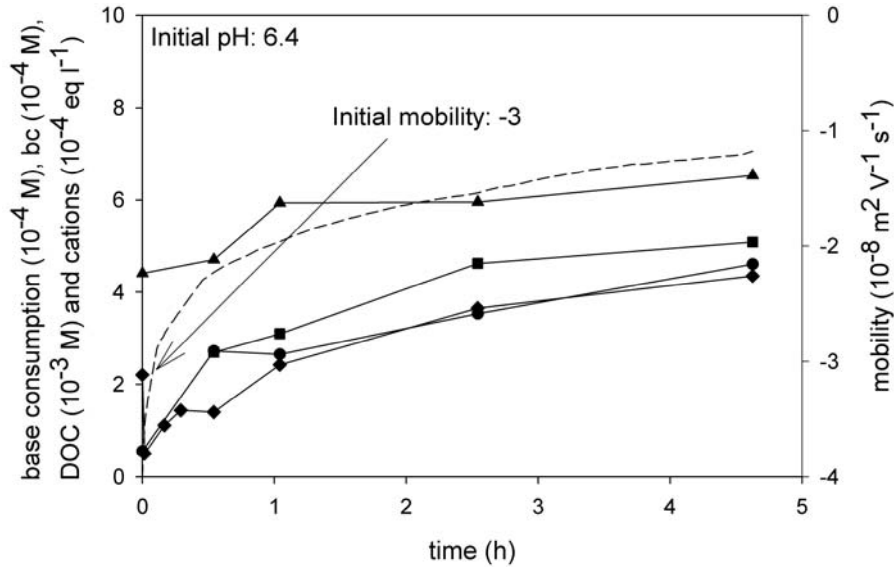


**Figure 2.7:** Base consumption, solution chemistry and electrophoretic cell mobility as function of time at pH 10, in 0.01 M NaCl (150 ml total volume,  $10^{11}$  cells  $L^{-1}$ ). Cells were cultured in LB-medium. See Figure caption 2.5 for additional details.

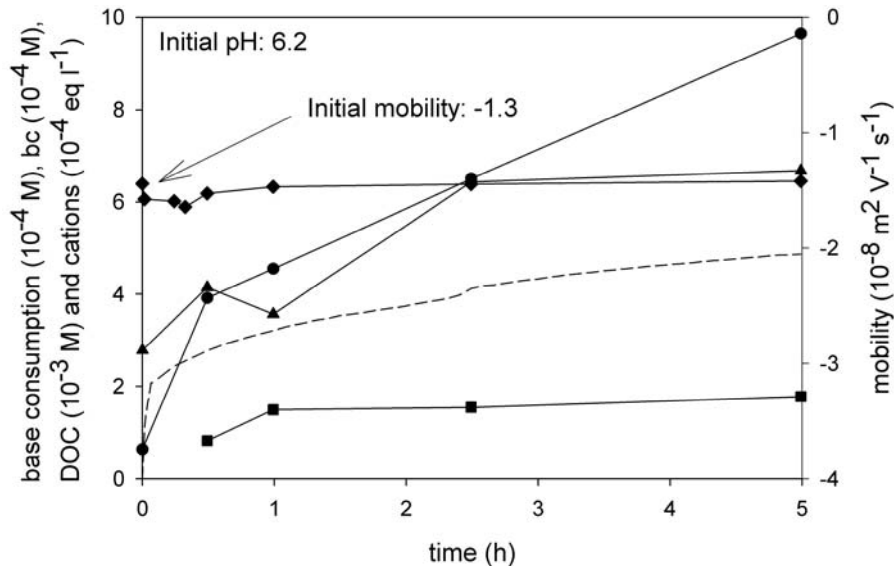


**Figure 2.8:** Base consumption, solution chemistry and electrophoretic cell mobility as function of time at pH 10, in 0.003 M  $MgCl_2$  (150 ml total volume,  $10^{11}$  cells  $L^{-1}$ ). Cells were cultured in LB-medium. See Figure caption 2.5 for additional details.

### 2.3.5 Release of cell wall components

SDS-PAGE of 0.15 and 0.01 M NaCl solutions in which bacteria had resided for 5 hours at pH 7 showed no evidence of dissolved proteins (not shown). At pH 10, poorly resolved bands (not shown) indicated that either the bacteria had released many different proteins with a large range of molar masses, or that the sample treatment had dissociated released proteins in many different fragments.

SDS-PAGE of the cell envelopes revealed the broad band characteristic of LPS from cell walls of Gram-negative bacteria (Fig. 2.9). Such bands did not appear in the SDS-PAGE of 0.15 and 0.01 M NaCl solutions in which bacteria had resided for 5 hours at pH 7. However, at pH 10, two weak, but distinct bands were observed at the position corresponding to the cell envelope LPS (channel 8 on Fig. 2.9).

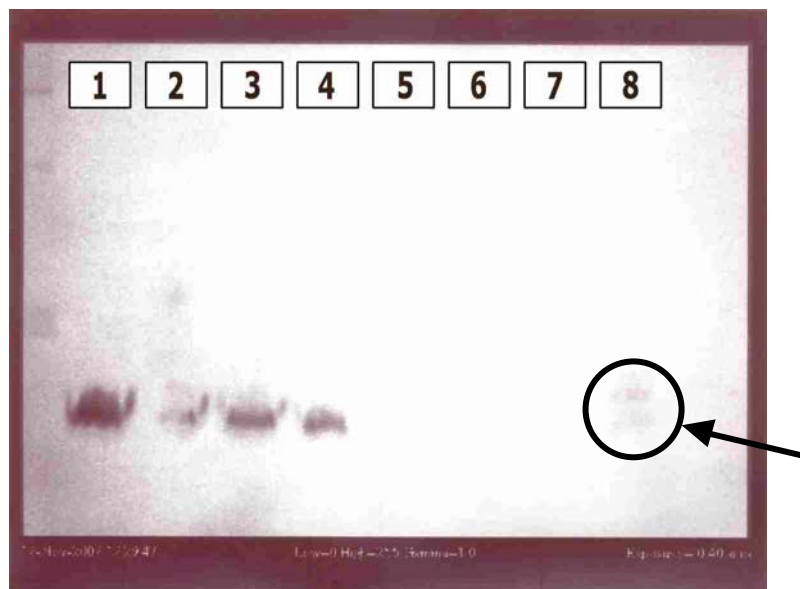


**Figure 2.9:** LPS gel electrophoresis of the cell envelopes (CE) and the solutions (S). Bacterial suspensions were kept for 5 hours under experimental conditions: Lane 1: CE of cultured cells, 2: CE 0.15 M NaCl pH 7, 3: CE 0.01 M NaCl pH 7, 4: CE 0.01 M NaCl pH 10, 5: S 0.15 M NaCl pH 7, 6: S 0.15 M NaCl pH 7, 7: S 0.01 M NaCl pH 7, 8: 0.01 M NaCl pH 10.

## 2.4 Discussion

Continuous acid-base titrations of mineral surfaces have been used extensively to acquire information on the types and amounts of surface functional groups. Their application has recently been extended to probe the functional groups present in microbial cell walls (Plette et al., 1995; Plette et al., 1996; Van der Wal et al., 1997a; Daughney et al., 1998; Daughney and Fein, 1998; Cox et al., 1999; Fowle and Fein, 1999; Fowle et al., 2000; Fowle and Fein, 2000; Daughney et al., 2001; Haas et al., 2001; Yee and Fein, 2001). At a given temperature and electrolyte composition, a mineral or microbial cell suspension has a unique titration curve if reversible protonation and deprotonation of a fixed set of exposed functional groups are the only processes responsible for proton exchange between solution and suspended matter. Our results, however, indicate that titration curves of suspensions of live cells of *S. putrefaciens* cannot be interpreted solely in terms of protonation and deprotonation of functional groups present in the cell wall. Even for relatively small equilibration times, on the order of minutes, the titration curves exhibit hysteresis.

As shown in this paper, pH stat experiments provide a useful approach to investigate the time-dependent processes affecting the acid-base activity of suspensions of live cells. The most striking result is the very different behavior of suspensions of *S. putrefaciens* at pH 4, compared to that observed under alkaline conditions. After exposure to pH 4, the cells are no longer viable, although they remain intact. The observed acid consumption, as well as the changes in electrophoretic mobility and solution composition, are consistent with a rapid initial protonation of functional groups of the cell wall (Fig. 2.5). The only long-term response of the bacteria is continued leakage of  $K^+$  into the extracellular medium.

In contrast to the behavior observed at pH 4, the cells remain viable even after being exposed for several hours at pH 10. At this pH value, a rapid initial response, most likely reflecting deprotonation of cell wall functional groups, is followed by long-term changes of the electrical charging of the bacteria and the chemical composition of the extracellular medium. At pH 8, a similar behavior is seen, although the initial response is less pronounced. At pH 8 and 10, base neutralizing capacity is continually generated by the bacterial cells over the entire duration of the experiments.

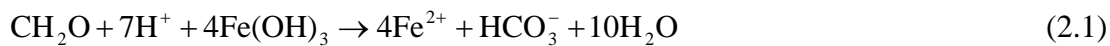
The increase in DOC concentration at pH 8 and 10 (Figs. 2.6-2.8) suggests that continued base neutralization is related to the release into solution of organic compounds.

These compounds could be organic acids synthesized intracellularly and then transported across the cell wall (Fig. 2.1, process 4), or they could be acidic cell wall components that are detached under high pH conditions (Fig. 2.1, process 6). Although the exact nature of continued base neutralization by the cells is currently unknown, it appears to involve an active metabolic response of the cells. After 5 hours at pH 10, live cells neutralize about twice as much base as heat-broken cells (Fig. 2.4). A live cell thus generates buffering capacity in excess of the initial capacity associated with its cytoplasm and cell wall.

SDS-PAGE results indicate that, at pH 10, cell wall constituents, in particular LPS and possibly also proteins, accumulate in solution (Fig. 2.9). These cell wall constituents contain a variety of acidic functional groups and can, therefore, contribute to the observed base neutralization capacity of the cell suspensions. The results presented, however, are preliminary. We are currently using SDS-PAGE to more completely characterize the pH-dependent release of macromolecules by bacterial suspensions, in combination with measurements of small organic acids. This work should permit to better constrain the relative contributions of cell wall and cytoplasm constituents to the base buffering capacity of the cell suspensions.

The electrical charging of the cells not only depends on the pH, but also on the background electrolyte. The electrophoretic mobility is more positive when cells are conditioned in a  $\text{MgCl}_2$  rather than a  $\text{NaCl}$  solution (Figs. 2.7 and 2.8), implying that cells of *S. putrefaciens* have a higher affinity for  $\text{Mg}^{2+}$  than for  $\text{Na}^+$ . Uptake of  $\text{Mg}^{2+}$  by the cell wall significantly reduces the initial response of the electrophoretic mobility to a shift to higher pH (Fig. 2.8). At pH 8 and 10, the cells' electrophoretic mobility in  $\text{NaCl}$  medium increases again after an initial drop to more negative values (Figs. 2.6 and 2.7). This recovery is accompanied by  $\text{Mg}^{2+}$  and  $\text{Ca}^{2+}$  removal from solution. Thus, the progressive loss of negative surface charge of cells exposed to pH 8 and 10 may result from release of negatively charged (deprotonated) cell wall constituents, as well as uptake of divalent cations by the cell wall. Although the electrical charging of the cells is dependent on the electrolyte ( $\text{NaCl}$  or  $\text{MgCl}_2$ ), the base consumption of the cell suspensions at pH 10 is similar. Moreover, experiments performed at different electrolyte concentrations (0.01 M or 0.15 M  $\text{NaCl}$ ) give the same results (Figs. 2.3A and B).

In cultures, *S. putrefaciens* grows best at near-neutral pH. As shown in this study, the bacterium dies when exposed to more acidic conditions, relative to the optimal pH range for growth, but survives under alkaline conditions. In the latter case, the bacterial cells actively generate base neutralizing capacity, countering the pH increase of the surrounding medium. The ability of *S. putrefaciens* to cope with alkaline conditions may be an adaptation related to its respiratory capabilities. *S. putrefaciens* is a well-known metal-reducing bacterium, which in natural environments utilizes iron and manganese (hydr)oxides as terminal electron acceptors (DiChristina, 1989). Dissimilatory reduction of these mineral phases, coupled to organic matter oxidation, has been shown to locally increase pH in aquatic sediments (Van Cappellen and Wang, 1996) and stratified water columns (Van Cappellen et al., 1998). The pH change is related to the large proton consumption in reactions such as



where  $\text{CH}_2\text{O}$  and  $\text{Fe}(\text{OH})_3$  are simplified representations of organic matter and ferric (hydr)oxides, respectively. We therefore speculate that iron and manganese reducing organisms may derive a competitive advantage from being able to deal with pH increases in their immediate environment.

## 2.5 Conclusions

This paper presents the results of a preliminary survey of the acid-base properties of suspensions of live cells of the facultative anaerobic bacterium *S. putrefaciens*. Under alkaline conditions (pH 8 and 10), the bacteria actively neutralize base during the 5 hour-long experiments. Several mechanisms are proposed to explain the continued generation of buffering capacity by the cells (Fig. 2.1), although further studies are needed to conclusively identify the dominant one(s). In contrast with the pH 8 and 10 experiments, exposure to pH 4 kills the bacteria. The acid neutralizing capacity is therefore limited by the initial availability of functional groups that undergo protonation at pH 4. Our results illustrate the complex response of cells of *S. putrefaciens* to changes in pH and electrolyte composition of the aqueous medium. As a result, it may not be straightforward to interpret titration curves of

living cell suspensions, or to predict the acid-base activity of natural microbial assemblages. Clearly more work is needed to characterize and understand the mechanisms and implications of the acid-base behavior of microorganisms in the environment.

### **Acknowledgments**

Prof. dr. J.P.M. Tommassen and H.A.M. Tommassen-van Boxtel (Department of Microbiology, Utrecht University) are acknowledged for assisting with the SDS-PAGE experiments and for discussions on bacterial physiology. Dr. D.M.E. Thies-Weesie and S. Sacanna (Van 't Hoff Laboratory for Physical and Colloid Chemistry, Utrecht University) are thanked for providing access to the electrophoretic mobility measurements. Two anonymous reviewers offered useful comments and suggestions. This research was financially supported by the Netherlands Organization for Scientific Research (NWO-Pionier Award).

---

## **Chapter 3**

### **Acid-base activity of live bacteria: Implications for quantifying cell wall charge**

Jacqueline Claessens, Yvonne van Lith, Anniet M. Laverman and Philippe Van Cappellen  
(2006) *Geochimica et Cosmochimica Acta*, 70, 267-276.

---

## Abstract

In order to distinguish the buffering capacity associated with functional groups in the cell wall from that resulting from metabolic processes, base or acid consumption by live and dead cells of the Gram-negative bacterium *Shewanella putrefaciens* were measured in a pH stat system. Live cells exhibited fast consumption of acid (pH 4) or base (pH 7, 8, 9 and 10) during the first few minutes of the experiments. At pH 5.5, no acid or base was required to maintain the initial pH constant. The initial amounts of acid or base consumed by the live cells at pH 4, 8 and 10 were of comparable magnitudes as those neutralized at the same pHs by intact cells killed by exposure to gamma radiation or ethanol. Cells disrupted in a French press required higher amounts of acid or base, due to additional buffering by intracellular constituents. At pH 4, acid neutralization by suspensions of live cells stopped after 50 minutes, because of loss of viability. In contrast, under neutral and alkaline conditions, base consumption continued for the entire duration of the experiments (5 hours). This long term base neutralization was, at least partly, due to active respiration by the cells, as indicated by the build-up of succinate in solution. Qualitatively, the acid-base activity of live cells of the Gram-positive bacterium *Bacillus subtilis* resembled that of *S. putrefaciens*. The pH-dependent charging of ionizable functional groups in the cell walls of the live bacteria was estimated from the initial amounts of acid or base consumed in the pH stat experiments. From pH 4 to 10, the cell wall charge increased from near-zero values to about  $-4 \times 10^{-16}$  mol cell<sup>-1</sup> and  $-6.5 \times 10^{-16}$  mol cell<sup>-1</sup> for *S. putrefaciens* and *B. subtilis*, respectively. The similar cell wall charging of the two bacterial strains is consistent with the inferred low contribution of lipopolysaccharides to the buffering capacity of the Gram-negative cell wall (on the order of 10 %).

### 3.1 Introduction

The presence and activity of microorganisms affect the redox state, acid-base properties and chemical speciation of environmental fluids. Interactions between microorganisms and their immediate surroundings are regulated via the cell wall, across which chemical substances enter and leave the cell. Furthermore, cell walls offer a variety of functional groups that provide binding sites for solute and colloidal species present in the environment. In particular, carboxylate, phosphate and amino groups have been identified as potential groups affecting the chemical functioning of the cell-water interface (e.g., Plette et al., 1995; van der Wal et al., 1997a; Haas et al., 2001).

As a result of protonation and deprotonation of functional groups, cell walls exhibit a pH-dependent charge. At most environmental pHs, cell walls of microorganisms, such as bacteria, carry an overall negative surface charge and, therefore, exhibit a high affinity for metal cations (e.g., Urrutia Mera et al., 1992; Agraz et al., 1994; Plette et al., 1996; Daughney et al., 2001; Haas et al., 2001; Kelly et al., 2002; Borrok and Fein, 2005). Metals complexed in the cell wall may serve as nucleation sites for mineral precipitation via counter adsorption of anions (Schultze-Lam et al., 1996).

Because the acid-base behavior of cell walls is crucial to understanding metal binding, cell-mineral adhesion, and microbially-induced mineralization or dissolution processes, there have been growing efforts to characterize the functional groups in cell walls. Acid-base titrations offer a powerful technique to quantify the protonation and deprotonation of functional groups, and they have been used widely to study the mineral-aqueous solution interface (Dzombak and Morel, 1990). Their application, however, has been extended to bacterial cell walls. While titrations were initially carried out mainly with dead bacterial cells or isolated cell walls (Goncalves et al., 1987; Plette et al., 1995; Van der Wal et al., 1997a), a number of recent studies have employed live cells of Gram-positive (Daughney and Fein, 1998; Daughney et al., 2001; Borrok and Fein, 2005) and Gram-negative bacteria (Haas, 2004).

The interpretation of acid-base titrations performed on live cells is not straightforward, however. In a previous study, we have shown that the acid and base consumption of suspensions of live cells of the Gram-negative bacterium *S. putrefaciens* cannot be explained

solely as a result of protonation and deprotonation of functional groups (Claessens et al., 2004). Hysteresis of continuous titration curves indicated the occurrence of irreversible processes, most likely related to cellular metabolism and, possibly, to the destabilization of the cell wall. Therefore, rather than performing traditional, continuous titrations, we measured the acid and base consumption of cell suspensions at constant pH, as a function of time (pH stat method).

The present study builds on our previous, preliminary findings. In order to separate the contributions of protonation and deprotonation of functional groups from those of other processes affecting the acid-base behavior of live cells, we performed new series of pH stat experiments with live cells, intact dead cells and disrupted cells of *S. putrefaciens*. In the experiments with live cells, the solutions were screened for the build-up of products indicative of metabolic activity, especially organic acids. In addition, we determined the buffering capacity of lipopolysaccharides, a major constituent of the cell wall of Gram-negative bacteria, and we compared the acid–base behavior of *S. putrefaciens* to that of the Gram-positive bacterium *B. subtilis*.

## **3.2 Materials and methods**

### **3.2.1 Bacteria**

A Gram-negative bacterium, *Shewanella putrefaciens* strain 200R, and a Gram-positive bacterium, *Bacillus subtilis*, were used. *S. putrefaciens* was originally isolated from crude oil, but its presence has been detected in a variety of aquatic and subsurface environments (Venkateswaran et al., 1999). *B. subtilis* is a common bacterium in soil and vegetation (Pinchuk et al., 2002). Pure cultures of *S. putrefaciens* strain 200R and *B. subtilis* were grown at room temperature in liquid Luria Bertani (LB) medium. The bacteria were harvested in mid-logarithmic phase and pelletized by centrifugation (5000 g for 20 min). The supernatant was discarded and the pelletized cells were resuspended in 150 mM NaCl salt solution. The washing procedure was repeated one more time, in order to obtain the bacterial stock suspensions used in the experiments. Cell densities of the bacterial stock suspensions were derived from the optical densities (OD) measured at 660 nm wavelength on the harvested cultures. The OD-values were calibrated by counting viable cells growing on solid

medium, and by using the acridine orange direct count (AODC) method (Lovley and Phillips, 1988). The harvested cultures contained on the order of  $10^9$  cells per ml.

Cell weights of *S. putrefaciens* and *B. subtilis* were determined by centrifuging pre-concentrated stock suspensions at 5000 g for 20 minutes, and discarding the supernatant. Wet weights were measured on pellets air-dried at room temperature for 2-3 hours, until no visible free water remained. Dry weights were determined on oven-dried pellets (40 °C, 7 hours). In contrast to air-drying, the pellet volume noticeably decreased as a result of oven drying. The weights of the pellets were corrected for salt contributions from the medium. Weight determinations were performed on triplicate aliquots; standard deviations were less than 2 %. For *S. putrefaciens* air-dried and oven-dried pellets yielded  $2 \times 10^{-12}$  and  $7 \times 10^{-13}$  g cell<sup>-1</sup>, respectively. For *B. subtilis* the corresponding values were  $6 \times 10^{-12}$  and  $4 \times 10^{-12}$  g cell<sup>-1</sup>. The higher and lower densities were considered to be representative of the wet and dry weights of the bacterial cells, respectively.

Intact dead cells of *S. putrefaciens* were prepared by exposing aliquots of the bacterial stock suspension to gamma radiation (25 kGr, Isotron Nederland B.V., Ede) and ethanol (1 hour in 50 % v/v ethanol). Gamma radiation damage to biological materials results from reactions with radicals produced from ionized water (Greenstock, 1981). In particular, gamma radiation breaks up DNA strands, thereby preventing the cells from replicating. Ethanol kills bacterial cells by denaturing proteins, although it may also partially dissolve membrane lipids (Prescott et al., 1996). After the treatments, the cells were pelletized by centrifugation (5000 g for 20 minutes) and resuspended in 150 mM NaCl, and the washing procedure was repeated.

Cells of *S. putrefaciens* were also disrupted in a French press at 8000 psi. The applied pressure causes the intracellular pressure to increase. As the cells are released through the outlet tube, the external pressure drops instantaneously to atmospheric pressure. The pressure differential between the outside and inside of the cells causes them to burst, releasing the intracellular contents. On the order of 10 % of the cells survived the French press treatment and were pelletized by centrifugation (5000 g for 20 minutes). The supernatant contained the envelopes and intracellular contents of the disrupted cells. In the following sections the supernatant is referred to as disrupted cells.

Gram-negative bacteria differ from Gram-positive bacteria by the presence of an outer membrane containing lipopolysaccharides (LPS) (Madigan et al., 1997). As LPS is specific for Gram-negative bacteria, its acid-base properties were studied separately. Pure LPS (Fluka 62326) from the Gram-negative bacterium, *Escherichia coli*, was dissolved in 150 mM NaCl to a final concentration of 1.203 g L<sup>-1</sup>.

### 3.2.2 pH stat experiments

The acid-base activity and properties of the live and dead cell suspensions, as well as LPS, were measured in a pH stat system (Claessens et al., 2004). The experiments were performed using an automated titrator (Metrohm 716S controlled by Metrohm Tinet 2.4) at 22 °C. The pH of a 150 mM NaCl solution (145 ml) was brought to the desired value of 4, 5.5, 8 or 10 by addition of 0.01 M HCl or 0.01 M NaOH solutions. Equal volumes (5 ml) of cell suspensions (live and dead) or LPS were added to final concentrations of 10<sup>8</sup> cells ml<sup>-1</sup> or 0.04 g L<sup>-1</sup> LPS. For suspensions of live cells of *S. putrefaciens*, additional pH stat experiments were carried out at pH 7 and 9. In two more experiments, suspensions of live cells of *S. putrefaciens* were pre-equilibrated at pH 4 for 1.4 hours, before adjusting the pH to 8 and 10 by adding NaOH.

The consumption of HCl or NaOH required to keep the pH constant was monitored for periods of up to 5 hours. The added titrant volumes were automatically recorded every minute. The total consumption of acid or base was corrected for the consumption by the salt solution alone, to derive the net consumption of protons or hydroxyls by the cells or LPS. The background consumption of acid or base by the salt solution alone was less than 15 % of that of the cell suspensions at pH 4 and 8, and less than 20 % at pH 10, except for ethanol treated cell suspensions where the background correction at pH 10 reached 30 % at the end of the experiment. The pH stat experiments with suspensions of live and ethanol treated cells of *S. putrefaciens* were performed at least in triplicate, and standard deviations were calculated. All other experiments were performed once.

In the experiments at pH 4, 5.5, 8 and 10 with live cells of *S. putrefaciens*, the solutions were analyzed for the presence of organic acids. At fixed times (0 h, 1 h, 2.5 h, 4 h and 5 h) an aliquot of 2.5 ml was collected, filtered through a 0.2 µm pore size filter, and analyzed by Ion Exclusion Chromatography (Dionex DX 120). A column (ICE-AS6) and

suppressor (AMMS-ICE II) were used for efficient separation of low molecular weight aliphatic organic acids. The eluent was a 0.4 mM heptafluorobutyric acid solution and the regenerant a 5 mM tetrabutylammoniumhydroxide solution. A standard solution of 1 mM formate, lactate, acetate, succinate and propionate was prepared, and diluted to final concentrations of 5, 10, 30, 50 and 100  $\mu\text{M}$  for calibration. The matrix of the standard solution was 150 mM NaCl to match that of the samples.

### 3.2.3 Electrophoretic mobility measurements

The electrophoretic mobility of *S. putrefaciens* cells was measured as function of pH in 1, 10 and 100 mM NaCl solutions. The pH of the cell suspensions was brought to pH 3.2 with 0.01 M HCl and equilibrated for 30 minutes. Subsequently, the pH was brought to pH 10 in steps of 0.4 pH units, with a 0.01 M NaOH solution. After each addition of base, the solution was allowed to equilibrate for 20 minutes. Unfiltered aliquots were directly injected in a Coulter Delsa 440sx and the electrophoretic mobility was measured at two positions in the measuring cell. At each position, the measurement was repeated four times.

## 3.3 Results

### 3.3.1 Acid-base activity of live cells

In pH stat experiments with live cells of *S. putrefaciens*, no acid or base was needed initially to keep the pH of the bacterial suspension constant at pH 5.5. At pH 4, rapid acid consumption occurred during the first few minutes after adding the cells, followed by more gradual acid consumption, which ended after 50 minutes (Fig. 3.1A). Similarly, under neutral and alkaline conditions (pH 7, 8, 9 and 10), base was consumed rapidly during the first few minutes of the experiments. In contrast with the experiments at pH 4, however, no cessation of the long-term base neutralization was observed. This is illustrated in Figure 3.1A, which shows ongoing base neutralization after 5 hours in the pH stat experiments at pH 8 and 10. Net base neutralization by suspensions of live *S. putrefaciens* cells measured after 5 hours increased systematically from pH 7 to pH 10. A small upward pH drift ( $0.13 \times 10^{-16} \text{ mol cell}^{-1} \text{ h}^{-1}$ ) also indicated some long-term acid consumption by the cell suspensions at pH 5.5.

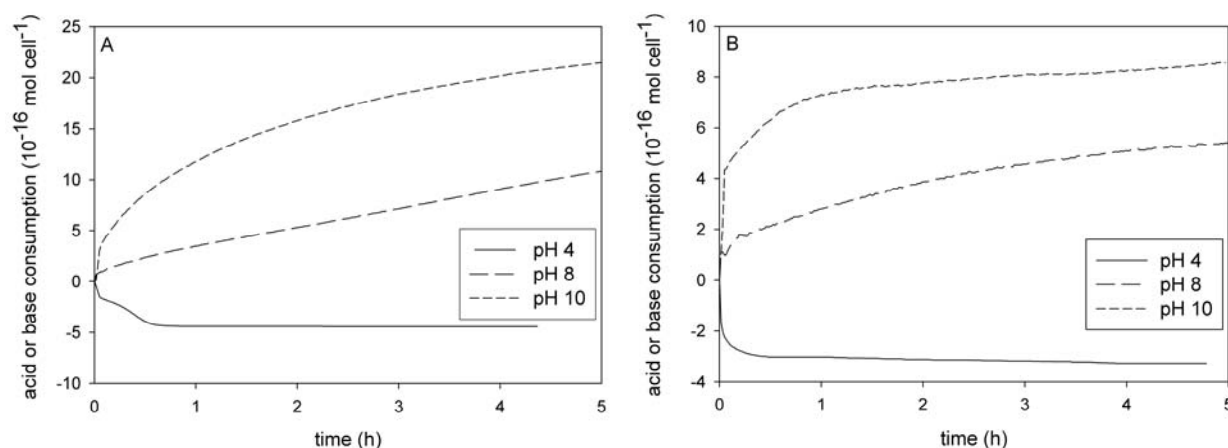


**Figure 3.1:** Acid and base consumption of live cells of *S. putrefaciens* (A) and *B. subtilis* (B) as function of time at pH 4, 8 and 10, in 150 mM NaCl, at a cell density of  $10^8$  cells  $\text{ml}^{-1}$  and a temperature of 22 °C.

The initial amounts of acid or base consumed by the bacterial suspensions were estimated by extrapolating the slow neutralization trends back to time zero, as shown in Figure 3.2. These estimates were quite reproducible. Standard deviations of the initial amounts of acid and base consumed by the suspensions of live cells of *S. putrefaciens* did not exceed 17 % (Table 3.1). The amounts of acid and base consumed after five hours had even lower standard deviations of 5 %, except at pH 10 where the standard deviations of the long-term (5 hours) base consumption were around 15 %.

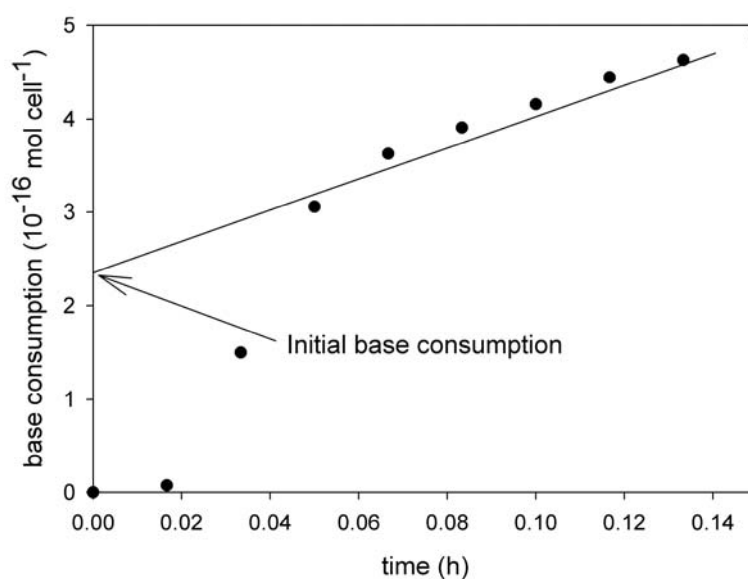


**Figure 3.2:** Example of the determination of initial base consumption by live cells of *S. putrefaciens* at pH 10.

**Table 3.1:** Initial acid (pH 4) or base (pH 8 and 10) consumption of live cells of *S. putrefaciens* (Sp) and *B. subtilis* (Bs), dead but intact cells of Sp, disrupted cells of Sp, and lipopolysaccharides (LPS) isolated from *E. coli* expressed in units of  $10^{-16}$  mol cell<sup>-1</sup>.

Cell suspensions	pH4	pH8	pH10
Live cells (Sp)	1.3 ± 0.13	0.7 ± 0.07	2.3 ± 0.40
Live cells (Bs)	2.0	1.4	4.1
Gamma radiated cells	2.8	1.8	2.6
Ethanol treated cells	2.7 ± 0.54	1.1 ± 0.22	1.7 ± 0.68
French press disrupted cells	6.7	3.5	13.7
LPS	0.1	0.1	0.3

Acid or base consumption curves by suspensions of live cells of *B. subtilis* exhibited features similar to those observed for *S. putrefaciens* (Fig. 3.1B). No acid or base was consumed when cells were added to pH 5.5 solutions. At pH 4, acid consumption lasted for about 20-30 minutes, beyond which no further acid addition was required to keep the pH constant. At pH 8 and 10, fast base consumption during the first few minutes was followed by slower, continuous base consumption for the remainder of the experiments. While the initial acid and base consumption per cell was higher for *B. subtilis* than for *S. putrefaciens* (Table 3.1), after 5 hours, base consumption at pH 8 and 10 was significantly lower for the cell suspensions of *B. subtilis*.

The base consumption of live cell suspensions of *S. putrefaciens* at pH 8 and 10 differed significantly whether or not the suspensions had been pre-equilibrated at pH 4 (compare Figs. 3.1A and 3.3). After exposing the cells to pH 4 for 1.4 hours, base addition during about 15 minutes was needed to change the pH of the suspensions to 8 or 10. For the remainder of the experiments, however, base consumption was much smaller than in the experiments with no pre-equilibration at pH 4.

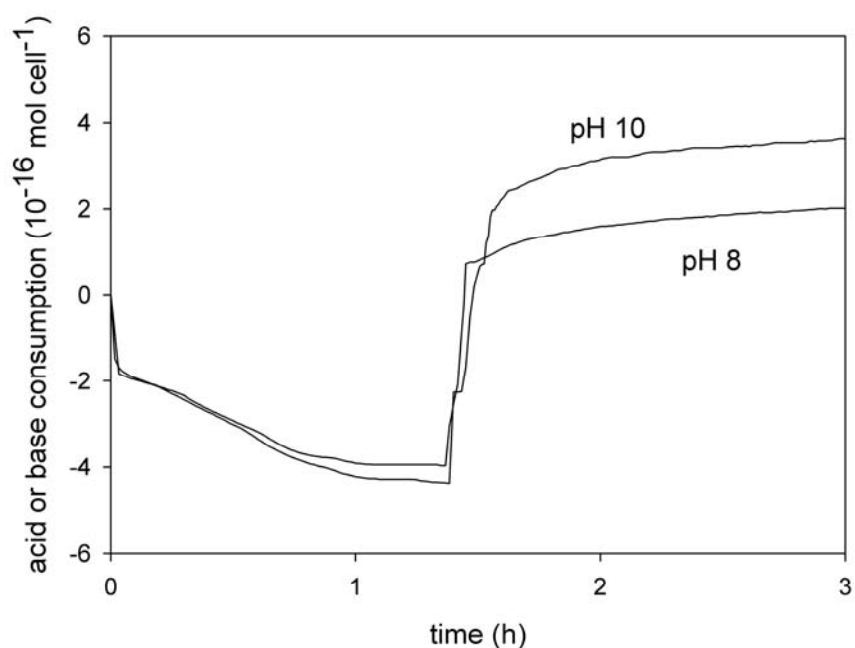


**Figure 3.3:** Acid and base consumption of live cells of *S. putrefaciens* exposed first to a constant pH of 4 for 1.4 hours, and then to a constant pH of 8 or 10. Experiments are conducted in 150 mM NaCl, at a cell density of  $10^8$  cells  $\text{ml}^{-1}$  and a temperature of 22 °C.

### 3.3.2 Acid and base buffering by dead cells and LPS

The acid or base activities of dead cells of *S. putrefaciens* in pH stat experiments was fundamentally different from that observed for the live cells, as shown in Figures 3.4A-C, for pH 4, 8 and 10, respectively. Rapid consumption of acid or base in suspensions of dead cells lasted a few minutes, and then ceased, or proceeded at a very slow rate. In Table 3.1, the initial acid (pH 4) or base (pH 8 and 10) consumption of the dead cells are compared to the initial acid or base consumption of live cells of *S. putrefaciens* and *B. subtilis*. The initial values listed in the table were determined by extrapolating the long term buffering trends back to time zero (Fig 3.2). This correction mainly affected the estimated initial acid or base consumption by the live cells, however.

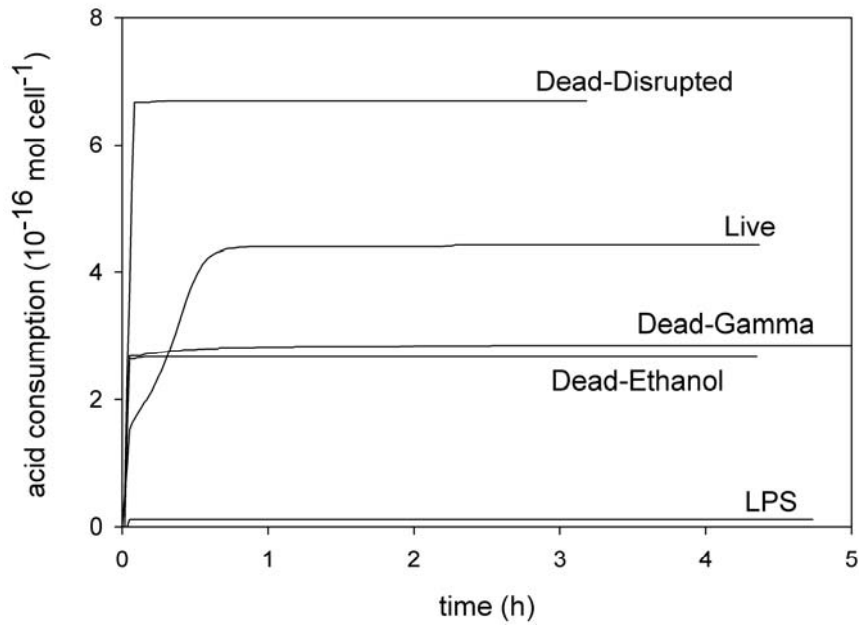


**Figure 3.4A:** Acid and base consumption of live cells, dead cells, disrupted cells of *S. putrefaciens*, and LPS as function of time at pH 4 in 150 mM NaCl, at a cell density of  $10^8$  cells  $\text{ml}^{-1}$  or  $0.04 \text{ g L}^{-1}$  LPS and  $22 \text{ }^\circ\text{C}$ .

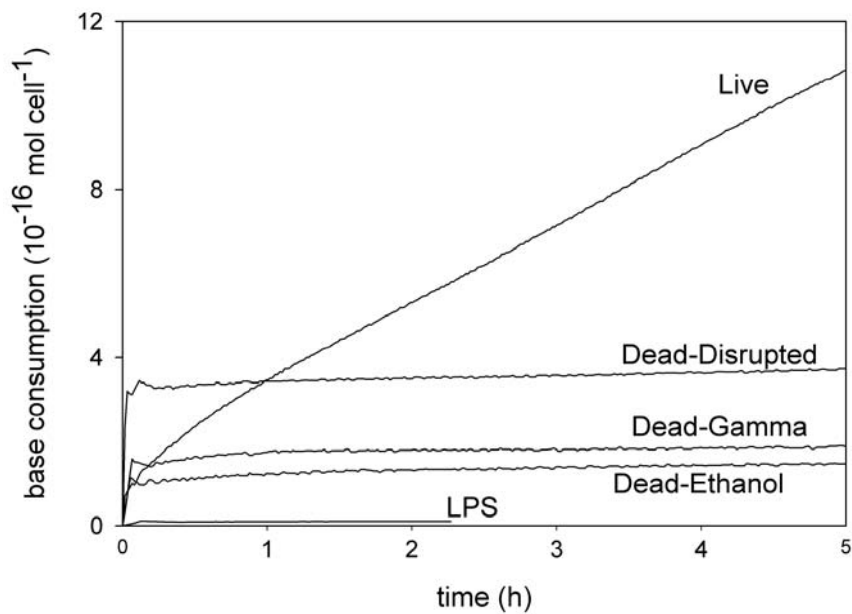


**Figure 3.4B:** Acid and base consumption of live cells, dead cells, disrupted cells of *S. putrefaciens*, and LPS as function of time at pH 8 in 150 mM NaCl, at a cell density of  $10^8$  cells  $\text{ml}^{-1}$  or  $0.04 \text{ g L}^{-1}$  LPS and  $22 \text{ }^\circ\text{C}$ .

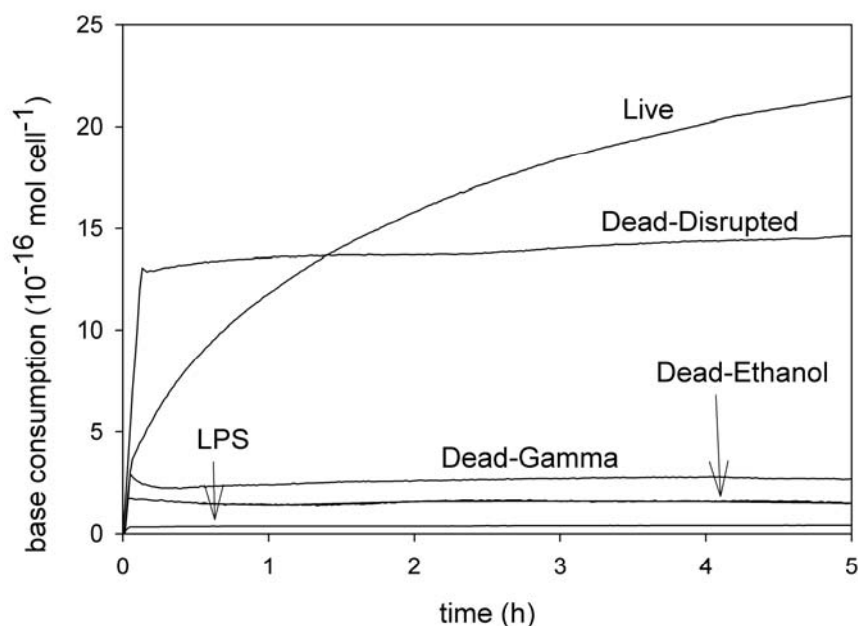


**Figure 3.4C:** Acid and base consumption of live cells, dead cells, disrupted cells of *S. putrefaciens*, and LPS as function of time at pH 10 in 150 mM NaCl, at a cell density of  $10^8$  cells  $\text{ml}^{-1}$  or  $0.04$  g  $\text{L}^{-1}$  LPS and  $22$  °C.

The amounts of acid or base consumed by gamma radiated and ethanol treated cells of *S. putrefaciens* were of comparable magnitude, although base consumption at pH 8 and 10 tended to be higher for cells killed by gamma radiation (Figs. 3.4B and C). Cells disrupted by the French press treatment exhibited systematically much higher acid and base consumption than dead, but intact cells. The initial amounts of acid or base consumed by live cell suspensions were comparable, within a factor of three, to those of the intact dead cells. The reproducibility of initial acid and base consumption in the replicate experiments with ethanol-killed cells, however, was not as good as for live cells, as can be inferred from the standard deviations in Table 3.1.

At pH 4, acid consumption by the live cells of *S. putrefaciens* reached values intermediate between those of intact dead cells and disrupted cells (Fig. 3.4A). At pH 8 and 10, base consumption at the end of the experiments was significantly higher for the live than for the dead cells (Figs. 3.4B and C). These results further highlight the very different buffering behavior of *S. putrefaciens* under acidic and basic conditions.

In order to estimate the potential contribution of lipopolysaccharides to the acid-base buffering capacity of cell walls of Gram-negative bacteria, the acid or base consumption measured in the LPS suspensions were expressed on a per cell basis (Table 3.1, Figs. 3.4A-C). The calculations assumed that the dry weight of *S. putrefaciens* cells is  $7 \times 10^{-13}$  g cell<sup>-1</sup> (section 3.2.1) and that LPS accounts for 3.4 % of the dry weight of Gram-negative bacteria (Madigan et al., 1997). According to the results, LPS may, at most, account for 10 % of the buffering capacity of the Gram-negative cell wall.

### 3.3.3 Organic acid production

Lactate and propionate were not detected in the filtered solutions of the pH stat experiments with live cells of *S. putrefaciens*. Measurable levels of acetate (5 mmol L<sup>-1</sup>) and formate (10 mmol L<sup>-1</sup>) were found at pH 4, 5.5, 8 and 10, but no clear trends with time were observed. Solutions of the experiments at pH 8 and 10 additionally contained succinate. In the case of succinate, however, the concentrations systematically increased with time (Fig. 3.5). The build-up of succinate was higher at pH 10 than at pH 8.

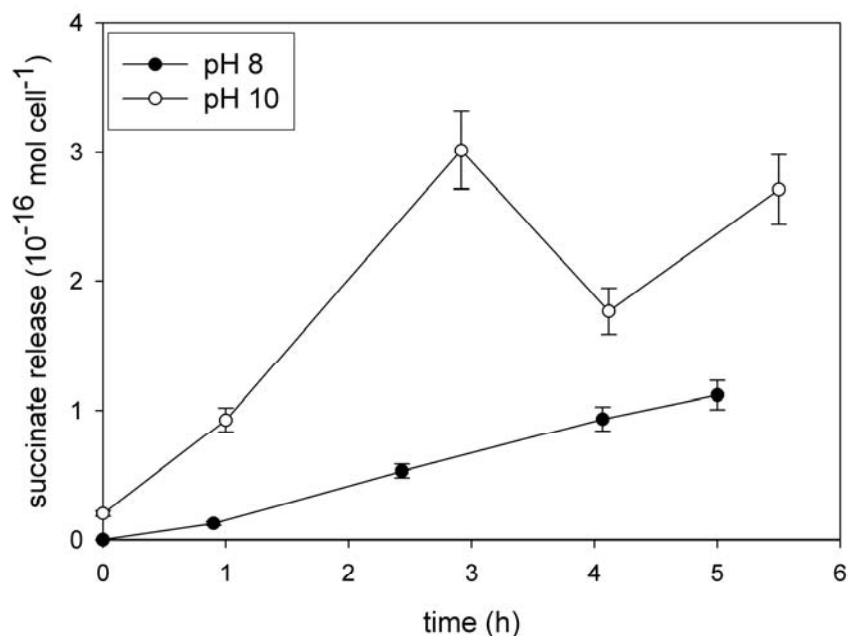


**Figure 3.5:** Release of succinate by live cells of *S. putrefaciens* as function of time at pH 8 and 10, in 150 mM NaCl, at a cell density of  $10^8$  cells ml<sup>-1</sup> and 22 °C.

### 3.3.4 Electrophoretic mobility

The isoelectric point (iep) of live cell suspensions of *S. putrefaciens* fell between pH 3.5 and 4, for the three electrolyte concentrations used (Fig. 3.6). With increasing pH, the electrophoretic mobility increased, consistent with the development of pH-dependent negative charge on the cells. The increase in electrophoretic mobility was more pronounced in 1 and 10 mM NaCl than in 100 mM NaCl. In 100 mM NaCl solution the electrophoretic mobility remained constant above pH 7, while in 1 and 10 mM NaCl solutions it continued to increase slowly until pH 10.

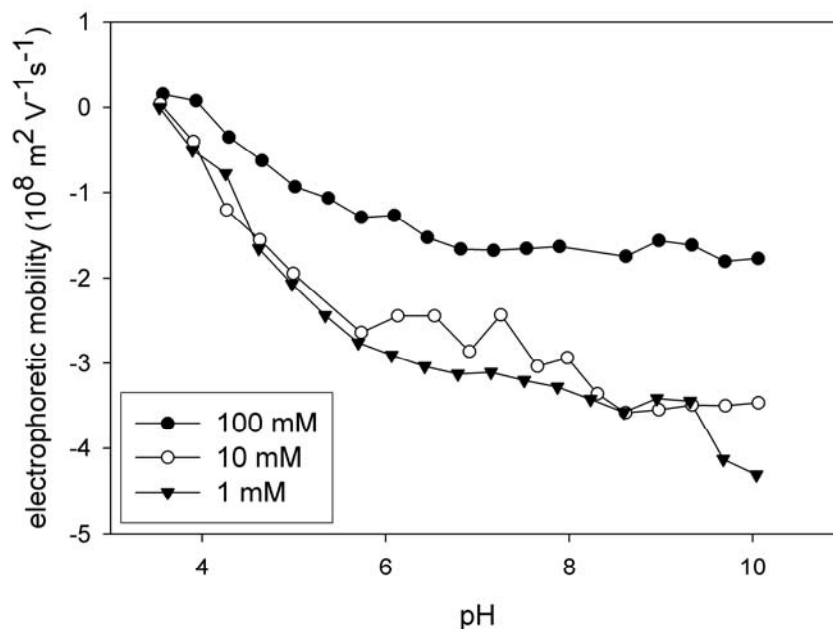


**Figure 3.6:** Electrophoretic mobility of cells of *S. putrefaciens* as function of pH in 1, 10 and 100 mM NaCl.

## 3.4 Discussion

### 3.4.1 Acid-base activity of bacterial cells

The acid and base consumption of live cells of *S. putrefaciens* differ greatly from those of dead cells (Figs. 3.4A-C). Dead cells exhibit little or no acid-base activity beyond the first few minutes of exposure to new pH conditions. The fast acid or base consumption by the dead cells most likely reflects the buffering capacity of the cell wall and, in the case of disrupted cells, also the intracellular content. Consequently, disrupted cells yield higher acid or base neutralization than dead, but intact cells (Table 3.1). The lack of long-term buffering by the

intact dead cells argues against a significant leakage of protons across their cytoplasmic membranes.

Physiologically active cells of *S. putrefaciens* also exhibit fast acid or base consumption during the first few minutes of the pH stat experiments. The initial amounts of acid or base neutralized are of similar magnitudes for live and intact dead cells, although some significant differences are observed (Table 3.1). At pH 8 and 10, the differences in initial buffering capacity between gamma radiated and ethanol treated cells, however, are of the same order of magnitude as those observed between live and dead bacteria. Furthermore, the replicate experiments with ethanol treated cells show a large variability, suggesting that the ethanol treatment creates artifacts in the cell wall buffering capacity.

Exposure of bacterial cells to ethanol causes denaturation of proteins and may dissolve membrane lipids (Prescott et al., 1996), while hydroxyl and superoxide radicals oxidize cell wall lipids and proteins during gamma radiation. In the latter case, the oxidative stress results in a reorganization of the fatty acid pattern and may alter the secondary structure of proteins (Benderitter et al., 2003). These various physical-chemical changes of the cell wall are likely to affect its acid-base properties. Therefore, we consider the initial acid or base consumption by the live cells to be the more accurate measure of the protonation or deprotonation of functional groups in the unaltered cell wall.

Viable cell counts show that *S. putrefaciens* cells die upon exposure to pH 4 (Claessens et al., 2004), which is consistent with the cessation of acid neutralization after 50 minutes observed at pH 4 (Fig. 3.4A), and with the much reduced base neutralization at pH 8 and 10 by cells pre-equilibrated at pH 4 (Fig. 3.3). The initial fast acid consumption in the pH stat experiments at pH 4 is not immediately followed by cessation of all acid neutralization activity, however (Fig. 3.4A). At pH 4, the cell suspensions continue to neutralize acid at a near-constant rate for about 50 minutes. Possibly, protons are pumped into the cell, where they are neutralized by the intracellular buffering capacity. Van der Wal et al. (1997a) similarly invoked proton transport across the cytoplasmic membrane to explain the hysteresis of continuous acid-base titration curves of whole live cells of a Gram-positive bacterium. Comparison of acid consumption by live and disrupted cells (Fig. 3.4A) indicates that the intracellular buffering capacity is sufficient to explain proton consumption beyond the fast initial acid buffering.

At pH 7 and higher, the evidence points to an additional mechanism of base neutralization. As shown in Figures 3.4B and C, base consumption by live cells of *S. putrefaciens* at pH 8 and 10 clearly exceeds that of disrupted cells. Therefore, the buffering capacities of cell wall and intracellular content together cannot account for the observed long-term (>1 hour) buffering. Aerobic respiration is the likely source of the long-term base neutralization, as indicated by the measurable build-up of succinate in the suspensions at pH 8 and 10 (Fig. 3.5). Succinate is one of the intermediate products of the tricarboxylic acid cycle (Madigan et al., 1997). During respiration, cells convert their intracellular sugar reserves, e.g. glucose, into pyruvate (glycolysis). Pyruvate is a substrate for the tricarboxylic acid cycle, and its transformation produces succinate and releases CO<sub>2</sub>. The acidity associated with CO<sub>2</sub> is then transferred to the extracellular solution, directly as CO<sub>2</sub> or as protons via the proton motive force across the cell membrane.

Interestingly, the intensity of long-term base neutralization by live cells of *S. putrefaciens* seems to be directly related to the pH of the surrounding medium. From pH 7 on, the net amount of base neutralization measured after 5 hours increases systematically with pH. We hypothesize that the cells adjust their respiration rate to the surrounding pH: the more the pH exceeds the optimal growth pH (7.0), the higher the respiratory activity and, hence, the larger the corresponding base neutralization. Obviously, the long-term base buffering in the pH stat experiments is limited by the intracellular reserves of carbon substrates for respiration. Substrate limitation may be responsible for the progressive slowing down of base neutralization observed at pH 10 (Fig. 3.1A).

Qualitatively, the acid and base consumption curves by live cells of the Gram-positive bacterium *B. subtilis* resemble those of the live cells of *S. putrefaciens*. A closer look at Figures 3.1A and B reveals some important differences, however. For instance, the initial amounts of acid and base consumed indicate that the cells of *B. subtilis* carry more functional groups than *S. putrefaciens* (Table 3.1). In contrast, the additional amounts of acid and base consumed are significantly lower for *B. subtilis*, implying a reduced intracellular acid buffering capacity and less long-term base neutralization by respiration, compared to *S. putrefaciens*. This is also illustrated in Table 3.2, where rates of proton release associated with intracellular buffering and respiration are systematically lower for *B. subtilis*.

**Table 3.2:** The rate of proton release by live cells of *S. putrefaciens* (Sp) and *B. subtilis* (Bs) expressed in units of  $10^{-16}$  mol cell<sup>-1</sup> h<sup>-1</sup> at pH 4, 5.5, 7, 8, 9 and 10 and 22 °C in 150 mM NaCl and  $10^8$  cells ml<sup>-1</sup>. The rate of proton release due to intracellular and metabolic buffering was calculated from the amounts of protons released in the pH stat experiments between respectively 3 and 18 minutes and 1.5 to 4 hours.

pH	Intracellular buffering		Metabolic buffering	
	Sp	Bs	Sp	Bs
4	-2.70	-2.31	0	-0.07
5.5	0	-	-0.13	-
7	2.17	-	0.84	-
8	3.80	3.14	1.87	0.67
9	5.68	-	-	-
10	9.45	4.98	2.79	0.25

The results discussed in this section highlight the large variability in acid-base activity of bacterial cells that may be caused by (1) variations in cell wall properties and the initial metabolic state resulting from cell preparation, (2) pH-dependent variations in cell viability and metabolic activity, and (3) inherent differences in cell wall and metabolism among bacterial species. The implications of these and other (e.g., cell wall destabilization, Claessens et al., 2004) sources of variability in acid-base activity for the determination of the cell wall charge associated with the reversible protonation and deprotonation of functional groups are explored further in the next section.

### 3.4.2 Cell wall charge

A number of different methods have been used to determine charge development in bacterial cell walls and characterize the responsible functional groups. The most common methods involve continuous acid-base titrations of dead cells (Goncalves et al., 1987), live cells (Daughney and Fein, 1998; Daughney et al., 2001; Haas, 2004), and isolated cell walls (Plette et al., 1995; Van der Wal et al., 1997a). The treatments used to kill the cells, by radiation or chemical agents, or to isolate the cell walls may cause chemical modifications that affect the results of the titrations, as illustrated by the differences in the acid and base consumption curves of *S. putrefaciens* cells treated with gamma radiation and ethanol (see section 3.4.1). Continuous titration curves of live cells may be affected by proton

consumption or production linked to active cellular processes or cell wall destabilization (Claessens et al., 2004; this study). For example, in continuous titrations of viable cells of *Rhodococcus erythropolis*, van der Wal et al. (1997a) observed that decreasing the rate of titration increased hysteresis, clearly indicating a contribution from irreversible processes to acid and base neutralization.

The pH stat method used here represents an alternative approach to estimate cell wall charging due to protonation and deprotonation of functional groups of macromolecules present in the unaltered cell wall of live bacteria. In addition, it provides insight into the potential influence of irreversible processes during continuous titrations of cells. For instance, comparison of the time-dependent acid and base consumption by live cells of *S. putrefaciens* and *B. subtilis* indicates that the relative contribution of irreversible processes is larger in the case of *S. putrefaciens* (Figs. 3.1A, 3.1B and Table 3.2). Therefore, under otherwise identical experimental conditions, continuous titrations of *S. putrefaciens* should exhibit more pronounced hysteresis than titrations of *B. subtilis*.

The results of the pH stat experiments also imply that continuous titration curves should depend on the direction of titration, because cell viability is differently affected by exposure to low and high pH (section 3.4.1). For the two bacterial species considered in this study, cellular activity should have less impact if live cell suspensions are first titrated acidimetrically, e.g. to pH 4, and then alkalimetrically, e.g. to pH 10. By first exposing the bacteria to acidic conditions, loss of viability should minimize the effects of metabolism during the remainder of the titration, as clearly shown by Figure 3.3. The opposite would be true if the cells were first titrated to pH 10 and then to pH 4.

From the initial amounts of acid and base consumed at pH 4 and 10 (Table 3.1) it is possible to calculate the concentrations of ionizable functional groups within the experimental pH range. The estimated concentrations are  $4.0 \times 10^{-16}$  mol cell<sup>-1</sup> for *S. putrefaciens*, and  $6.5 \times 10^{-16}$  mol cell<sup>-1</sup> for *B. subtilis* (units are in mol H<sup>+</sup> equivalents). These concentrations are minimum estimates of the total concentrations of ionizable functional groups in the cell walls, because all groups are not necessarily (de)protonated in the pH range 4 to 10.

Cell wall charges of live cells of *S. putrefaciens* as a function of pH can be calculated from the initial amounts of acid and base consumed, by assuming that the point of zero charge (pzc) coincides with the measured isoelectric point of the cells (iep = 3.75, Fig. 3.6). The

results are shown in Figure 3.7 (full symbols). For comparison, the cell wall charges inferred for live cells of *B. subtilis* are also shown, assuming the same pzc (Fig. 3.7, open symbols), although recent evidence suggests that the pzc of *B. subtilis* may be lower than 3.75 (Fein et al., 2005).

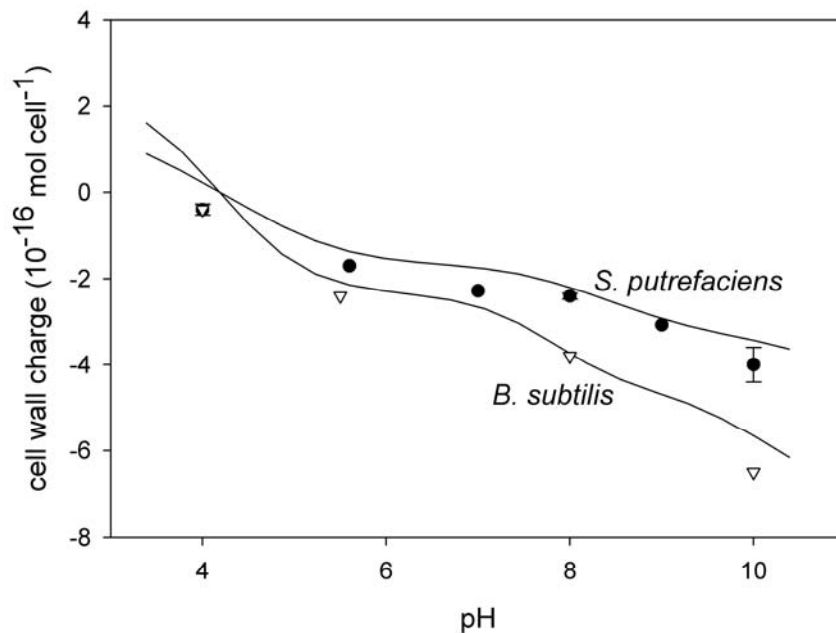


**Figure 3.7:** Cell wall charge of live cells of *S. putrefaciens* and *B. subtilis* as function of pH in 150 mM NaCl, at a cell density of  $10^8 \text{ cells ml}^{-1}$  and 22 °C. The symbols correspond to cell wall charges calculated from the initial acid or base consumptions in the pH stat experiments (Table 3.1), assuming a pzc of 3.75. The continuous curves are cell wall charges predicted using a three-site model comprised of carboxylate ( $pK = 4.3$ ), phosphate ( $pK = 7.8$ ) and amino ( $pK = 9.9$ ) groups. The three sites are assumed to be present in 2:1:1 proportions. The constant capacitance model is used to correct for electrostatic effects, assuming a capacitance of  $5 \text{ F m}^{-2}$ , and specific surface areas of  $55 \text{ m}^2 \text{ g}^{-1}$  for *S. putrefaciens* (Haas et al., 2001) and  $140 \text{ m}^2 \text{ g}^{-1}$  for *B. subtilis* (Fein et al., 1997). See text for detailed discussion.

For complex macromolecular structures such as cell walls, the assumption that the pzc and iep are equal is questionable. For example, Gélabert et al. (2004) recently showed that the pzc of diatom cells may be several pH units higher than their iep. They interpret these large differences in terms of the spatial disposition of functional groups within the three dimensional cell wall structure. Much smaller differences are reported by van der Wal et al.

(1997a) for bacterial cell walls with *pzc* values typically about 0.5 units higher than the corresponding *iep* values. A similar difference would produce a *pzc* for *S. putrefaciens* on the order of 4.25, causing a small upward shift of the cell wall charges plotted in Figure 3.7.

Often the concentrations of functional groups are reported per unit mass bacteria (Daughney and Fein, 1998; Daughney et al., 2001; Haas, 2004), although one also finds concentrations expressed per unit mass or surface area of cell wall (van der Wal et al., 1997a; Haas et al., 2001). Here, we opt to express the concentrations per cell. The cell is the basic physiological unit, and normalization to cell numbers is common when expressing microbial rates. Comparison of the functional group concentrations determined here with those in other studies, however, is hindered by the uncertainties and methodological biases associated with the determination of cell (or cell wall) masses. This is illustrated in Table 3.3 where concentrations of ionizable functional groups from a number of studies are converted into cell-normalized values, using the originally reported cell (or cell wall) masses and those obtained here.

**Table 3.3:** Cell wall functional group densities.

Bacterium	Reported value	Conversion	Concentration in $10^{-16}$ mol cell <sup>-1</sup>	
<i>R. opacus</i> <sup>a</sup> (Gram+)	0.7 mmol g <sup>-1</sup> cell wall	$2 \times 10^{-12}$ g cell <sup>-1</sup> and 0.29 g cell wall g <sup>-1</sup> cell	e a	4
<i>B. subtilis</i> <sup>b</sup> (Gram+)	0.3 mmol g <sup>-1</sup> cell	$2.5 \text{ g L}^{-1} \equiv 10^{10}$ cells ml <sup>-1</sup> $6 \times 10^{-12}$ g cell <sup>-1</sup>	b e	0.75 18
<i>S. putrefaciens</i> <sup>c</sup> (Gram-)	0.14 mmol g <sup>-1</sup> cell	$1.3 \times 10^{-13}$ g cell <sup>-1</sup> $2 \times 10^{-12}$ g cell <sup>-1</sup>	c e	0.18 2.7
<i>S. putrefaciens</i> <sup>d</sup> (Gram-)	1.77 $\mu$ mol mg <sup>-1</sup> cell	$2 \times 10^{-12}$ g cell <sup>-1</sup>	e	35

<sup>a</sup> van der Wal et al., 1997a

<sup>b</sup> Daughney and Fein, 1998

<sup>c</sup> Haas, 2004

<sup>d</sup> Sokolov et al., 2001

<sup>e</sup> this study

For example, for the Gram-positive bacterium *Rodococcus opacus*, the total concentration of ionizable groups reported by van der Wal et al. (1997a) is  $0.7 \text{ mmol g}^{-1}$  cell wall. This bacterium is of similar shape as *S. putrefaciens*, although somewhat larger. Its  $\text{iep}$  is 3.4, and it exhibits very similar dependencies of the electrophoretic mobility on pH and electrolyte concentration as *S. putrefaciens* (van der Wal et al., 1997b). If we assume that *S. putrefaciens* cells have the same cell wall density of functional groups ( $0.7 \text{ mmol g}^{-1}$  cell wall) and the same cell wall to cell mass ratio (29 %) as *R. opacus*, then, using a wet cell mass of  $2 \times 10^{-12} \text{ g cell}^{-1}$  (section 3.2.1), we obtain a concentration of functional groups of  $4.0 \times 10^{-16} \text{ mol cell}^{-1}$  (Table 3.3), which matches the estimate given above. This apparent agreement, however, hinges on the validity of the assumptions made.

In contrast, based on fitting continuous titration curves of live cells of the same strain of aerobically grown *S. putrefaciens* as used here, Haas (2004) derived a total functional group concentration of  $0.14 \text{ mmol g}^{-1}$  bacteria. Using the (wet) cell mass reported by this author,  $1.3 \times 10^{-13} \text{ g cell}^{-1}$ , yields a concentration of  $0.18 \times 10^{-16} \text{ mol cell}^{-1}$  (Table 3.3), that is, a value significantly lower than found here. The discrepancy, however, seems to be mostly related to the large difference in cell mass between the two studies. If we use the wet cell mass measured here,  $2 \times 10^{-12} \text{ g cell}^{-1}$  (section 3.2.1), the corresponding functional group density is  $2.7 \times 10^{-16} \text{ mol cell}^{-1}$  (Table 3.3), which is of the same order of magnitude as that derived from the pH stat experiments. A mass on the order of  $10^{-12} \text{ g cell}^{-1}$  is more in line with cell weights of *S. putrefaciens* determined by DiChristina (1989). However, combining a cell mass of  $2 \times 10^{-12} \text{ g cell}^{-1}$  with the functional group concentration of Sokolov et al. (2001), yields a much higher cell-normalized functional group concentration of  $35 \times 10^{-16} \text{ mol cell}^{-1}$  (Table 3.3).

Daughney and Fein (1998) performed acid-base titrations on live cells of *B. subtilis* and obtained functional group concentrations on the order of  $0.3 \text{ mmol g}^{-1}$ . Together with the wet cell mass determined here,  $6 \times 10^{-12} \text{ g cell}^{-1}$  (section 3.2.1), this equals a concentration of  $18 \times 10^{-16} \text{ mol cell}^{-1}$  (Table 3.3). According to Fein et al. (1997), however,  $2.5 \text{ g L}^{-1}$  of *B. subtilis* cells correspond to  $10^{10} \text{ cells ml}^{-1}$  and, hence, the functional group concentration should only be  $0.75 \times 10^{-16} \text{ mol cell}^{-1}$  (Table 3.3). The value derived from the pH stat experiments ( $6.5 \times 10^{-16} \text{ mol cell}^{-1}$ ) falls somewhere in between these two extremes.

For both bacterial species, the cell wall charge dependence on pH (Fig. 3.7) shows the characteristic sigmoidal shape that is also observed in continuous titrations of whole cells and isolated cell walls (e.g., van der Wal et al., 1997a; Daughney and Fein, 1998). The shape is attributed to the existence of weak acid and base groups in the cell wall, whose distinct dissociation constants ( $pK$ s) give rise to the inflection points of the cell wall charge versus pH curve. Equilibrium models that include a limited number (2-5) of discrete functional groups successfully capture this behavior (e.g., Plette et al., 1995; Fein et al., 1997; Daughney and Fein, 1998; Cox et al., 1999; Haas et al., 2001; Sokolov et al., 2001).

Carboxylate, phosphate and amino groups are commonly invoked to explain cell wall charging of both Gram-positive and Gram-negative bacteria, although in some models the positively ionizing amino groups are replaced by negatively ionizing hydroxyl groups (e.g., Fein et al., 1997; Daughney and Fein, 1998; Haas, 2004). Inclusion of amino groups allows for the development of a net positive cell wall charge at sufficiently low pH. Models that exclusively include negatively ionizing functional groups (e.g., carboxylate, phosphate and hydroxyl groups) can obviously only produce negative charge.

By combining chemical analyses and titration curves of isolated cell walls of a variety of Gram-positive bacteria, Plette et al. (1995) and van der Wal et al. (1997a) proposed that carboxylate, phosphate and amino groups are present roughly in the ratio of 2:1:1. They further report average  $pK$  values of 4.3, 7.8 and 9.9 for their deprotonation reactions (Plette et al., 1995)



Cell wall charges predicted by this three-site model are shown in Figure 3.7. The model curves in the figure were generated using the constant capacitance model to account for electrostatic effects, while the total functional group (carboxylate + phosphate + amino) concentration was treated as adjustable parameter.

The model curves reproduce the general shape of the pH dependence of the cell wall charge of both bacteria (Fig. 3.7), with a somewhat higher (cell-normalized) total functional

group concentration for *B. subtilis* ( $9.3 \times 10^{-16}$  mol cell<sup>-1</sup>) than for *S. putrefaciens* ( $6.5 \times 10^{-16}$  mol cell<sup>-1</sup>). The model predicted pzc values, however, exceed the measured iep of *S. putrefaciens* by about 0.5 pH units (Fig. 3.6), in line with the findings of van der Wal et al. (1997a) for isolated cell walls of five different Gram-positive bacteria. Better agreement between model and data would be possible by adjusting the various model parameters but, without additional constraints, particularly on the pzc and cell wall functional group composition of the bacteria, this represents merely a curve fitting exercise.

The development of cell wall charge is very similar for *S. putrefaciens* and *B. subtilis* (Fig. 3.7), despite large differences in macromolecular structures of the cell walls. In particular, the more complex cell wall of Gram-negative bacteria is characterized by an outermost layer made up principally of lipopolysaccharides (LPS) (Madigan et al., 1997). A possible explanation is that the LPS layer does not contribute significantly to the charging of the Gram-negative cell wall. This is consistent with the observed low buffering capacity of LPS isolated from *E. coli* (Figs. 3.4A-C), although it must be kept in mind that the chemical compositions of LPS of *S. putrefaciens* and *E. coli* are different (Jansson, 1999).

### 3.5 Conclusions

Time-dependent acid and base consumption curves by live bacterial cells are interpreted to consist of the following three contributions. (1) The near-instantaneous (time scale of minutes) buffering capacity associated with the functional groups present in the cell wall, (2) the short-term (< 1 hour) utilization of the intracellular buffering capacity, and (3), under basic conditions, the long-term (1-5 hours) release of (acidic) metabolic byproducts. By measuring the initial acid or base consumption at different pH values, the passive buffering capacity of the cell wall can thus be determined as a function of the pH of the medium.

The functional group concentrations and the pH dependent cell wall charges inferred from the pH stat experiments for *S. putrefaciens* and *B. subtilis* are in general agreement with those obtained with continuous titrations. Large uncertainties in cell weight (and cell surface areas), however, are currently a major obstacle when comparing results from different research groups. A concerted effort to design standardized procedures to determine these basic cell characteristics would go a long way in generating consistent data sets.

Lipopolysaccharides (LPS), the major constituent of the outermost layer of the cell wall of Gram-negative bacteria, appear to contribute little to the buffering capacity of the intact cell wall. Thus, while LPS may be important in regulating cell adhesion of Gram-negative bacteria, it may not offer many anionic binding sites for metal cations, which must therefore migrate deeper inside the cell wall. The relatively minor buffering capacity associated with LPS may also explain the very similar cell wall charging behavior of Gram-positive and Gram-negative bacteria.

### **Acknowledgments**

The Associate Editor, Johnson R. Haas, and three anonymous reviewers are thanked for their constructive comments and suggestions. This research was financially supported by the Netherlands Organization for Scientific Research (NWO-Pionier Award).

---

## **Chapter 4**

# **Response of *Shewanella putrefaciens* to pH stress and possible geochemical implications**

Jacqueline Claessens, Anniet M. Laverman, Yvonne van Lith and Philippe Van Cappellen  
submitted to Geomicrobiology Journal

---

## Abstract

The acid or base consumption, and the release of metabolic products by live cells of *Shewanella putrefaciens* were monitored in a pH stat system under oxic or anoxic conditions and at variable pH and temperature. Acid conditions (pH 4) resulted in a loss of viability of the cells. At pH 7, 8 and 10, however, after an initial rapid base consumption (minutes) associated with the buffering capacity of the cell walls, slower continuous base consumption was observed (hours). The continuous base consumption is due to the release of acids, produced by cellular metabolism. Dissolved organic acids and dissolution of metabolically produced CO<sub>2</sub> were the main sources of the continued base consumption. The environmental conditions (redox, pH and temperature) determined the type and rates of acid release. Under oxic conditions, a build-up of succinate, an intermediate product of the tricarboxylic acid cycle during aerobic respiration, was observed. Under anoxic conditions, fermentation reactions resulted in the release of acetate (pH 7 and 8) and succinate (pH 10). However, because carbon dioxide production due to fermentation reactions was small compared to aerobic respiration, the overall proton production under anoxic conditions was smaller than under oxic conditions. The release of protons, organic acids and CO<sub>2</sub> systematically increased with pH and temperature. The pH dependent acid release by *S. putrefaciens*, a model iron and manganese reducing organism, should compensate the alkalinity production during the reductive dissolution of iron and manganese oxides and, hence, help maintain favorable pH conditions in the immediate vicinity of the cell. The production of protons and organic ligands also affects metal binding to the cell wall, and mineral weathering reactions.

## 4.1 Introduction

The reduction potential, pH and temperature are key environmental variables. In lakes, marine basins and subsurface environments the redox conditions may change from fully oxidized to completely reduced with depth (Schlesinger, 1997). This variability in reduction potential modulates microbial activity through the availability of electron acceptors and nutrient cycling. In addition to the reduction potential, microbial metabolic processes depend on pH and temperature, which may vary daily and seasonally. Enzymatic reactions function most rapidly at their optimum temperature and pH.

The pH of subsurface environments is well buffered by mineral precipitation-dissolution reactions (Schlesinger, 1997). Under acidic conditions, precipitation-dissolution reactions of silicate-aluminum minerals control the pH of the pore water solution, whereas under alkaline conditions the pH is buffered by precipitation-dissolution reactions of carbonates. Furthermore, microbial activity contributes to the alkalinity and proton balances of natural waters. In particular, the release of CO<sub>2</sub> due to microbial respiration may alter the proton activity of the solution. Also concentrations of organic and inorganic carbon are affected by microbial metabolic reactions. The concentrations of metabolic products can build up to concentrations in the extracellular environment that may affect the solubility reactions of minerals (Hiebert and Bennett, 1992; Bennett et al., 2001).

In a previous study, the effect of microorganisms on the acid-base chemistry of their surrounding solution was investigated (Claessens et al. 2006a). The acid and base consumptions by live cells of *Shewanella putrefaciens* and *Bacillus subtilis* were measured in a pH stat system. The results showed a near-instantaneous (time scale of minutes) buffering capacity associated with the functional groups present in the cell wall. This initial buffering, however, was followed by a short-term (< 1 h) utilization of the intracellular buffering capacity, and, under basic conditions, a long-term (> 1 h) release of acidic metabolic products.

The aim of the present study was to quantify the rates of proton uptake or release, as well as the rates of production of organic acids and inorganic carbon by the heterotrophic microorganism *Shewanella putrefaciens*. In particular, the dependence of these rates on redox conditions, pH and temperature were determined. *S. putrefaciens* was chosen because it is one of the most extensively studied organisms capable of dissimilatory iron and manganese

reduction (DiChristina, 1989). The reduction of Fe (III) and Mn (III, IV) oxides, however, consumes protons and, hence, tends to increase the pH and decrease the redox potential. It is thus important to determine how the microorganisms responsible for the reduction of Fe (III) and Mn (III, IV) respond to changes in pH and redox conditions.

## 4.2 Materials and Methods

### 4.2.1 Bacteria

To determine the effect of pH, temperature and redox conditions on the release and/or uptake of protons and organic acids, we used the Gram-negative bacterium *S. putrefaciens* strain 200R. *S. putrefaciens* was originally isolated from crude oil, but its presence has been detected in a variety of aquatic and subsurface environments (Venkateswaran et al., 1999). Pure cultures of the bacteria were grown at room temperature in liquid Luria Bertani (LB) medium. In the mid-logarithmic growth phase the bacteria were pelleted by centrifugation (5000 g for 15 min). The supernatant was discarded and the cell pellets were resuspended in 150 mM NaCl salt solution. The washing procedure was repeated once to obtain the bacterial stock suspensions used in the experiments. Cell densities of the bacterial stock suspensions were derived from the optical densities (OD) measured at 660 nm wavelength on the harvested cultures. The OD-values were calibrated by counting colony-forming units on solid medium and by using the acridine orange direct count (AODC) method (Lovley and Phillips, 1988). The harvested cultures contained on the order of  $10^9$  cells ml<sup>-1</sup>.

Bacteria were disrupted in a French press at 8000 psi and intact cells and cell debris were pelleted by centrifugation (5000 g for 15 minutes). The supernatant, containing cell envelopes and intracellular components, was used as control of non-living cells.

### 4.2.2 pH stat experiments

The acid-base activity of the live and disrupted cell suspensions was measured in a pH stat system (Claessens et al., 2004). The experiments were performed using an automated titrator (Metrohm 716S controlled by Metrohm Tinet 2.4) at 22 °C unless stated otherwise. The pH of a 150 mM NaCl solution (60 ml final volume) was brought to the desired value of 4, 5.5, 7, 8 or 10 by addition of 0.01 M HCl or 0.01 M NaOH solutions. Live and disrupted cell suspensions were added to final concentrations of  $10^9$  cells ml<sup>-1</sup> and an equivalent of  $10^8$

cells ml<sup>-1</sup>, respectively. The experiments at pH 7, 8 and 10 were carried out open to the atmosphere and by continuously purging with air (oxic conditions) or in a closed system by continuously purging with N<sub>2</sub> (anoxic conditions). Experiments at pH 4 and 5.5 were performed open to the atmosphere.

The consumption of HCl or NaOH required to keep the pH constant was monitored during a period of 5 hours. The added titrant volumes were recorded every minute automatically. The total consumption of acid or base was corrected for the consumption by the electrolyte solution alone to derive the net consumption of protons or hydroxyls by the cells. After 5 h, the background consumption of acid or base by the electrolyte solution alone was less than 15 % of that of the cell suspensions under oxic conditions and less than 5 % under anoxic conditions.

In the experiments with suspensions of live cells of *S. putrefaciens* at pH 7, 8 and 10, the solutions were analyzed for the presence of organic acids. At 1 h intervals, an aliquot of 2.5 ml was collected and filtered through a 0.2 µm pore size filter. An aliquot of the filtered solutions was diluted with UHQ water to a final concentration of the background electrolyte (NaCl) of 15 mM, and analyzed by Ion Exclusion Chromatography (Dionex DX 120). A column (ICE-AS6) and suppressor (AMMS-ICE II) were used for efficient separation of low molecular weight aliphatic organic acids. The eluent was a 0.4 mM heptafluorbutyric acid solution and the regenerant a 5 mM tetrabutylammoniumhydroxide solution. A standard solution of 1 mM formate, lactate, acetate, succinate and propionate was prepared and diluted to final concentrations of 5, 10, 40, 70 and 100 µM for calibration. The matrix of the standard solution was 15 mM NaCl to match that of the samples. Also, an aliquot of the suspensions of disrupted cells was analyzed for low molecular weight aliphatic organic acids.

In the experiments with live cells of *S. putrefaciens* carried out at pH 10 (oxic and anoxic conditions) dissolved inorganic carbon (DIC) was measured. An aliquot of 4 ml was collected at 1, 3 and 5 hours, and filtered through a 0.2 µm pore size filter. The DIC of the filtrate was measured with a Shimadzu TOC analyzer 5050.

### 4.2.3 Analysis of base consumption curves

#### Rates of intracellular and metabolic proton release

The rates of intracellular and metabolic proton release were calculated from the amount of base consumed between 6 min -1 h (mid-term base consumption) and 1-2.5 h (long-term base consumption), respectively (Fig. 4.1; Claessens et al., 2006a). The temperature dependencies of metabolic proton excretion were expressed as apparent activation energies,  $E_a$ , and  $Q_{10}$  values (Winkler et al., 1996).

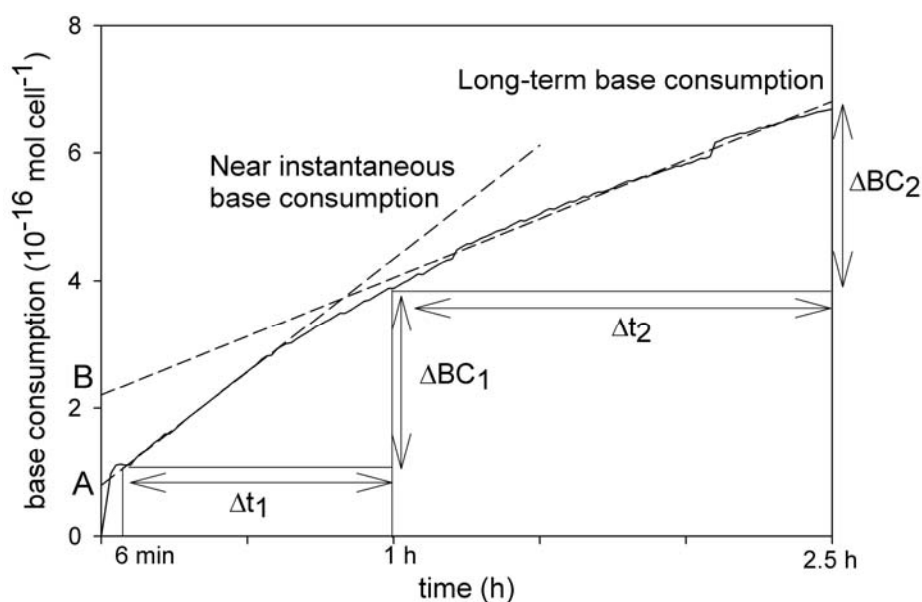


**Figure 4.1:** Example of the determination of the rates of metabolic and intracellular proton release, as well as the buffering capacities associated with the cell walls and intracellular contents of live cells of *S. putrefaciens* at pH 8. The buffering capacity of the cell walls (A) was determined by extrapolation of the near-instantaneous base consumption (6-18 min) to time 0. The buffering capacity of the intracellular content (B-A) was determined from extrapolation of the long-term base consumption (1-2.5 h) to time 0 and by subtracting the buffering capacity of the cell walls. The rates of intracellular and metabolic proton release were calculated from the amounts of base consumed between 6 min -1 h ( $\Delta BC_1$ ,  $\Delta t_1$ ) (mid-term base consumption) and 1-2.5 h (long-term base consumption), respectively.

### **Buffering capacity of cell walls and intracellular content**

The initial base consumption by live cell suspensions was determined by extrapolation of the near-instantaneous base consumption (6-18 min) to time 0 (Fig. 4.1). The buffering capacity of cell walls of live cells was calculated from this initial base consumption (Claessens et al., 2006a). The buffering capacity of the intracellular content was determined from extrapolation of the long-term base consumption (1-2.5 h) to time 0 and by subtracting the buffering capacity of the cell walls (Fig. 4.1). The buffering capacity of cell walls plus that of the intracellular content was compared to the buffering capacity of suspensions of disrupted cells.

### **Rates of organic acid and CO<sub>2</sub> release**

The rates of organic acid release were determined between 1 and 4 hours. The temperature dependencies of organic acid production were expressed as apparent activation energies,  $E_a$ , and  $Q_{10}$  values (Winkler et al., 1996). The rate of metabolic CO<sub>2</sub> release at pH 10 was calculated from the concentrations of DIC measured at 1, 3 and 5 h after correction for dissolved atmospheric CO<sub>2</sub>. The amount of DIC due to dissolution of atmospheric CO<sub>2</sub> was calculated from the base consumption (proton release) by the electrolyte solution alone and contributed 10 % to the total DIC.

## **4.3 Results**

### **4.3.1 Proton release by live cells**

#### **The effect of pH on proton release**

In oxic pH stat experiments with live cells of *S. putrefaciens*, no acid was needed initially to keep the pH of the bacterial suspension constant at 5.5 (Fig. 4.2A). Little acid consumption by the live cell suspensions was observed over 2.5 h at pH 5.5 ( $0.13 \times 10^{-16}$  mol cell<sup>-1</sup> h<sup>-1</sup>). In contrast, at pH 4, rapid acid consumption occurred during the first few minutes after adding the cells, followed by more gradual acid consumption, which ended after 50 min. Similarly, under neutral and alkaline conditions (pH 7, 8 and 10), base was consumed rapidly during the first few minutes of the experiments, followed by more gradual base consumption, up to 2.5 (pH 7) and 5 h (pH 8 and 10). However, after exposing the cells for 6 hours to pH 10, base consumption ceased and was  $35 \times 10^{-16}$  mol cell<sup>-1</sup>.

Under anoxic conditions (Fig. 4.2B), the base consumption curves measured at pH 7, 8 and 10 had a similar shape as to those measured under oxalic conditions. The fast initial base consumption was followed by a long-term base neutralization that increased with pH. At pH 8 and 10, base consumption continued during the 5 h but the net base neutralization was smaller than that under oxalic conditions. At pH 7, base consumption also continued for 5 h, at least twice as long as under oxalic conditions.

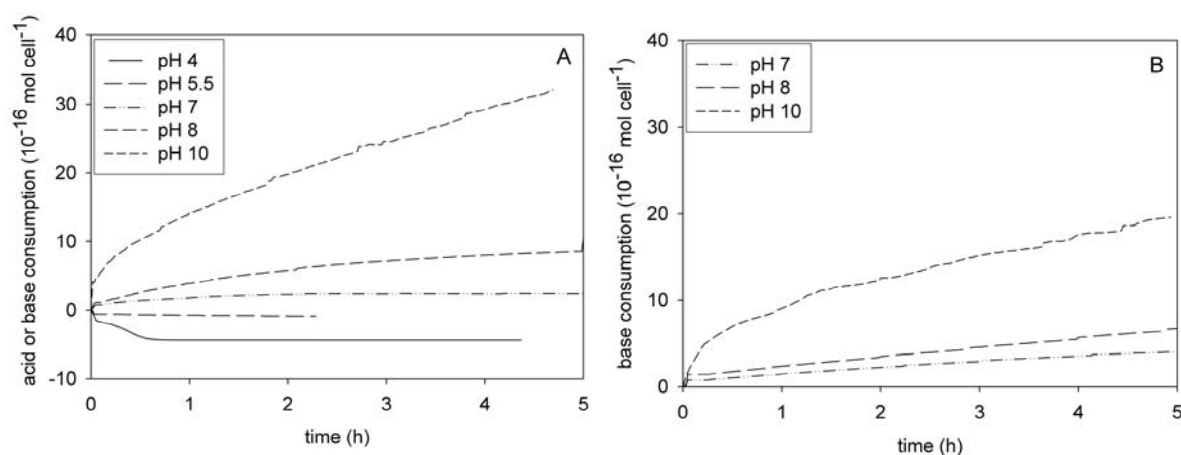


**Figure 4.2:** Acid and base consumption of live cells of *S. putrefaciens* as function of time at pH 4, 5.5, 7 and 8, in 150 mM NaCl, at a cell density of  $10^9$  cells  $\text{ml}^{-1}$  and 22 °C under oxalic (A) and anoxic (B) conditions.

The buffering capacity of cell walls and intracellular content systematically increased with pH and was similar under oxalic and anoxic conditions (Fig. 4.3). The buffering capacity of cell walls and intracellular content did not exceed that of disrupted cells (Fig. 4.3). The rates of intracellular proton release were higher than those of metabolic proton release (Fig. 4.4; Table 4.1). Both rates systematically increased with pH and were higher under oxalic than anoxic conditions.

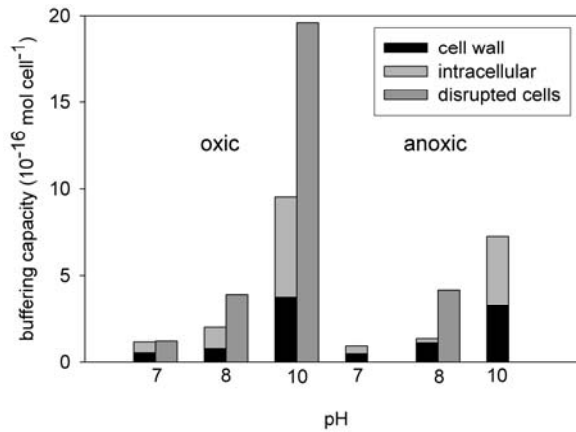


**Figure 4.3:** Buffering capacities of cell walls, intracellular contents and disrupted cells as function of pH at 22 °C in 150 mM NaCl and  $10^8$  cells  $\text{ml}^{-1}$  (disrupted cells) or  $10^9$  cells  $\text{ml}^{-1}$  (cells walls and intracellular content) under oxic and anoxic conditions.

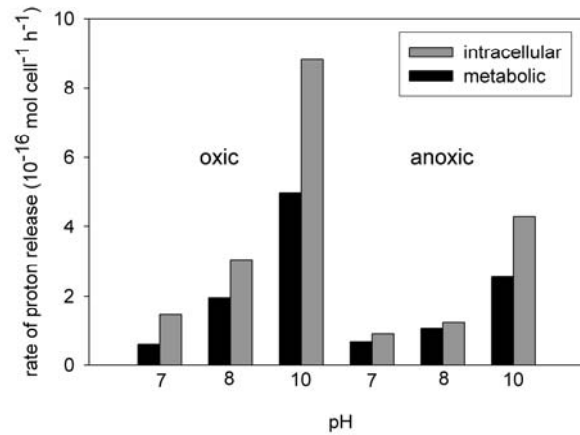


**Figure 4.4:** Rates of proton release due to intracellular and metabolic buffering as function of pH at 22 °C in 150 mM NaCl and  $10^9$  cells  $\text{ml}^{-1}$  under oxic and anoxic conditions.

**Table 4.1:** Measured rates of proton, organic acid and  $\text{CO}_2$  release expressed in  $10^{-16}$  mol cell<sup>-1</sup> h<sup>-1</sup> and the ratios of proton or  $\text{CO}_2$  to organic acid release.

redox	pH	T (°C)	protons	organic acids	$\text{CO}_2$	protons: organic acids	$\text{CO}_2$ : organic acids
oxic	7	22	0.6	0.04	-	15.0	-
	8	12	0.9	0.1	-	8.2	-
	8	22	2.0	0.2	-	10.9	-
	8	32	2.2	0.4	-	5.1	-
	10	22	5.0	0.9	1.3	5.7	1.5
anoxic	7	22	0.7	0.3	-	2.5	-
	8	12	0.4	0.2	-	2.0	-
	8	22	1.1	0.4	-	2.4	-
	8	32	1.5	0.6	-	2.8	-
	10	22	2.6	0.05/0.5 <sup>a</sup>	0.7	5.2	1.4

<sup>a</sup>  $0.05 \times 10^{-16}$  mol cell<sup>-1</sup> h<sup>-1</sup> corresponds to acetate release and  $0.5 \times 10^{-16}$  mol cell<sup>-1</sup> h<sup>-1</sup> corresponds to succinate release.

### The effect of temperature on proton release

At pH 8, the fast initial base consumption was similar at 12, 22 and 32 °C (Figs. 4.5A and B). In contrast, the long-term base consumption systematically increased with temperature both under oxic and anoxic conditions. However, net base consumption was smaller under anoxic conditions compared to oxic conditions. Under oxic conditions, the rate of base consumption clearly decreased during the experiment at all temperatures (Fig. 4.5A). In contrast, the decrease in rate of base consumption under anoxic conditions was small compared to those under oxic conditions (Fig. 4.5B).

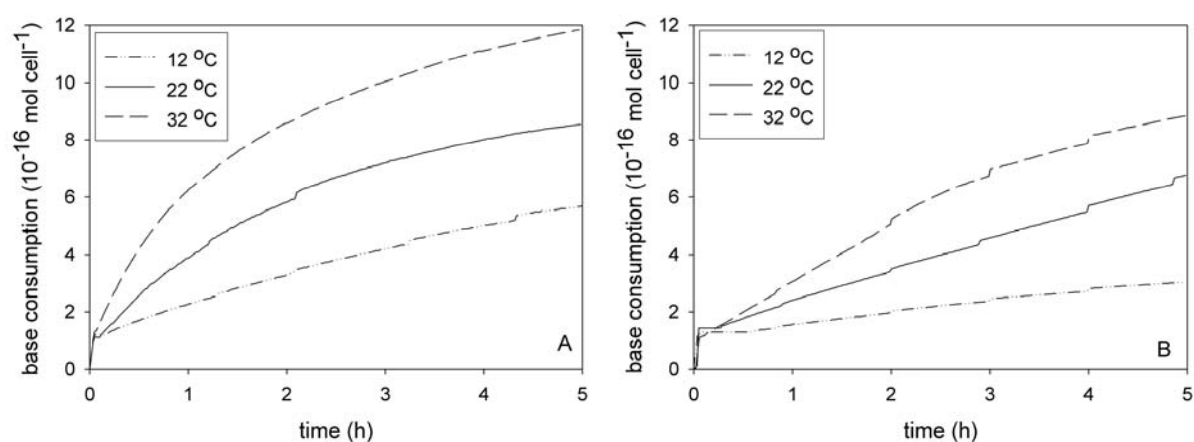


**Figure 4.5:** Base consumption by cells of *S. putrefaciens* as function of time at pH 8 and 12, 22 and 32 °C in 150 mM NaCl and  $10^9$  cells  $\text{ml}^{-1}$  under oxic (A) and anoxic (B) conditions.

At pH 8, the buffering capacity of the cell walls and disrupted cells was similar at all temperatures (Fig. 4.6). In contrast, the buffering capacity of intracellular contents increased with temperature. The buffering capacity of the cell walls and intracellular content combined never exceeded that of disrupted cells (Fig. 4.6).

The rates of intracellular and metabolic release of protons by live cells systematically increased with temperature (Fig. 4.7; Table 4.1). The rate of intracellular proton release was higher than that of metabolic proton release and the rates were systematically lower under anoxic conditions compared to oxic conditions. Apparent activation energies and  $Q_{10}$  values for metabolic excretion of protons were calculated to be  $33 \text{ kJ mol}^{-1}$  and  $49 \text{ kJ mol}^{-1}$  and 1.6 and 2.0 for respectively oxic and anoxic conditions (Table 4.2).

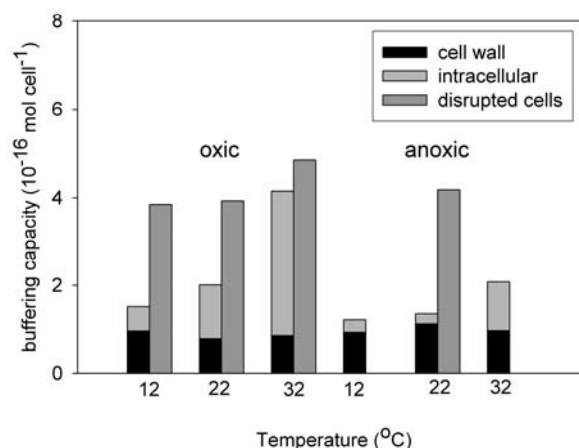


**Figure 4.6:** Buffering capacities of cell walls, intracellular contents and disrupted cells as function of temperature at pH 8 in 150 mM NaCl and  $10^8$  cells  $\text{ml}^{-1}$  (disrupted cells) or  $10^9$  cells  $\text{ml}^{-1}$  (cell walls and intracellular contents) under oxic and anoxic conditions.

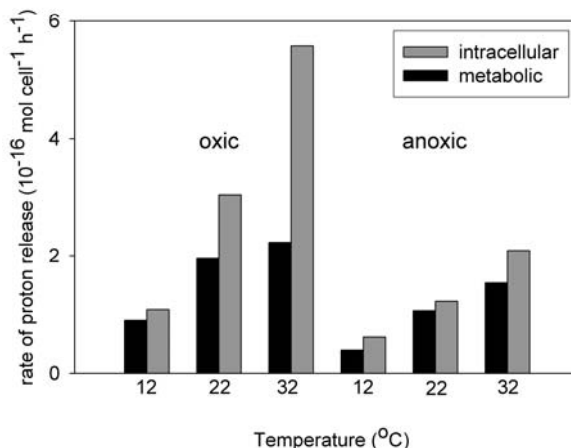


**Figure 4.7:** Rates of proton release due to intracellular and metabolic buffering as function of temperature at pH 8 in 150mM NaCl and  $10^9$  cells  $\text{ml}^{-1}$  under oxic and anoxic conditions.

**Table 4.2:** Activation energies and  $Q_{10}$  values determined at pH 8.

		$E_a$ (kJ $\text{mol}^{-1}$ )	$Q_{10}$
oxic	protons	33	1.6
	succinate	37	1.7
anoxic	protons	49	2.0
	acetate	50	2.0

### 4.3.2 Release of organic acids by live cells

#### The effect of pH on organic acid release

At pH 7, 8 and 10, a build-up of succinate and acetate was measured (Figs. 4.8A and B). Under oxic conditions, the concentrations of succinate systematically increased with pH (Fig. 4.8A). Under anoxic conditions, however, the concentrations of acetate were significantly lower at pH 10 compared to pH 7 and 8 (Fig. 4.8B). The solution of the experiment carried out at pH 10 under anoxic conditions showed the additional build-up of succinate with time (Fig. 4.8A), whereas a constant concentration of succinate ( $\sim 100$  mM or  $\sim 0.9 \times 10^{-16}$  mol cell<sup>-1</sup>) was detected in time in the experiments carried out at pH 7 and 8 under anoxic conditions. Lactate, formate and propionate were not detected in the pH stat

experiments with live cells. The suspension of disrupted cells contained succinate (~200 mM), acetate (~200 mM), lactate (~25 mM), and formate (~100 mM).

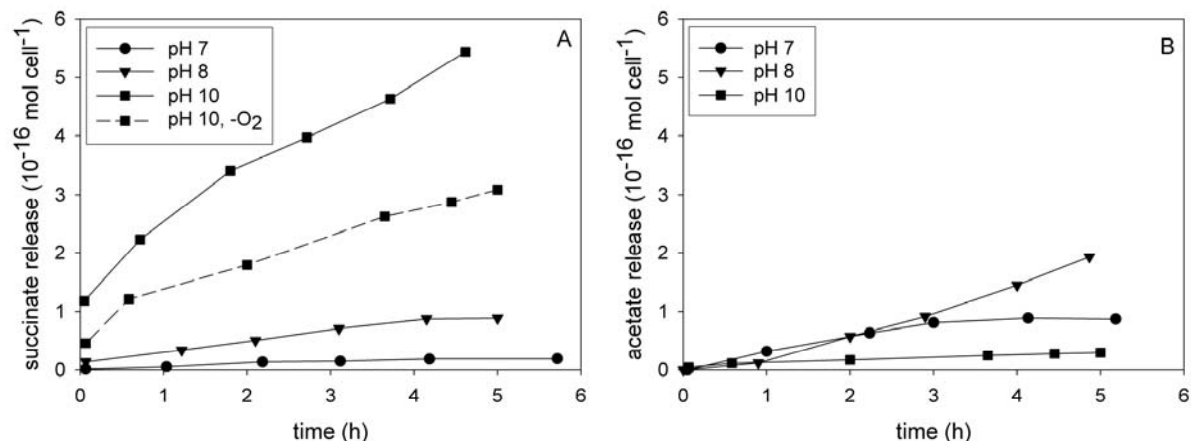


**Figure 4.8:** Release of succinate and acetate by cells of *S. putrefaciens* as function of time at pH 7, 8 and 10 and at 22 °C in 150 mM NaCl and  $10^9$  cells ml $^{-1}$  under oxic (A) and anoxic (B) conditions. The dashed line in plot A shows succinate release at pH 10 under anoxic conditions.

The rates of organic acid release systematically increased with pH (Fig. 4.9; Table 4.1). At pH 7 and 8, the rate of acetate production under anoxic conditions was higher than that of succinate production under oxic conditions (Table 4.1). The rates of organic acid were significantly lower than the rates of proton excretion in the same experiment.

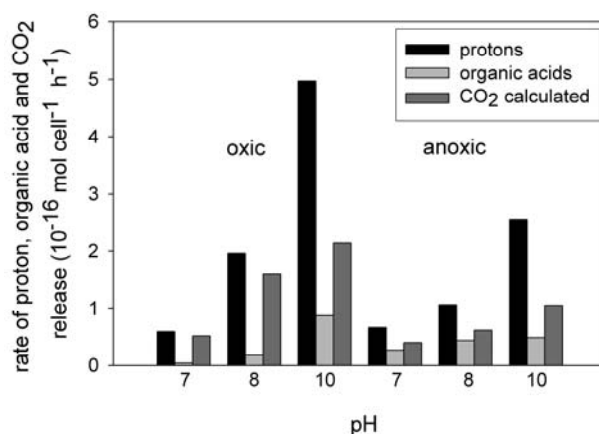


**Figure 4.9:** Rates of proton, organic acid and CO<sub>2</sub> release due to metabolic buffering as function of pH at 22 °C in 150 mM NaCl and  $10^9$  cells ml $^{-1}$  under oxic and anoxic conditions. The rates of CO<sub>2</sub> release are calculated from the amount of released protons that are not associated with organic acid release (see section 4.4.1).

### The effect of temperature on organic acid release

At pH 8, the release of succinate and acetate by the live cell suspensions systematically increased with temperature (Figs. 4.10 and 4.11). Production of succinate was observed from the beginning of the experiment, whereas acetate production started after 1 hour. Activation energies and  $Q_{10}$  values of  $37 \text{ kJ mol}^{-1}$  and  $50 \text{ kJ mol}^{-1}$  and 1.7 and 2.0 were calculated for respectively succinate and acetate release under oxic and anoxic conditions (Table 4.2). The rates of both succinate and acetate production were significantly lower than the rates of proton excretion in the same experiment.

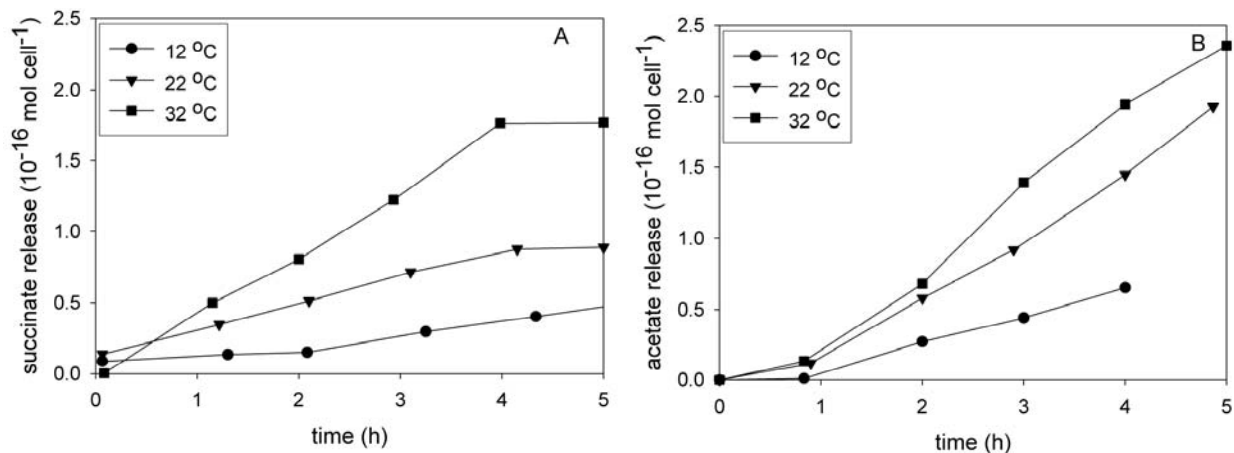


**Figure 4.10:** Release of succinate by cells of *S. putrefaciens* as function of time at pH 8 and 12, 22 and 32 °C in 150 mM NaCl and  $10^9 \text{ cells ml}^{-1}$  under oxic (A) and anoxic (B) conditions.

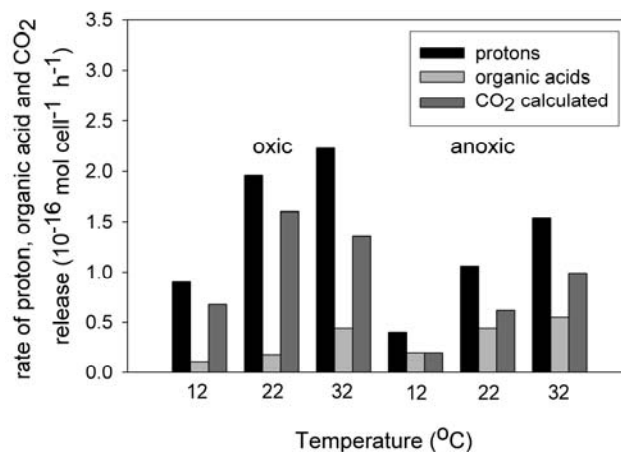


**Figure 4.11:** Rates of proton, organic acid and CO<sub>2</sub> release due to metabolic buffering as function of temperature at pH 8 in 150 mM NaCl and  $10^9 \text{ cells ml}^{-1}$  under oxic and anoxic conditions. The rates of CO<sub>2</sub> release are calculated from the amount of released protons that are not associated with organic acid release (see section 4.4.1).

### 4.3.3 CO<sub>2</sub> release

At pH 10, CO<sub>2</sub> was released rapidly during the first hour of the experiment followed by a more gradual release of CO<sub>2</sub> (Fig. 4.12). The CO<sub>2</sub> production under oxic conditions was higher than under anoxic conditions. The measured rate of CO<sub>2</sub> release was higher than the rate of succinate and acetate production but smaller than the rate of proton excretion in the same experiment (Table 4.1).

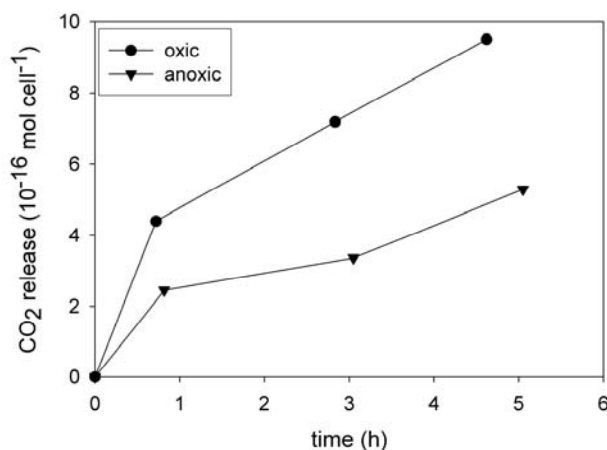


**Figure 4.12:** Release of CO<sub>2</sub> by cells of *S. putrefaciens* as function of time at pH 10 and 22 °C in 150 mM NaCl and 10<sup>9</sup> cells ml<sup>-1</sup> under oxic and anoxic conditions. CO<sub>2</sub> release is calculated from DIC analyzed in the solutions.

## 4.4 Discussion

### 4.4.1 Acid-base activity of live cells

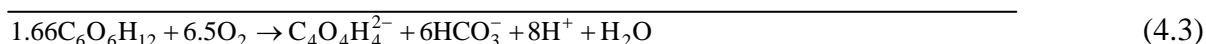
The calculated activation energies and Q<sub>10</sub> values (Table 4.2) suggest that the long-term base consumption is an enzymatic-controlled process. The build-up of succinate under oxic conditions and acetate under anoxic conditions, at pH 7 and 8, indicates that different metabolic processes are responsible for acid release. Under oxic conditions, *Escherichia coli*, a facultative anaerobe bacterium, releases succinate as the major product in the tricarboxylic acid (TCA) cycle (Lin et al., 2005). *E. coli* can also grow under anoxic conditions by using sugars, for example glucose, as sole carbon and energy source in fermentation reactions, releasing different organic acids, such as succinate, acetate, formate and lactate (Clark, 1989; Sanchez et al., 2005).

It is likely that the facultative anaerobe bacterium, *S. putrefaciens*, releases succinate as an intermediate product of the TCA cycle and acetate as the end product of fermentation reactions as is reported for *E. coli* (Lin et al., 2005; Sanchez et al., 2005). *S. putrefaciens* may use cell material or internal reserves, such as glycogen, to neutralize the pH of the surrounding solution by releasing acids. Our experiments show that the rate of organic acid release by live cells of *S. putrefaciens* depends on the pH, temperature and redox state of the solution (Figs. 4.8 and 4.10; Table 4.1).

In addition to organic acids, protons are excreted as a result of metabolic reactions. The proton release determined from the base consumption curves (Figs. 4.2 and 4.5) represent the total acidity excreted by the cells. Different processes contribute to the released acidity. Succinate, the intermediate product of aerobic respiration, has two (acidic) carboxyl groups, which are protonated during metabolic release. These two carboxyl groups will deprotonate in solutions with pH above 5.6 because the pK values are respectively 4.2 and 5.6. Thus, in the experiments carried out at pH 7, 8 and 10, the metabolic production of 1 mol succinate results in the release of 2 mol protons (Fig. 4.13).

In addition to deprotonation of produced organic acids, another source of acidity is the dissolution of CO<sub>2</sub>, the end product of respiration. CO<sub>2</sub> dissolution results in an increase of carbonic acid in solution. Since the pK values of the acid-base equilibria of carbonic acid are 6.3 and 10.2, dissolution of 1 mol CO<sub>2</sub> at pH 7 and 8 results in an increase of 1 mol bicarbonate in solution and the release of 1 mol protons (Fig. 4.13). At pH 10, however, dissolution of CO<sub>2</sub> results in an increase of equal amounts of bicarbonate and carbonate ions and consequently dissolution of 1 mol CO<sub>2</sub> results in the release of 1.5 mol protons.

At pH 8, the mean stoichiometry of proton and succinate release by cells of *S. putrefaciens* at 12, 22 and 32 °C is 8:1 (Table 4.1). Assuming that dissolution of CO<sub>2</sub> is responsible for the proton excretion not accounted for by succinate deprotonation, the following reactions describe aerobic respiration by *S. putrefaciens* at pH 8 (Fig. 4.13), assuming glucose (C<sub>6</sub>O<sub>6</sub>H<sub>12</sub>) is the substrate for metabolism,



In Figures 4.9 and 4.11 the rates of proton release and organic acid production are compared. The CO<sub>2</sub> release shown in Figures 4.9 and 4.11 is calculated from the released protons that are not accounted for by succinate deprotonation.

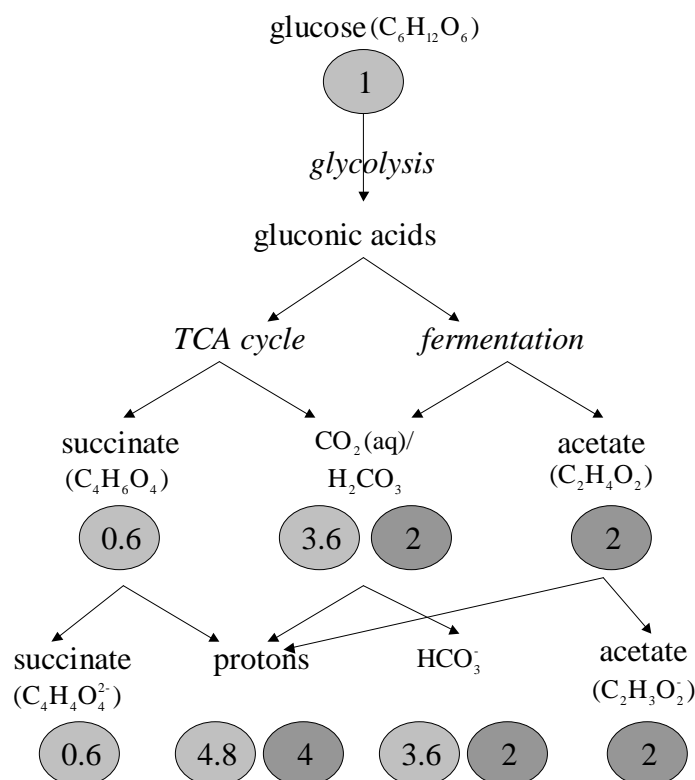
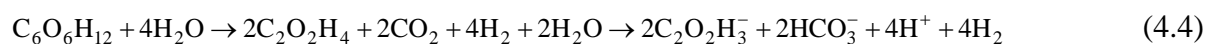


**Figure 4.13:** Schematic representation of the conversion of 1 mol glucose in its metabolic products due to respiration (light gray boxes) and fermentation (dark gray boxes) at pH 8 by *S. putrefaciens*. It was assumed that succinate is released due to aerobic respiration and acetate as a result of fermentation.

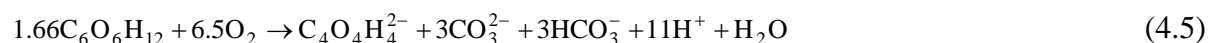
Under anoxic conditions, acetate is produced which has only one carboxyl group with a  $pK$  value of 4.75. Therefore, at pH 8, the metabolic production of 1 mol acetate results in the release of 1 mol protons (Fig. 4.13). However, similarly as for aerobic respiration, production of CO<sub>2</sub> is also a source of acidity during fermentation. At pH 8 under anoxic conditions, the stoichiometry of proton and acetate release is approximately 2:1 at various temperatures (Table 4.1). Then, similarly as done for aerobic respiration, the following reaction describes fermentation by cells of *S. putrefaciens* (Fig. 4.13)



For the calculations, it was assumed that all produced CO<sub>2</sub> remains in the electrolyte solutions and that all acidity due to the dissolved CO<sub>2</sub> is measured. However, CO<sub>2</sub> dissolves in water only up to concentrations of the order of 10<sup>-4</sup>, 10<sup>-3</sup> and 10<sup>-1</sup> M at pH 7, 8 and 10, respectively (Stumm and Morgan, 1996). At the beginning of the experiments, before adjusting the pH, the DIC concentration of the salt solution was 2x10<sup>-6</sup> M, being undersaturated with respect to dissolved CO<sub>2</sub>. However, at pH 7 and 8 under oxic conditions, the rate of proton release significantly decreased during the 5 h of the experiment (Figs. 4.2A and 4.5A). Because of the relatively high CO<sub>2</sub> production, these solutions become saturated with respect to dissolved CO<sub>2</sub> and the dissolution of CO<sub>2</sub> decreased. Therefore, in these experiments, the rate of metabolic proton release, determined from the base consumption curves between 1 and 2.5 h, was slightly underestimated. In contrast, at pH 10, the decrease in the rate of proton excretion was much smaller over the duration of the experiment (Fig. 4.2A). At pH 10, CO<sub>2</sub> may dissolve in water up to concentrations of 10<sup>-1</sup> M, a concentration higher than the CO<sub>2</sub> released during the experiment. This is supported by the measured rate of CO<sub>2</sub> release, which did not decrease over time (Fig. 4.12).

As pH 7-8 is the optimum pH for *S. putrefaciens* (Venkateswaran et al., 1999), live cells experience more stress at pH 10 than at pH 7 and 8. Therefore, the increased rates of proton and succinate release at pH 10 compared to pH 7 and 8 (Figs. 4.2 and 4.8; Table 4.1) may be considered a response of the cells to stress. Apparently, cells of *S. putrefaciens* are able to neutralize the unfavorable pH conditions by their respiratory activity. Even so, growth rates would be expected to decrease under pH 10 conditions.

At pH 10, the stoichiometry of proton and succinate release in the overall reaction that describes aerobic respiration (reaction 4.3) changes because half of the bicarbonate deprotonates to carbonate. Then, at pH 10, aerobic respiration can be described by



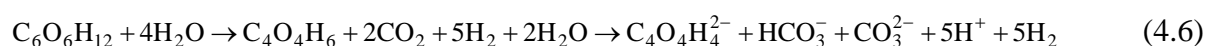
The measured rates of proton and CO<sub>2</sub> release normalized by moles of produced succinate (5.7 and 1.5 (Table 4.1)) are within the same order of magnitude as expected from reaction 4.5, namely 11 and 6. Furthermore, the measured rate of CO<sub>2</sub> production of 1.3 mol cell<sup>-1</sup> h<sup>-1</sup>

(Table 4.1) was comparable with the rate of CO<sub>2</sub> release, calculated from the difference between the release of total acidity and succinate (2.1 mol cell<sup>-1</sup> h<sup>-1</sup>) (Fig. 4.9).

At pH 10 under oxic conditions, the maximum base consumption or proton release by live cells of *S. putrefaciens* was 36x10<sup>-16</sup> mol cell<sup>-1</sup>, which is considerably higher than the buffering capacity of disrupted cells at the same pH (19.6x10<sup>-16</sup> mol cell<sup>-1</sup>; Fig. 4.3). This indicates that the release of acidity is a result of microbial activity and not a passive effect of the cell walls or cell content. Base consumption by the live cells exceeded that of disrupted cells at pH 8 and 10 in no longer than 1.5 h (Claessens et al., 2006a). Using the stoichiometry of reaction 4.5 (protons:glucose = 6.8:1), this maximum proton release corresponds to a glucose storage of 5.3x10<sup>-16</sup> mol cell<sup>-1</sup> or 9.2x10<sup>-14</sup> g cell<sup>-1</sup>. Assuming a dry weight for cells of *S. putrefaciens* of 7x10<sup>-13</sup> g cell<sup>-1</sup> (Claessens et al., 2006a), this corresponds to glucose storage of 13 % of the dry weight of a cell. Bacteria grown under suitable conditions can easily reach internal carbon storages on the order of 90 % (Schlegel, 1986).

Under anoxic conditions at pH 10, the rate of acetate production was small compared to that at pH 7 and 8 (Fig. 4.8B; Table 4.1), probably due to a decrease in fermentation activity under those stress conditions. Interestingly, at this high pH, succinate was produced in addition to acetate (Figs. 4.8A and B) and proton release was significantly higher than that at pH 7 and 8 (Fig. 4.2B; Table 4.1). Possibly, at pH 10, cells use a different fermentation pathway in order to be able to neutralize the alkaline stress condition more efficiently by releasing succinate instead of acetate. Both fermentation reactions involving the production of acetate and succinate has been described for *E. coli* (Sanchez et al., 2005). However, under these conditions (pH 10) a different electron acceptor might become available. In the presence of another electron acceptor respiration occurs resulting in the release of succinate.

At pH 10 under anoxic conditions, the stoichiometry of proton, CO<sub>2</sub> and succinate release by cells of *S. putrefaciens* is 5.2 to 1.4 to 1 (Table 4.1) and dissolved CO<sub>2</sub> is present in equal amounts of bicarbonate and carbonate. At this pH, fermentation can be described by the following reaction



Thus, at this high pH, fermentation results in the production of succinate and a high release of protons.

In contrast to the high base-neutralization at pH 7, 8 and 10, little acid-neutralization was observed at pH 5.5 (Fig. 4.2A). At pH 5.5, the release of CO<sub>2</sub> and succinate, the products of aerobic respiration, rather result in proton release instead of proton uptake. A possible explanation for the acid neutralization is uptake of protons or release of small basic compounds into the extracellular solution due to the pH gradient across the cell wall. The slower acid-neutralization at pH 5.5 compared to the base neutralization at pH 7, 8 and 10 (Fig. 4.2A) suggests that (1) at pH 5.5, cells cannot use their metabolism to neutralize the pH as efficiently as at pH 7, 8 and 10, or (2) pH 5.5 conditions are not stressful and therefore cells are not stimulated to neutralize the external pH. This is also observed for different facultative anaerobic and strictly aerobic bacteria that neutralize basic solutions much faster than acidic ones (Rius et al., 1998).

#### 4.4.2 Possible implications for biogeochemical processes

*S. putrefaciens* was selected for the experiments because this strain is often used as a model organism in studies to determine metal reduction rates (e.g. Liu et al., 2001). Our results can thus be interpreted in relation to reported metal reduction rates. *S. putrefaciens* has been detected in a variety of aquatic and subsurface environments (Venkateswaran et al., 1999). In natural environments, *S. putrefaciens* utilizes iron and manganese (hydr)oxides as terminal electron acceptors (DiChristina, 1989). Dissimilatory reduction of these mineral phases, coupled to organic matter oxidation, has been shown to locally increase pH in aquatic sediments (Van Cappellen and Wang, 1996) and stratified water columns (Van Cappellen et al., 1998). The pH increase is related to the large proton consumption in metal reduction reactions such as



where CH<sub>2</sub>O and Fe(OH)<sub>3</sub> are simplified representations of organic matter and ferric (hydr)oxides, respectively.

The ability of *S. putrefaciens* to cope with alkaline conditions (Fig. 4.2) may be an adaptation related to its respiratory capabilities. Metal reducing organisms may release acids in solution to deal with pH increases in their immediate environment as a result of metal reduction reactions. Iron reduction rates of 0.3 mmol Fe (II) L<sup>-1</sup> h<sup>-1</sup> are reported at cell densities of 0.6x10<sup>9</sup> cells ml<sup>-1</sup> for *Shewanella alga* (Roden and Zachara, 1996) and of 1 mmol Fe (II) L<sup>-1</sup> h<sup>-1</sup> at cell densities of 50x10<sup>6</sup> cells ml<sup>-1</sup> for *S. putrefaciens* (Liu et al., 2001). This results in iron reduction rates of 5x10<sup>-16</sup> mol cell<sup>-1</sup> h<sup>-1</sup> for *S. alga*, a value similar to that of acid release determined in this study, and an iron reduction rate of 2x10<sup>-14</sup> mol cell<sup>-1</sup> h<sup>-1</sup> for *S. putrefaciens*, a significantly higher rate than that of acid release by *S. putrefaciens* determined in this study (Table 4.1).

For enrichment cultures of anaerobic bacteria iron reduction rates are reported of 0.5 mmol L<sup>-1</sup> day<sup>-1</sup> at cell densities of 10<sup>8</sup> cells ml<sup>-1</sup> (Bell et al., 1987) and 12 mmol L<sup>-1</sup> day<sup>-1</sup> at cell densities of 2.3x10<sup>7</sup> cells ml<sup>-1</sup> (Roden and Wetzel, 2001). This results in a similar range of iron reduction rates as reported for pure cultures, namely between 10<sup>-16</sup> mol cell<sup>-1</sup> h<sup>-1</sup> and 10<sup>-14</sup> mol cell<sup>-1</sup> h<sup>-1</sup>. The rates of acid release by live cells of *S. putrefaciens* determined in this study fall well within this range.

The alterations in proton and Fe (II) concentrations by iron reducing bacteria in environmental systems will affect dissolution and precipitation reactions of secondary iron (II) minerals, such as magnetite, vivianite and siderite (Bell et al., 1987). Magnetite formation occurs at high pH, whereas vivianite and siderite, may precipitate at lower pH conditions, e.g. pH 6 or 7, in the presence of sufficient phosphate and carbonate. However, microbial production of organic acids, such as succinate and acetate, may complex Fe (II) and thereby increase the solubility of these Fe (II) minerals.

Also, the solubility of silicate and carbonate minerals is affected by the release of metabolic products. The effects of released metabolic products, such as protons, organic acids and inorganic carbon, on silicate and carbonate dissolution reactions have been extensively studied (e.g., Chou et al., 1989; Welch and Ullman, 1993; Bennett et al., 2001). As an example, based on a rate of metabolic proton release of 10<sup>-16</sup> mol cell<sup>-1</sup> h<sup>-1</sup> (Table 4.1) we estimate that an active bacterial population of 10<sup>7</sup> cells g<sup>-1</sup> dry sediment can produce up to 10<sup>-9</sup> mol protons g<sup>-1</sup> dry sediment h<sup>-1</sup>. Typical dissolution rates of silicate minerals are 10<sup>-11</sup> mol m<sup>-2</sup> s<sup>-1</sup> at neutral pH (Welch and Ullman, 1993; Bennet et al., 2001). Using a specific

surface area of  $0.07 \text{ m}^2 \text{ g}^{-1}$  (Welch and Ullman, 1993) and 5 % mass percentage of silicate minerals in the sediment, this rate corresponds to  $10^{-10} \text{ mol g}^{-1} \text{ h}^{-1}$ . Similarly, calcite dissolution rates are reported of  $10^{-10} \text{ mol s}^{-1} \text{ cm}^{-2}$  (Cubillas et al., 2005). Using a specific surface area of  $195 \text{ cm}^2 \text{ g}^{-1}$  (Cubillas et al. 2005) and 5 % mass percentage of carbonates in the sediment, this rate corresponds to  $10^{-6} \text{ mol g}^{-1} \text{ h}^{-1}$ .

The rate of metabolic release of acidity by live cells of *S. putrefaciens* is thus of the same order as dissolution rates of silicate minerals but significantly lower than those of carbonate minerals. However, as most bacteria exist attached to mineral surfaces in natural environments, released metabolic products accumulate near mineral surfaces (Hiebert and Bennet, 1992). Therefore, bacteria may contribute to silicate and carbonate dissolution in a quantitatively significant manner, especially at or near mineral surfaces.

This study is a first attempt to relate microbial reaction rates of released acidity to those of metal reduction or mineral dissolution processes. The determined rates are rough estimates for the release of products from metabolic reactions by live cells in natural solutions. In addition to the release of acids, microorganisms have an impact on the geochemistry of natural environments by the surface properties of their cell walls. In a previous study, we have quantified the functional group concentration of cell walls of live cells (Claessens et al., 2006a). While the functional groups in bacterial cell walls are important binding sites for metal ions (e.g. Fein et al., 1997), they also contribute to the pH buffering of environmental solutions by protonation or deprotonation reactions. Furthermore, the buffering capacities of intracellular contents are significant compared to that of the cell walls (Figs. 4.3 and 4.6). This acidity associated with intracellular buffering is released at higher rates than that of metabolic buffering (Figs. 4.4 and 4.7). Buffering by the cell walls and intracellular contents are particularly important for the contribution of dead cells to the buffering of natural solutions. In general, a significant part of the bacterial population of environmental systems is dead or dormant.

## 4.5 Conclusions

The long-term base neutralizing capacity of cells of *S. putrefaciens* at  $\text{pH} \geq 7$  is ascribed to the release of acidity due to metabolic reactions. In addition to the observed temperature dependence, the higher proton release by live cells at pH 10, compared to the

buffering capacity of disrupted cells at the same pH, indicates that the release of acidity is partly caused by metabolic activity. Release of organic acids and dissolution of metabolically produced CO<sub>2</sub> are the main sources of acidity. The redox, pH and temperature conditions regulate the type and rates of excreted metabolic products. Succinate exudation and its associated acidity are caused by aerobic respiration. Furthermore, CO<sub>2</sub> production is higher under oxic conditions resulting in a high proton release in the solutions. In contrast, fermentation reactions under anoxic conditions result in the production of acetate (pH 7 and 8) and succinate (pH 10). In general, production of CO<sub>2</sub> and release of its associated acidity is lower for fermentation reactions than respiration. In all experiments, the release of protons, organic acids and CO<sub>2</sub> systematically increases with pH and temperature.

Natural environments are characterized by fluctuations in pH, redox and temperature conditions. The response of microorganisms to these changing conditions has a major effect on the surrounding solution chemistry. The rate of metabolic release of protons by *S. putrefaciens* under various conditions is of the same order of magnitude as reported rates of iron reduction. By releasing protons, metal-reducing bacteria may compensate for the alkalinity production during the reductive dissolution of iron and manganese oxides and thereby keep their direct environment favorable for metal reduction. The rates of proton release measured in this study are also of the same order of magnitude as silicate weathering. This demonstrates the quantitatively significant effect microorganisms may have on mineral dissolution in their surrounding environment, especially when they are attached to mineral surfaces.

### **Acknowledgments**

Prof. dr. J.P.M. Tommassen and S. Loucaides are acknowledged for critically reading the manuscript. G. Nobbe is acknowledged for technical assistance with IC analyses. This research was financially supported by the Netherlands Organization for Scientific Research (NWO-Pionier Award).

---

## **Chapter 5**

# **Competitive binding of $\text{Cu}^{2+}$ and $\text{Zn}^{2+}$ to cells of *Shewanella putrefaciens***

Jacqueline Claessens and Philippe Van Cappellen  
submitted to Environmental Science and Technology

---

## Abstract

The binding of  $\text{Cu}^{2+}$  and  $\text{Zn}^{2+}$  to cells of *Shewanella putrefaciens* was measured at pH 4, 5.5 and 7, for dissolved metal concentrations ranging from 0.1 to 100  $\mu\text{M}$ . Release of organic compounds by the cells resulted in concentrations of dissolved organic carbon (DOC) between 0.5 and 1.6 mM. A surface complexation modeling approach was used to obtain affinity constants for  $\text{Cu}^{2+}$  and  $\text{Zn}^{2+}$  binding to cell wall functional groups. The binding of  $\text{Zn}^{2+}$  increased with increasing pH, over the entire range of dissolved metal concentration. This behavior could be explained by invoking two types of binding sites: carboxylate and phosphate groups. No electrostatic corrections were required to reproduce the pH-dependent binding of  $\text{Zn}^{2+}$ . Binding of  $\text{Cu}^{2+}$  exhibited a more complex pH dependence: at dissolved metal concentrations below 1  $\mu\text{M}$ , binding to the cells actually increased with decreasing pH. This behavior could be reproduced by (1) assuming the existence of a fraction of high affinity carboxylate groups (on the order of 10 %), and (2) including metal complexation by dissolved organic ligands. The latter compete with cell wall phosphate groups and decrease  $\text{Zn}^{2+}$  and  $\text{Cu}^{2+}$  binding at pH 5.5 and 7. Model parameters derived from the single metal binding isotherms were able to account for the observed competition of  $\text{Zn}^{2+}$  and  $\text{Cu}^{2+}$  for cell wall sites when both metals were present.

## 5.1 Introduction

Binding of metal ions to natural materials has a major impact on metal mobility in environmental systems (Xue and Sigg, 1999; Weng et al., 2002; Gustafsson et al., 2003; Toner et al., 2006). Sorption of metals to mineral surfaces and humic substances has been studied extensively. More limited metal binding experiments have been carried out with isolated cell walls (Plette et al., 1996), dead cells (Agraz et al., 1994) and live cells of Gram-positive (Fein et al., 1997) and Gram-negative bacteria (Haas et al., 2001). Metal interactions with bacterial cells can be understood by considering the cell wall to be a macromolecular array of reactive ligands.

Cell walls of microorganisms contain functional groups, such as carboxylate, phosphate and amino groups, which are protonated or deprotonated dependent on the pH of the outside solution (e.g., Plette et al., 1995; van der Wal et al., 1997a; Claessens et al., 2006a). Therefore, microbial cell walls exhibit a pH dependent charge. At most environmental pHs, cell walls are negatively charged and thus exhibit a high affinity for metal cations (e.g., Fein et al., 1997; Daughney et al., 2001; Haas et al., 2001). The acid-base behavior of cell walls is crucial for the understanding of metal binding, cell-mineral adhesion, and microbially induced mineralization or dissolution processes.

Acid-base titrations offer a simple, but powerful, technique to quantify the protonation and deprotonation reactions of functional groups, and they have been applied widely to study the mineral-aqueous solution interface (Dzombak and Morel, 1990). More recently, their application has been extended to microbial cells (e.g., Fein et al., 1997; Haas et al., 2004). However, our previous work has shown that the acid-base behavior of live bacterial cells differs fundamentally from that of mineral surfaces (Claessens et al., 2004; 2006a). Using pH stat experiments, we were able to separate the contributions of protonation and deprotonation of cell wall functional groups from those of other, irreversible, processes of base or acid neutralization by suspensions of live bacteria.

Microbial cells release metabolic and structural compounds to the surrounding solution, including organic ligands (Lin et al., 2005; Sanchez et al., 2005; Claessens et al., 2006b) and other exudates, such as polypeptides and siderophores (Xue and Sigg, 1990). The exudates affect aqueous metal speciation and, in particular, decrease the amounts of free

metals in solution. Binding of metals to the functional groups in the cell walls therefore competes with complexation reactions in solution. Furthermore, natural solutions are characterized by a variety of (metal) ions that are present at different concentrations. Therefore, in natural solutions metal cations also compete with one another for the available binding sites in bacterial cell walls.

Charging of bacterial cell walls and binding of metal cations to cell wall functional groups have been modeled using surface complexation models that include electrostatic corrections (e.g., Fein et al. 1997; Daughney et al., 2001; Haas et al., 2001). The electrostatic correction terms were originally developed to account for electrostatic interactions at two-dimensional surfaces. Bacterial cell walls, however, are truly three-dimensional macromolecular structures, instead of two-dimensional arrays of functional groups. It has been argued that the gradual change of surface charge with pH observed for bacterial cell walls is caused by a distribution of proton affinity constants of the functional groups, rather than by strong electrostatic interactions in the cell wall (Plette et al., 1995).

In the present study the binding of  $\text{Cu}^{2+}$  and  $\text{Zn}^{2+}$  to live cells of *Shewanella putrefaciens*, a facultative anaerobic Gram-negative bacterium, was quantified in one- and two-metal systems. The experiments were performed over a wide range of metal concentrations at three pH values (4, 5.5 and 7). Affinity constants for binding of  $\text{Cu}^{2+}$  and  $\text{Zn}^{2+}$  to bacterial cells were derived using a simple cell wall complexation model. In order to understand the mechanisms of metal binding, we compared one- and two-site binding models. Furthermore, the effects of electrostatic corrections and the presence of organic ligands in solution were investigated.

## **5.2 Materials and Methods**

### **5.2.1 Bacterial cultures**

*S. putrefaciens* was originally isolated from crude oil, but its presence has been detected in a variety of aquatic and subsurface environments (Venkateswaran et al., 1999). Pure cultures of the bacteria were grown at room temperature in liquid Luria Bertani (LB) medium. The bacteria were harvested in the mid-logarithmic phase and pelletized by centrifugation (5000 g for 15 min). The supernatant was discarded and the cell pellets were resuspended in 150 mM NaCl salt solution. The washing procedure was repeated one more

time to obtain the bacterial stock suspensions used in the experiments. Cell densities of the bacterial stock suspensions were derived from the optical densities (OD) measured at 660 nm wavelength on the harvested cultures. The OD-values were calibrated by counting colony-forming units on solid medium and by using the acridine orange direct count (AODC) method (Lovley and Phillips, 1988). The harvested cultures contained on the order of  $10^9$  cells per ml.

### 5.2.2 Metal binding experiments

Solutions with final metal (Cu or Zn) concentrations ranging from 2.5 to 150  $\mu\text{M}$  were prepared in 150 mM NaCl using stock solutions of 1 mM  $\text{CuCl}_2$  and  $\text{ZnCl}_2$  (final volumes 10 ml). The solution pH was adjusted to the desired value by addition of 0.01 M NaOH or 0.01 M HCl. For pH values of 4 and 5.5, the adjustment was carried out before adding the cells. For the series of experiments at pH 7, the pH was adjusted after adding the cells in order to minimize precipitation of oxide phases prior to binding of the metal to the cell walls. Chemical equilibrium speciation calculations with MINEQL+ showed that all solutions were undersaturated with respect to metal oxides, except in the experiments with Cu at pH 7. The competitive effect of  $\text{Zn}^{2+}$  on  $\text{Cu}^{2+}$  binding was determined in a series of variable Cu concentration experiments at pH 5.5, in the presence of a total Zn concentration of 59  $\mu\text{M}$ . The competitive effect of  $\text{Cu}^{2+}$  on  $\text{Zn}^{2+}$  binding was determined by performing three additional series of experiments at pH 5.5, with variable Zn concentrations and total Cu concentrations of 5, 143 and 1285  $\mu\text{M}$ .

Aliquots of the stock suspension of live cells were added to the metal containing solutions to final cell densities of  $7 \times 10^8$  cells  $\text{ml}^{-1}$ . The solutions were allowed to equilibrate for 2 hours under continuous shaking. After 20 minutes, 1 hour and 2 hours, the pH of the solutions was checked and readjusted if necessary by addition of 0.01 M NaOH or HCl solutions. The added volumes of NaOH or HCl were always less than 3 % of the total volume. After 2 hours, the cells were separated from the solutions by centrifugation (3000 g for 20 minutes). An aliquot of 0.5 ml of the supernatant was transferred in 4.5 ml of a 0.1 M  $\text{HNO}_3$  solution. The concentrations of Cu and Zn were determined by Inductively Coupled Plasma Mass Spectrometry (ICP-MS). DOC (dissolved organic carbon) concentrations in the supernatants were measured with a Shimadzu TOC analyzer 5050.

To check whether aqueous metal removal might be due to processes other than metal binding to the cells, such as precipitation of metal oxides or metal binding to the experimental tubes, control experiments were carried out without cells for concentrations of 50  $\mu\text{M}$  of Zn or Cu. At pH 4 and 5.5, the decrease in aqueous Cu in the control experiments was less than 8 % of the total concentration. At pH 7, however, 99 % of aqueous Cu was removed, due to oxide mineral precipitation. The decrease in aqueous Zn concentration in the control experiments was below 20 %, at pH 4 and 5.5, but increased to about 40 % at pH 7.

The significant decrease in aqueous Zn concentrations observed in the control experiments could reflect binding of metal to the tubes. To check for this possibility, cells were equilibrated with solutions of 50  $\mu\text{M}$  total Zn, at pH 4, 5.5 and 7. After centrifugation of the equilibrated suspensions, the pellets were resuspended and the suspensions were discarded. The tubes were dried carefully with a tissue and then filled with a solution of 0.1 M  $\text{HNO}_3$ , in order to release any Zn bound to the tubes. The Zn concentrations recovered in the acid solutions were always less than 1 % of the total amount of Zn, implying that nearly all aqueous Zn removal was due to binding to the cells.

## 5.3 Model description

### 5.3.1 Acid-base properties of cell walls

Carboxylate, phosphate and amino groups are commonly invoked to explain cell wall charging of both Gram-positive and Gram-negative bacteria (Haas, 2001, and references therein). The deprotonation reactions of these functional groups are



where R represents the cell wall. The corresponding mass action equations are

$$K_{(1)} = \frac{[\text{R} - \text{COO}^-]a_{\text{H}^+}}{[\text{R} - \text{COOH}]} \quad (5.4)$$

$$K_{(2)} = \frac{[\text{R} - \text{PO}_4^-]a_{\text{H}^+}}{[\text{R} - \text{PO}_4\text{H}]} \quad (5.5)$$

$$K_{(3)} = \frac{[\text{R} - \text{NH}_2] a_{\text{H}^+}}{[\text{R} - \text{NH}_3^+]} \quad (5.6)$$

where  $K$  corresponds to the acid dissociation constant of the given cell wall functional group,  $a_{\text{H}^+}$  is the proton activity and the brackets correspond to site concentrations in the cell wall.

By combining chemical analyses and titration curves of isolated cell walls of a variety of Gram-positive bacteria, Plette et al. (1995) and van der Wal et al. (1997a) proposed that the average ratios of carboxylate, phosphate and amino groups are 2:1:1. They further report average  $pK_a$  values of 4.3, 7.8 and 9.9 for the deprotonation reactions given above (Plette et al., 1995). Using the 2:1:1 distribution of functional groups and the reported  $pK_a$  values, plus the constant capacitance model to correct for electrostatic interactions, the cell wall charging of live cells of *S. putrefaciens* as a function of pH could be reproduced, resulting in a total functional group concentration of  $6.5 \times 10^{-16}$  mol cell<sup>-1</sup> (Claessens et al., 2006a; Table 5.1).

**Table 5.1:** Site densities and acid dissociation constants of cell wall functional groups of *S. putrefaciens*.

Model parameter	Value	Units
[R-COOH] <sup>a</sup>	3.25	10 <sup>-16</sup> mol cell <sup>-1</sup>
[R-PO <sub>4</sub> H] <sup>a</sup>	1.63	10 <sup>-16</sup> mol cell <sup>-1</sup>
[R-NH <sub>2</sub> ] <sup>a</sup>	1.63	10 <sup>-16</sup> mol cell <sup>-1</sup>
[R-HA] <sup>b</sup>	0.32	10 <sup>-16</sup> mol cell <sup>-1</sup>
$pK_1^c$	4.3	-
$pK_2^c$	7.8	-
$pK_3^c$	9.9	-
$pK_{a(\text{HA})}^b$	4.3	-

<sup>a</sup> Claessens et al., 2006a

<sup>b</sup> this study

<sup>c</sup> Plette et al., 1995

### 5.3.2 Metal binding to cell walls

The negatively charged (deprotonated) functional groups in the bacterial cell wall provide binding sites for positively charged aqueous metal ions. Metal binding behavior to cell walls has been modeled assuming one and two binding sites below and above pH 5.5, respectively (Fein et al., 1997). At low pH (< 5.5), carboxylate groups that are deprotonated ( $pK_a = 4.3$ ) serve as metal ion binding sites (one-site model). With increasing pH (above pH 5.5), however, phosphate groups also deprotonate ( $pK_a = 7.8$ ) and, hence, also become available for additional metal ion binding (two-site model).

Binding of divalent aqueous metal cations ( $\text{Me}^{2+}$ ) to the negatively charged functional groups in the bacterial cell walls can be represented by the following reactions



with the corresponding mass action equations

$$K_{(\text{COOMe}^+)} = \frac{[\text{R} - \text{COOMe}^+]}{[\text{R} - \text{COO}^-][\text{Me}^{2+}]} \quad (5.9)$$

$$K_{(\text{PO}_4\text{Me}^+)} = \frac{[\text{R} - \text{PO}_4\text{Me}^+]}{[\text{R} - \text{PO}_4^-][\text{Me}^{2+}]} \quad (5.10)$$

where  $K$  corresponds to the equilibrium constant for complex formation between the metal and a cell wall functional group. The  $K$  values are obtained by fitting binding isotherms of Cu and Zn to the cells measured in one-metal systems.

### 5.3.3 Electrostatic effect of the cell wall

In analogy with mineral surfaces, the effect of the net electrical charge of the bacterial cell wall on the binding of aqueous metal ions to cell wall functional groups is usually accounted for using the following relationship

$$K = K_{\text{int}} \exp\left(\frac{-\Delta Z F \psi}{RT}\right) \quad (5.11)$$

where  $F$  and  $R$  are Faraday's constant and the gas constant,  $T$  is absolute temperature,  $K_{\text{int}}$  is the complex formation constant at zero cell wall charge and zero metal binding,  $\psi$  is the electric potential produced by the cell wall charge, and  $\Delta Z$  is the change in charge accompanying the binding of the metal ion (Dzombak and Morel, 1990).

In the case of low surface potentials or high ionic strengths, the diffuse layer created by the net cell wall charge is compressed and the electric potential is proportional to the surface charge according to the constant capacitance model (Dzombak and Morel, 1990)

$$\psi = \frac{\sigma}{C} \quad (5.12)$$

where  $\sigma$  is the surface charge and  $C$  the capacitance of the diffuse layer. The constant capacitance model represents the simplest model relating potential to charge at a surface and has been used for describing cell wall charging and metal binding to cell walls (e.g., Fein et

al., 1997; Haas et al., 2001; Claessens et al., 2006a). Use of an electrostatic model intended for planar surfaces, however, is questionable for cell walls and is, therefore, further assessed in this study.

#### 5.3.4 Solution speciation

Chemical equilibrium speciation calculations using MINEQL+ imply that, in the absence of dissolved organic ligands, 99 % of the Zn and Cu in solution occur as free metal ( $\text{Me}^{2+}$ ) or chloride complexes ( $\text{MeCl}^+$  and  $\text{MeCl}_2$ ). The exception are the experiments with Cu at pH 7, where on the order of 40 % of metal in solution occurs as aqueous hydroxide complexes,  $\text{Cu}(\text{OH})_2^0$ ,  $\text{Cu}(\text{OH})^+$  and  $\text{Cu}_2(\text{OH})_2^{2+}$ . However, live cells of *S. putrefaciens* release cell wall components (Claessens et al., 2004) and metabolic products, including organic acids and  $\text{CO}_2$ , to solution (Claessens et al., 2006a; 2006b) The presence of additional dissolved ligands especially affects free metal concentrations resulting in a competition between metal complexation in solution and complexation with cell wall functional groups.

As the experimental solutions were open to the atmosphere, the potential contribution of aqueous metal-carbonate complexes was estimated by assuming equilibrium with atmospheric  $\text{CO}_2$  at the different pH values. Carbonate complexes were negligible, except for the experiments with copper at pH 7, where 3 % of the metal in solution should be present as the carbonate species  $\text{CuHCO}_3^+$  and  $\text{CuCO}_3$ .

Because the nature and properties of DOC released to solution by the cells are not well constrained, it is less straightforward to account for metal complexation by organic ligands in solution. The DOC concentrations in the metal binding experiments were on the order of  $0.7 \pm 0.2$  mM ( $7\text{-}14 \times 10^{-16}$  mol DOC cell<sup>-1</sup>, Table 5.2). Organic acids released as a result of cellular metabolism account for up to 10 % of the DOC (Claessens et al., 2006b). These acids are assumed to represent the main metal complexing agents of the DOC. To assess the sensitivity of metal binding at the cell wall to the presence of competing dissolved organic ligands, citric acid was selected as a model compound representing the organic acids in solution. The citric acid concentration was set to 10  $\mu\text{M}$ , which corresponds to approximately 10 % of the average DOC concentrations.

**Table 5.2:** Concentrations of DOC measured in metal binding experiments at different pH values and metal concentrations.

pH	Zn ( $\mu\text{M}$ )	Cu ( $\mu\text{M}$ )	DOC (mM)	DOC ( $10^{-16}$ mol cell $^{-1}$ )
4	-	11	0.7	10.2
4	97	-	0.8	12.0
5.5	-	11	0.5	6.6
5.5	132	-	0.5	8.6
5.5	61	4.2	0.5	7.0
5.5	59	53	0.8	13.6
5.5	66	143	0.7	10.3
5.5	64	1290	0.8	11.1
7	-	11	1.6	24.1
7	128	-	0.6	11.8

### 5.3.5 Modeling strategy

The primary aim of the modeling was to help with the mechanistic interpretation of the binding behavior of the metals to the cells. As shown below, the pH-dependent binding of  $\text{Zn}^{2+}$  to the cells was more straightforward than that of  $\text{Cu}^{2+}$ , and was therefore used as starting point for the modeling. The first step consisted in deriving the simplest complexation model explaining the  $\text{Zn}^{2+}$  binding data. Next the  $\text{Cu}^{2+}$  binding data were considered, and the model was expanded to reproduce the more complicated pH dependence of the  $\text{Cu}^{2+}$  binding isotherms. Model complexity was increased progressively, in as far needed to account for the various trends observed in the  $\text{Cu}^{2+}$  binding data. At each step, the model parameters describing  $\text{Zn}^{2+}$  binding were updated so that the isotherms of both metals measured in one-metal systems could be reproduced simultaneously by the model. In the final step, the predictive capability of the model was tested by forecasting competitive metal binding in cell suspensions to which both  $\text{Zn}^{2+}$  and  $\text{Cu}^{2+}$  were added.

## 5.4 Results

### 5.4.1 Binding of $\text{Zn}^{2+}$

Binding of  $\text{Zn}^{2+}$  to cells of *S. putrefaciens* increased with pH and increasing aqueous Zn concentration (Fig. 5.1). At pH 4 and 5.5, the observed binding behavior of  $\text{Zn}^{2+}$  could be reproduced by a one-site binding model (carboxylate groups only), without the need to invoke electrostatic corrections. The site concentration ( $3.25 \times 10^{-16}$  mol cell $^{-1}$ ) imposed in the model calculations was derived assuming that 50 % of the total cell wall functional groups are

carboxylate groups (section 5.3.1; Table 5.1). Since no electrostatic correction was necessary to account for the observed pH-dependent binding behavior of  $\text{Zn}^{2+}$ , the only adjustable parameter was the affinity constant for  $\text{Zn}^{2+}$  binding to carboxylate groups. The corresponding  $\log K$  value was 4.3 (model 1 in Table 5.3).

The one-site binding model could not account for the observed increase in  $\text{Zn}^{2+}$  binding from pH 5.5 to 7 (Fig. 5.1). This is consistent with the complete deprotonation of the carboxylate groups at pH above 5.5 ( $\text{p}K_a = 4.3$ ). A two-site binding model (carboxylate and phosphate groups), without electrostatic correction, was able to reproduce the binding behavior of  $\text{Zn}^{2+}$  at the three experimental pHs (Fig. 5.1). The  $\log K$  value of the affinity constant for  $\text{Zn}^{2+}$  binding to the phosphate groups was 5.5 (model 1 in Table 5.3). The one- and two-site models yielded identical results at pH 4. At pH 5.5, the two-site binding model predicted slightly enhanced binding of  $\text{Zn}^{2+}$  at high dissolved Zn concentrations ( $> 100 \mu\text{M}$ ). At pH 5.5 and 7, the one- and two-site models underestimated the binding of  $\text{Zn}^{2+}$  at low aqueous Zn concentrations ( $< 10 \mu\text{M}$ ) (Fig. 5.1).

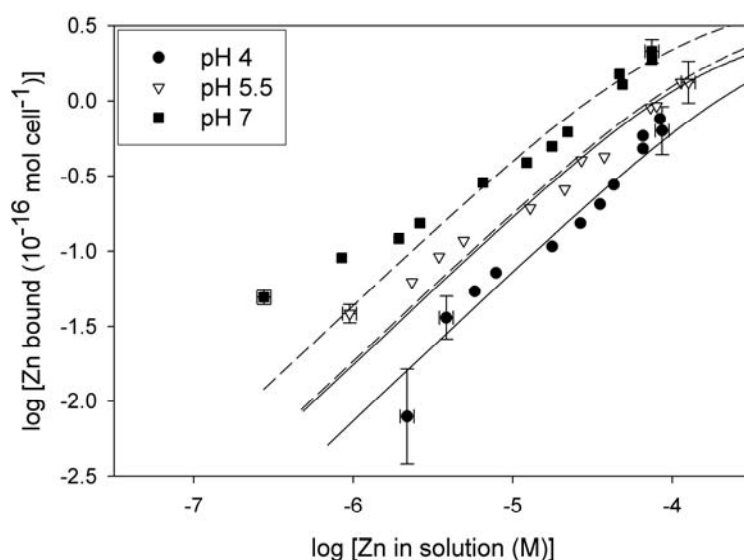


**Figure 5.1:** Binding of  $\text{Zn}^{2+}$  to cells of *S. putrefaciens* as a function of dissolved Zn concentration at pH 4, 5.5 and 7, in 150 mM NaCl and for a cell density of  $7 \times 10^8$  cells  $\text{ml}^{-1}$ . The solid and dashed lines represent model calculations with a one- (carboxylate) and two-site (carboxylate and phosphate) binding model, respectively. The affinity constants for  $\text{Zn}^{2+}$  binding to the sites used in the calculations are given in Table 5.3 (model 1). See Table 5.1 for further model parameters. The errors on experimental data assume an uncertainty of  $\pm 10\%$  on the ICP-MS analyses.



### 5.4.2 Comparison of $\text{Zn}^{2+}$ and $\text{Cu}^{2+}$ binding

At pH 4 and 5.5, binding of  $\text{Cu}^{2+}$  to the cells exceeded that of  $\text{Zn}^{2+}$  (Figs. 5.2A and B), particularly at low dissolved metal concentrations ( $< 20 \mu\text{M}$ ). The shapes of the  $\text{Cu}^{2+}$  isotherms also deviated significantly from those of  $\text{Zn}^{2+}$  at these two pH values. At pH 7, binding of  $\text{Cu}^{2+}$  was comparable to that of  $\text{Zn}^{2+}$ , up to dissolved metal concentrations of  $10 \mu\text{M}$  (Fig. 5.2C). Above  $10 \mu\text{M}$ , binding of  $\text{Cu}^{2+}$  exceeded that of  $\text{Zn}^{2+}$ . The pH-dependent binding behavior of  $\text{Cu}^{2+}$  was far more complex than that of  $\text{Zn}^{2+}$  (compare Figs. 5.1 and 5.3). At high dissolved Cu concentrations ( $> 10 \mu\text{M}$ ),  $\text{Cu}^{2+}$  binding to the cells increased with pH, as expected (Fig. 5.3). However, at dissolved Cu concentrations below  $10 \mu\text{M}$ ,  $\text{Cu}^{2+}$  binding was lower at pH 7 than at pH 5.5. At aqueous Cu concentrations below  $1 \mu\text{M}$ , the highest  $\text{Cu}^{2+}$  binding was observed for pH 4 (Fig. 5.3).

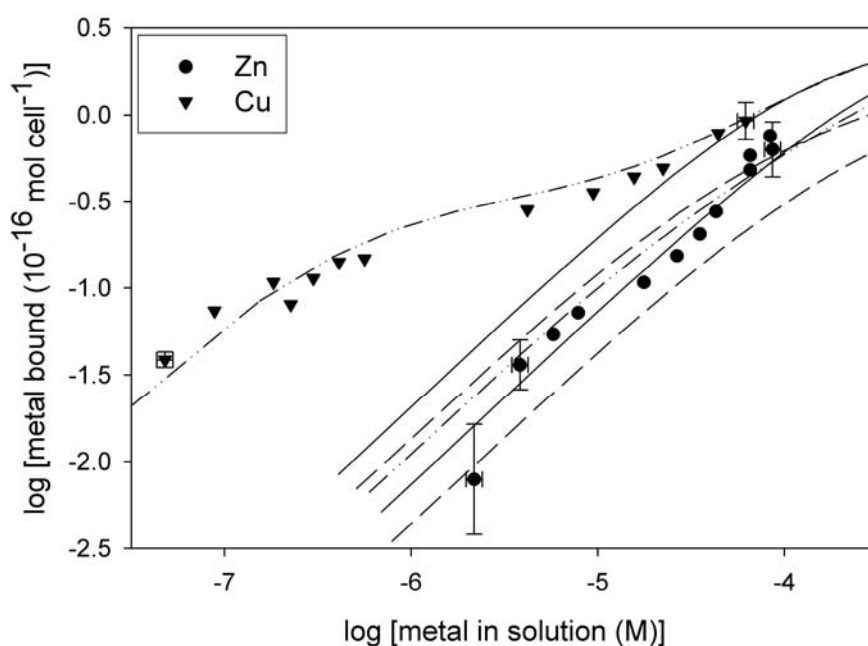


**Figure 5.2A:** Binding of  $\text{Zn}^{2+}$  and  $\text{Cu}^{2+}$  to cells of *S. putrefaciens* as a function of dissolved metal concentration at pH 4, in 150 mM NaCl and for a cell density of  $7 \times 10^8 \text{ cells ml}^{-1}$ . The solid and dashed lines represent model calculations with a two-site (carboxylate and phosphate) binding model without and with electrostatic correction, respectively (model 1 in Table 5.3). The dashed-dotted lines represent model calculations of a two-site binding model with a 10 % fraction of high affinity carboxylate sites (model 2 in Table 5.3).

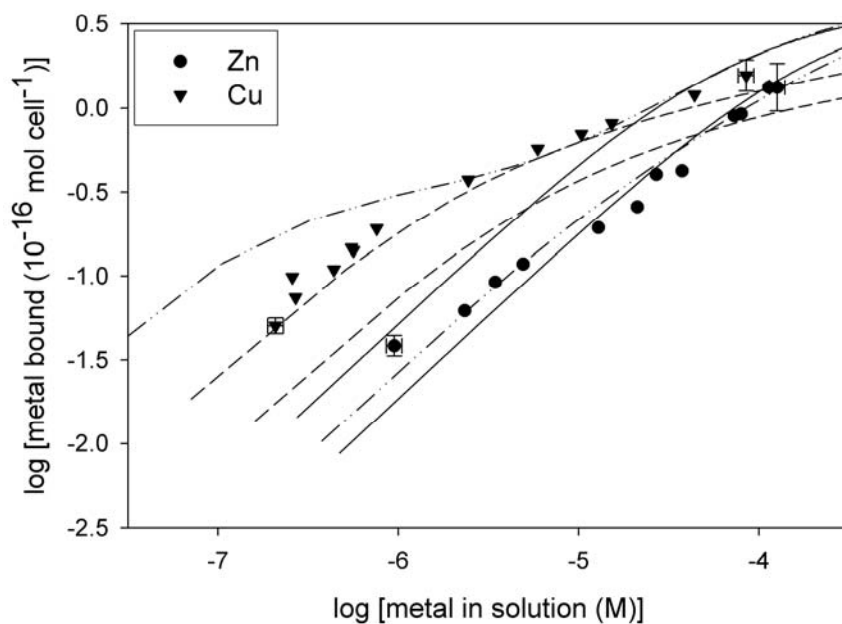


**Figure 5.2B:** Binding of Zn<sup>2+</sup> and Cu<sup>2+</sup> to cells of *S. putrefaciens* as a function of dissolved metal concentration at pH 5.5, in 150 mM NaCl and for a cell density of  $7 \times 10^8$  cells ml<sup>-1</sup>. See Figure caption 5.2A for additional details.

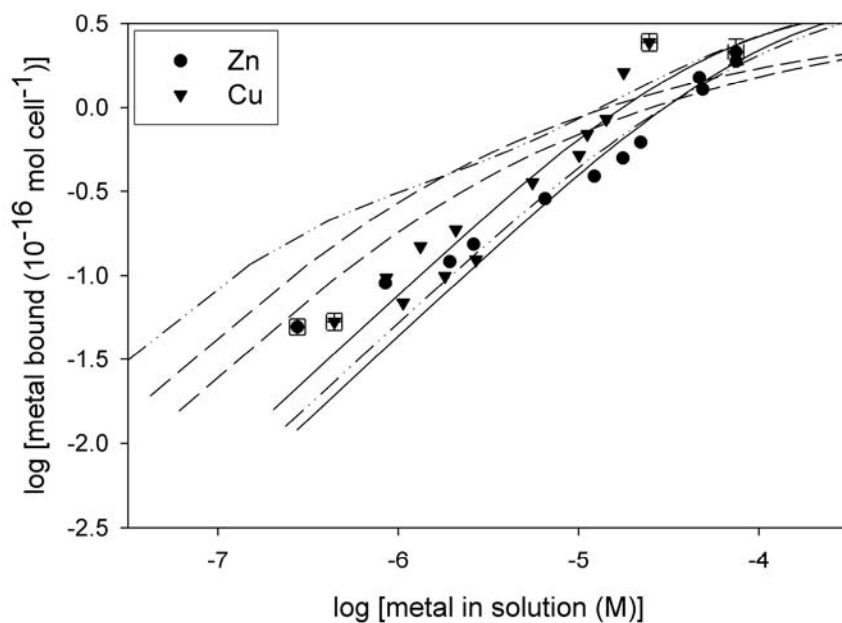


**Figure 5.2C:** Binding of Zn<sup>2+</sup> and Cu<sup>2+</sup> to cells of *S. putrefaciens* as a function of dissolved metal concentration at pH 7, in 150 mM NaCl and for a cell density of  $7 \times 10^8$  cells ml<sup>-1</sup>. See Figure caption 5.2A for additional details.

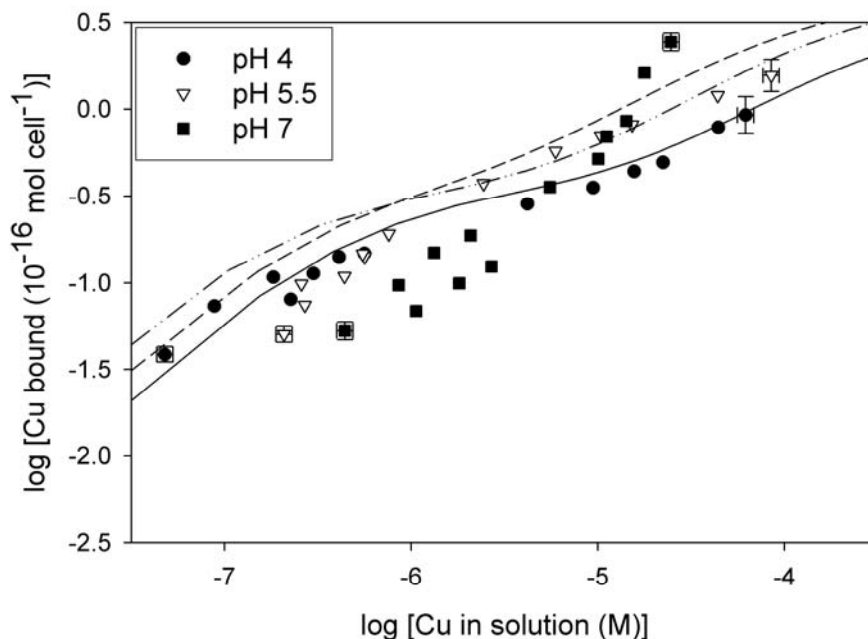


**Figure 5.3:** Binding of  $\text{Cu}^{2+}$  to cells of *S. putrefaciens* as a function of dissolved Cu concentration at pH 4, 5.5 and 7, in 150 mM NaCl and for a cell density of  $7 \times 10^8$  cells  $\text{ml}^{-1}$ . The lines represent model calculations of a two-site binding model with a 10 % fraction of high affinity carboxylate sites (model 2 in Table 5.3). The solid, dashed-dotted and dashed lines correspond to pH 4, 5.5 and 7, respectively.

In contrast to  $\text{Zn}^{2+}$ , the two-site binding model was unable to reproduce the shapes of the  $\text{Cu}^{2+}$  isotherms at pH 4 and 5.5 (Figs. 5.2A and B; model 1 in Table 5.3). At pH 7, the isotherms of both metals had fairly similar shapes, and the two-site binding model was able to provide an approximate fit to the  $\text{Cu}^{2+}$  binding data (Fig. 5.2C). First estimates of the affinity constants of  $\text{Cu}^{2+}$  to the cell wall functional groups were obtained by only considering the highest aqueous  $\text{Cu}^{2+}$  concentrations ( $> 30 \mu\text{M}$ ). Using the pH 4 and 5.5 data, a  $\log K$  value for  $\text{Cu}^{2+}$  binding to the carboxylate groups of 4.8 was estimated (model 1 in Table 5.3). Similarly, a  $\log K$  value of 6.0 for the affinity constant for  $\text{Cu}^{2+}$  binding to the phosphate groups was derived by fitting the high concentration data at pH 5.5 and 7 (model 1 in Table 5.3).

The observed shape of the binding isotherm of  $\text{Cu}^{2+}$  at pH 5.5 could be reproduced by including an electrostatic correction in the two-site model using Equations 5.11 and 5.12 (Fig. 5.2B). A good fit was obtained by adjusting the capacitance to  $5 \text{ F m}^{-2}$ , and imposing a specific surface area of *S. putrefaciens* cells of  $55 \text{ m}^2 \text{ g}^{-1}$  (as reported by Haas et al., 2001).

The same electrostatic correction failed to reproduce the  $\text{Cu}^{2+}$  isotherms at pH 4 and 7, however (Figs. 5.2A and B). Furthermore, at pH 5.5 and 7, the predicted shapes of the  $\text{Zn}^{2+}$  isotherms deviated significantly from the observed ones when the electrostatic correction was applied (Figs 5.2B and C). Thus, the two-site model, with or without electrostatic correction (model 1 in Table 5.3), was unable to provide a consistent explanation of the entire set of single metal binding isotherms.

The  $\text{Cu}^{2+}$  isotherm at pH 4 was satisfactorily reproduced by assuming that a small fraction of the carboxylate groups in the cell wall have an enhanced binding affinity for metal cations (Figs. 5.2A and 5.3, model 2 in Table 5.3). The corresponding model curves in Figures 5.2 and 5.3 assume that 10 % of the carboxylate groups (or  $0.32 \times 10^{-16}$  mol cell<sup>-1</sup>; Table 5.1) are high affinity sites. Fitting the  $\text{Cu}^{2+}$  isotherm at pH 4, without electrostatic correction, then yielded a  $\log K$  for the affinity constant of  $\text{Cu}^{2+}$  binding to the high affinity sites of 7.3. At pH 5.5 and 7, the same model overpredicted  $\text{Cu}^{2+}$  binding to the cells at dissolved metal concentrations below 1 and 10  $\mu\text{M}$ , respectively (Figs. 5.2B and 5.2C). The two-site binding model with high affinity sites was able to reproduce the  $\text{Zn}^{2+}$  isotherms at the three pHs using a unique value for the binding constant of  $\text{Zn}^{2+}$  to the high affinity sites ( $\log K = 5.4$ ) (Fig. 5.2). In fact, the presence of the high affinity sites slightly improved the fit to the  $\text{Zn}^{2+}$  binding data at pH 5.5 and 7.

Although the inclusion of a fraction of high affinity carboxylate groups did not yield a systematic fit to the  $\text{Cu}^{2+}$  isotherms at the three pHs, it did reproduce an important feature of the data. As can be seen in Figure 5.3, at aqueous  $\text{Cu}^{2+}$  concentrations below 1  $\mu\text{M}$ , the model predicted lower  $\text{Cu}^{2+}$  binding at pH 7 compared to pH 5.5, as also observed in the experimental data. In part, this effect was due to the lowering of the concentration of free  $\text{Cu}^{2+}$  ions in solution at pH 7, as a result of the formation of aqueous hydroxide complexes, which, according to equilibrium speciation calculations, accounted for about 40 % of total Cu at pH 7.

The fraction of high affinity carboxylate sites and the affinity constant of metal binding to these sites are interdependent fitting parameters. Choosing a different fraction of high affinity sites therefore yields different values for the affinity constants, as illustrated for  $\text{Cu}^{2+}$  in Table 5.3. Nonetheless, as shown in Figure 5.4, good fits of the  $\text{Cu}^{2+}$  isotherm at pH 4 were only obtained for a fraction of high affinity carboxylate groups in the range 5-10 %. In

all further calculations, 10 % of the carboxylate groups are assumed to be high affinity metal binding sites.

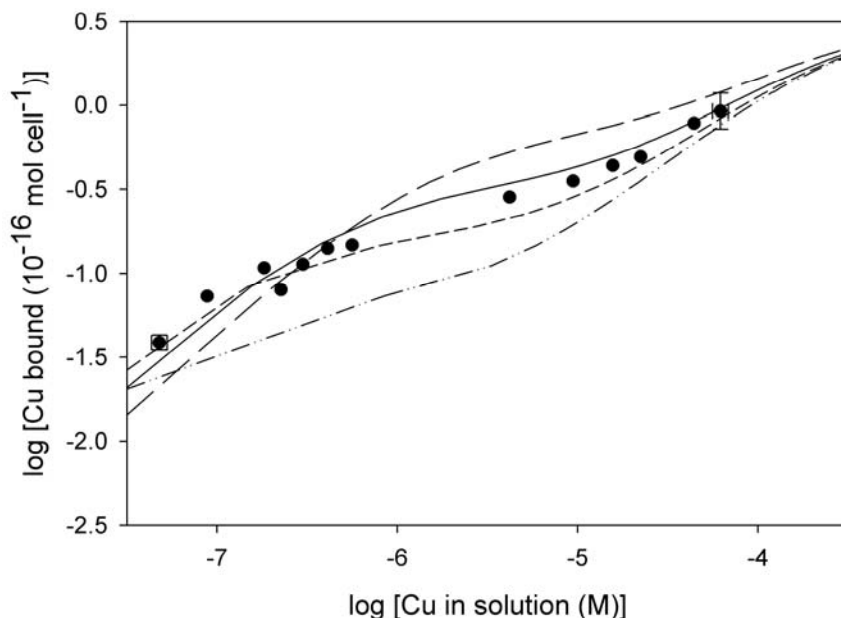


**Figure 5.4:** Binding of  $\text{Cu}^{2+}$  to cells of *S. putrefaciens* as a function of dissolved Cu concentration at pH 4, in 150 mM NaCl and for a cell density of  $7 \times 10^8$  cells  $\text{ml}^{-1}$ . The lines represent model calculations of a two-site binding model with a variable fraction of high affinity carboxylate sites (model 2 in Table 5.3). The dashed-dotted, short-dashed, solid and long-dashed lines correspond to 2, 5, 10 and 20 % high affinity sites, respectively.

The acid dissociation constant of the high affinity sites was also an adjustable parameter. When the  $\text{p}K_a$  of the high affinity sites was reduced from 4.3 to 3.5, the model produced exactly the same  $\text{Cu}^{2+}$  isotherm at pH 4 by changing the  $\log K$  value of the affinity constant from 7.3 to 7.0 (Table 5.3). The lower  $\text{p}K_a$  value implies complete deprotonation of the high affinity sites at pH 4. As a consequence, the  $\text{Cu}^{2+}$  ions no longer have to compete with protons for binding to the sites, which results in a lower apparent affinity constant. In all further calculations a  $\text{p}K_a$  value of 4.3 is assumed for the high affinity carboxylate sites.

### 5.4.3 Organic complexation in solution

As  $\text{Cu}^{2+}$  ions more strongly complex to common organic acids released by cell metabolism (e.g., formate, acetate, succinate, citrate) than  $\text{Zn}^{2+}$ , the different pH dependencies of binding of the metals to the cells (Fig. 5.2) could in part be due to differences in organic

complexation in solution. This possibility was investigated by including citric acid as a model compound in the equilibrium speciation calculations (model 3 in Table 5.3).

At pH 4, the presence of 10  $\mu\text{M}$  citric acid had no effect on the model-calculated  $\text{Zn}^{2+}$  binding to the cells (Fig. 5.5). At pH 5.5 and 7, however,  $\text{Zn}^{2+}$  binding to the cells slightly decreased because of complexation of Zn to citrate. The effect was more pronounced at pH 7 than at pH 5.5. In order to compensate for the effects of citrate complexation at pH 5.5 and 7, the  $\log K$  value for the affinity constant of  $\text{Zn}^{2+}$  binding to the cell wall phosphate groups was increased from 5.5 to 5.7 (model 3 in Table 5.3).

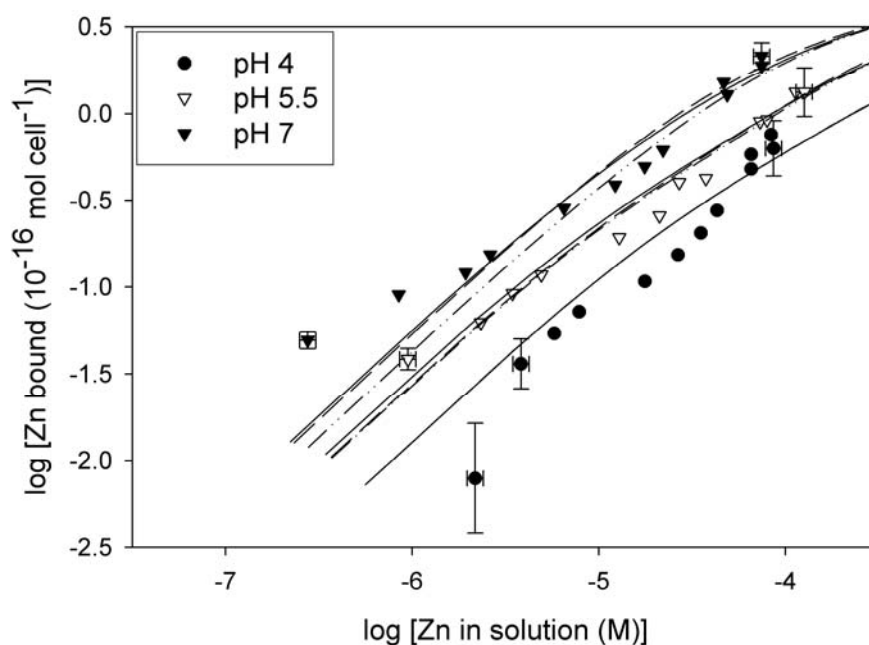


**Figure 5.5:** Binding of  $\text{Zn}^{2+}$  to cells of *S. putrefaciens* as a function of dissolved Zn concentration at pH 4, 5.5 and 7, in 150 mM NaCl and for a cell density of  $7 \times 10^8$  cells  $\text{ml}^{-1}$ . The solid lines represent model calculations of a two-site binding model with a 10 % fraction of high affinity carboxylate sites, in the absence of dissolved organic ligands (model 2 in Table 5.3). The dashed-dotted and dashed lines correspond to model calculations of a two-site binding model with high affinity carboxylate sites, in the presence of 10  $\mu\text{M}$  citric acid, using the parameter set of models 2 and 3 in Table 5.3, respectively.

As for  $\text{Zn}^{2+}$ , model-calculated  $\text{Cu}^{2+}$  binding at pH 4 was not affected by the presence of 10  $\mu\text{M}$  of citric acid (compare Figs. 5.4 and 5.6), but decreased significantly at pH 5.5 and

7 (compare Figs. 5.3 and 5.6). To compensate for citrate complexation, the  $\log K$  value of the affinity constant of  $\text{Cu}^{2+}$  binding to the cell wall phosphate groups was raised from 6.0 to 6.2 (model 3 in Table 5.3). Most importantly, by taking into account the complexation of  $\text{Cu}^{2+}$  by citrate, the observed pH dependency of  $\text{Cu}^{2+}$  binding to the cells was reproduced (Fig. 5.6). At low dissolved metal concentrations ( $< 3 \mu\text{M}$ ), binding to the cells was predicted to increase with decreasing pH, while the opposite trend was predicted at higher dissolved metal concentrations.

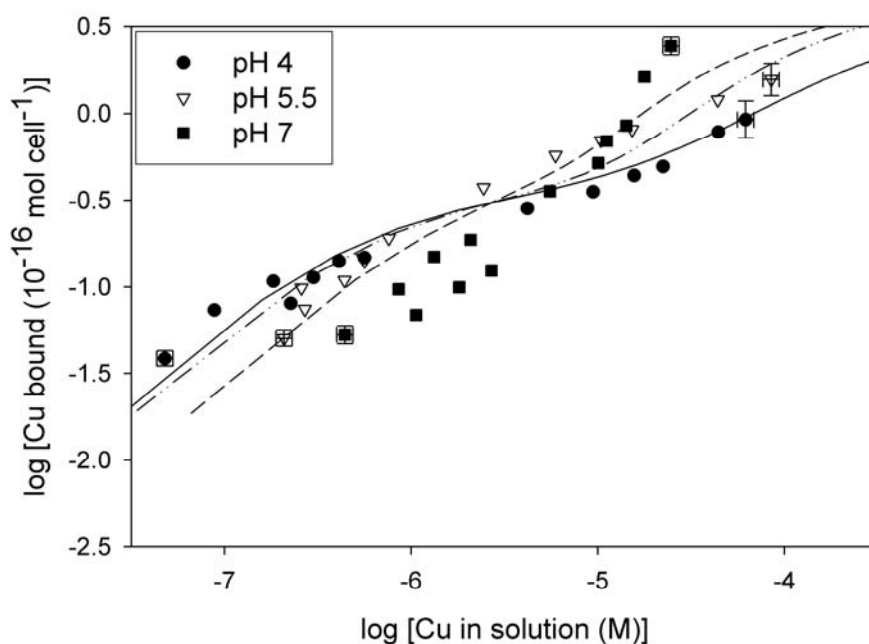


**Figure 5.6:** Binding of  $\text{Cu}^{2+}$  to cells of *S. putrefaciens* as a function of dissolved Cu concentration at pH 4, 5.5 and 7, in 150 mM NaCl and for a cell density of  $7 \times 10^8$  cells  $\text{mL}^{-1}$ . The lines represent model calculations of a two-site binding model, with a 10 % fraction of high affinity carboxylate sites plus 10  $\mu\text{M}$  citric acid in solution (model 3 in Table 5.3). The solid, dashed-dotted and dashed lines correspond to pH 4, 5.5 and 7, respectively.

As expected, changes in the concentration and metal complex formation constants assigned to the model dissolved organic acid affect the model-predicted metal binding isotherms. For instance, increasing the  $\log K$  of the formation constant of the  $\text{CuCit}^{-1}$  aqueous complex from 7.3 to 7.8 markedly improved the fit to the pH 7  $\text{Cu}^{2+}$  binding data at low dissolved metal concentrations (results not shown). One feature that could not be reproduced,

however, was the upward trend of  $\text{Cu}^{2+}$  binding at the highest dissolved concentrations (Fig. 5.6).

#### 5.4.4 Competitive binding of $\text{Zn}^{2+}$ and $\text{Cu}^{2+}$

At pH 5.5, the presence of Zn at a total concentration of 59  $\mu\text{M}$  did not have a measurable effect on the binding of  $\text{Cu}^{2+}$  to the cells (Fig. 5.7). Even at low Cu concentrations ( $\leq 1 \mu\text{M}$ ) no competitive effect of Zn on  $\text{Cu}^{2+}$  binding was observed. The absence of a significant competitive effect of  $\text{Zn}^{2+}$  on  $\text{Cu}^{2+}$  binding to the cells was consistent with predictions based on the model parameters derived from the single metal binding isotherms (Fig. 5.7; model 3 in Table 5.3). At low dissolved  $\text{Cu}^{2+}$  concentrations, the model calculations actually predict a slight increase in  $\text{Cu}^{2+}$  binding in the presence of  $\text{Zn}^{2+}$ . This effect is due to complexation of  $\text{Zn}^{2+}$  by citrate in solution, which lowers the complexation of  $\text{Cu}^{2+}$  to citrate, hence allowing more  $\text{Cu}^{2+}$  ions to bind to the cell wall.

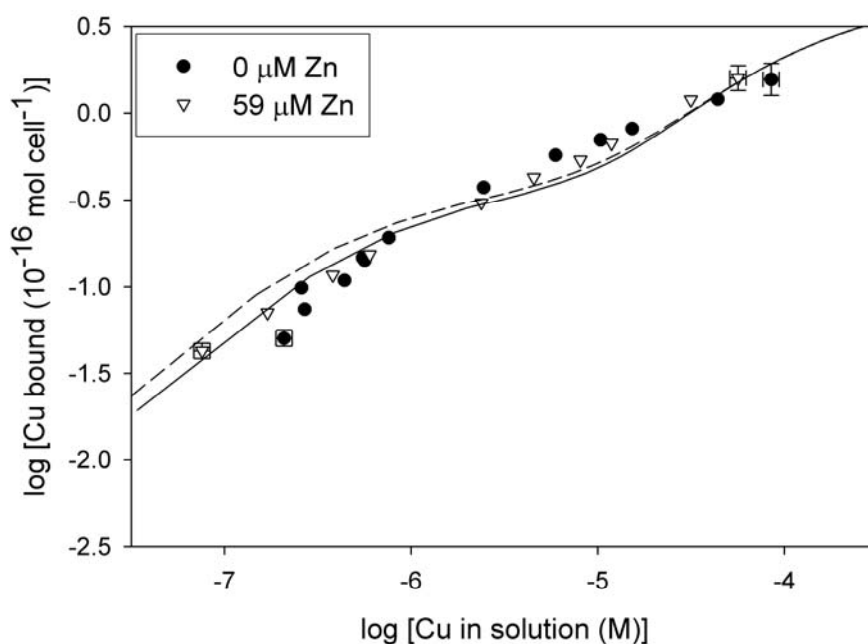


**Figure 5.7:** Effect of  $\text{Zn}^{2+}$  on the binding of  $\text{Cu}^{2+}$  to cells of *S. putrefaciens* as a function of dissolved Cu concentration at pH 5.5, in 150 mM NaCl, for a cell density of  $7 \times 10^8$  cells  $\text{ml}^{-1}$ . The lines represent model calculations of a two-site binding model, with a 10 % fraction of high affinity carboxylate sites plus 10  $\mu\text{M}$  citric acid in solution (model 3 in Table 5.3). The solid and dashed lines correspond to 0 and 59  $\mu\text{M}$  total Zn, respectively.

As expected from the higher affinity constants of  $\text{Cu}^{2+}$  for cell wall carboxylate and phosphate groups (Table 5.3),  $\text{Zn}^{2+}$  binding to the cells decreased in the presence of Cu (Fig. 5.8). Already at low concentrations (4.8  $\mu\text{M}$ ),  $\text{Cu}^{2+}$  ions had a measurable competitive effect on  $\text{Zn}^{2+}$  binding at pH 5.5 (Fig. 5.8). The competitive effect increased with increasing  $\text{Cu}^{2+}$  addition. The two-site model with high affinity sites (model 3 in Table 5.3) could reasonably well reproduce the relative decrease in  $\text{Zn}^{2+}$  binding at the lowest two  $\text{Cu}^{2+}$  concentrations (4.8 and 143  $\mu\text{M}$ ), but overpredicted the competitive effect at the highest concentration (1285  $\mu\text{M}$ ).

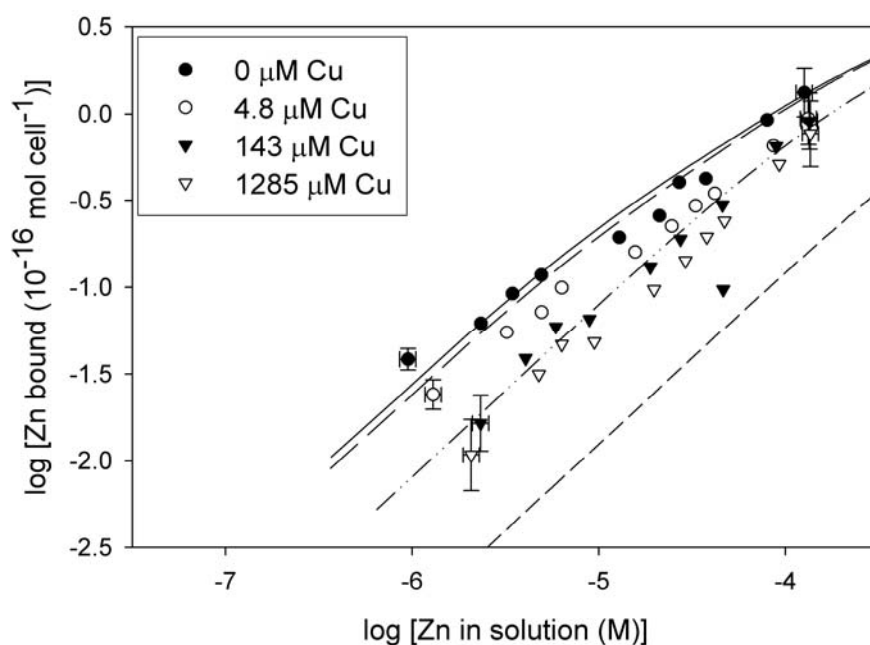


**Figure 5.8:** Effect of  $\text{Cu}^{2+}$  on the binding of  $\text{Zn}^{2+}$  to cells of *S. putrefaciens* as a function of dissolved Zn concentration at pH 5.5, in 150 mM NaCl, for a cell density of  $7 \times 10^8$  cells  $\text{ml}^{-1}$ . The lines represent model calculations of a two-site binding model, with a fraction of high affinity carboxylate sites (10 %) plus 10  $\mu\text{M}$  citric acid in solution (model 3 in Table 5.3). The solid, long-dashed, dashed-dotted and short-dashed lines correspond to 0, 4.8, 143 and 1285  $\mu\text{M}$  total Cu, respectively.

## 5.5 Discussion and Conclusions

The pH-dependent binding of  $\text{Zn}^{2+}$  to cells of *S. putrefaciens* indicates that carboxylate and phosphate functional groups are the likely metal binding sites in the cell wall (see also, Plette et al., 1995; Fein et al., 1997; Haas et al., 2001). The  $\text{Cu}^{2+}$  binding data further suggest

that a small proportion (5-10 %) of the carboxylate groups exhibit enhanced affinity for metal cations. High affinity sites have been invoked to explain binding of a variety of metals, especially  $\text{Cu}^{2+}$ , to humic substances and live algal cells (Benedetti et al., 1995; Gonzalez-Davila et al., 1995; Tipping et al., 2002). The effect of the high affinity sites on  $\text{Cu}^{2+}$  binding to *S. putrefaciens* is most pronounced at low dissolved metal concentrations ( $\leq 1 \mu\text{M}$ ), that is, under conditions typically encountered in environmental settings.

Live microorganisms are known to release organic compounds to the surrounding solution. The release of polysaccharides, polypeptides and siderophores by algal cells, for instance, has been well documented (Xue and Sigg, 1990; Vasconcelos et al., 2002). While difficult to avoid when working with live cells, the presence of these organic exudates affects the chemical speciation of aqueous metals and, hence, metal binding to the cell wall. In the experiments carried out in this study, the competition between binding to the cell wall and organic ligands in solution causes a reversal in the pH dependence of  $\text{Cu}^{2+}$  binding at low versus high dissolved metal concentrations (Fig. 5.6). As a consequence, at dissolved  $\text{Cu}^{2+}$  concentrations  $\leq 1 \mu\text{M}$ , increasing pH actually decreases binding to *S. putrefaciens* in the pH range 4-7. The organic ligands most likely competing with cell wall functional groups for the metal cations are small organic acids released by bacterial metabolism (Lin et al., 2005; Sanchez et al., 2005; Claessens et al., 2006a).

When solution speciation effects and the presence of high affinity carboxylate sites are taken into account, a two-site (carboxylate plus phosphate sites) cell wall complexation model is able to consistently explain the binding trends of  $\text{Zn}^{2+}$  and  $\text{Cu}^{2+}$  over wide ranges of aqueous metal concentration and pH, in both one- and two-metal systems. In particular, the model predicts pronounced differences in the cell wall and solution complexation behavior of the two metals (Fig. 5.9). It must be kept in mind, however, that the affinity constants of  $\text{Zn}^{2+}$  and  $\text{Cu}^{2+}$  binding to the cell wall functional groups reported here are model-dependent fitting parameters. In order to better constrain these constants, further work is needed to reduce the uncertainties associated with the density and acidity of the high affinity sites, as well as the binding capacities and metal complexation constants of the dissolved organic ligands released by the cells.

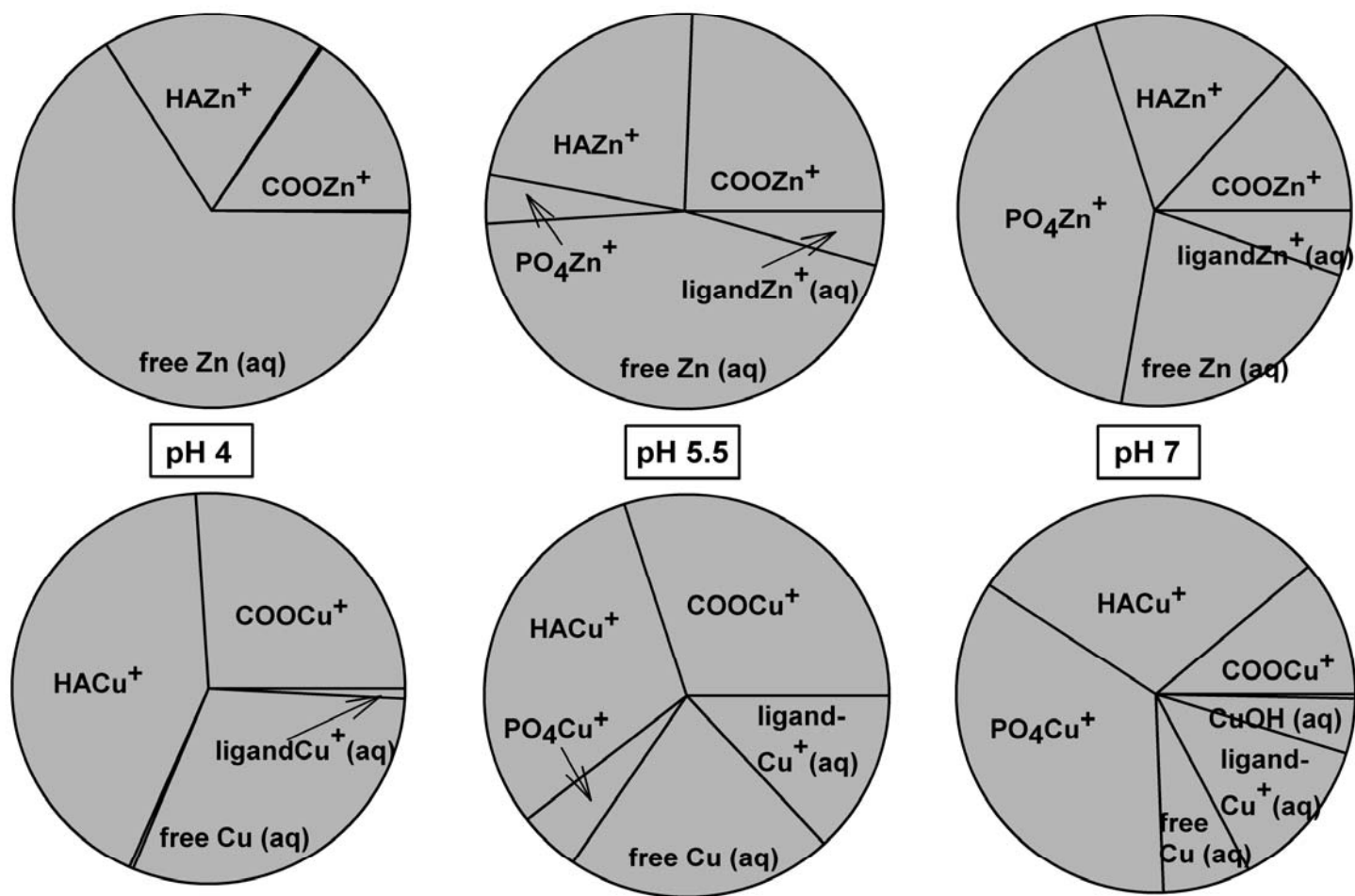


**Figure 5.9:** Chemical speciation of Zn and Cu in  $7 \times 10^8$  cells  $\text{ml}^{-1}$  suspensions of *S. putrefaciens* (150 mM NaCl) as a function of pH, according to model 3 in Table 5.3. The total concentrations of the metals are 51  $\mu\text{M}$ .

The upward trend of  $\text{Cu}^{2+}$  binding observed for the highest dissolved  $\text{Cu}^{2+}$  concentrations at pH 7 (Fig. 5.2C) cannot be reproduced by any of the complexation models presented. A likely explanation is that under these conditions part of the  $\text{Cu}^{2+}$  removal from solution is due to the precipitation of Cu oxide phases. At pH 7, already 1  $\mu\text{M}$  dissolved  $\text{Cu}^{2+}$  is sufficient to create supersaturation with respect to tenorite ( $\log K_{\text{sp}} = 7.65$ , Stumm and Morgan, 1996). Similarly, the small effect on  $\text{Zn}^{2+}$  binding observed when the total  $\text{Cu}^{2+}$  concentration is increased from 148 to 1285  $\mu\text{M}$  may, possibly, be due to mineral precipitation or binding of  $\text{Cu}^{2+}$  to the experimental tubes (section 5.2.2) at the highest  $\text{Cu}^{2+}$  concentration.

The  $\text{Cu}^{2+}$  and  $\text{Zn}^{2+}$  binding data can be reproduced without explicitly invoking electrostatic corrections in the cell wall. This contrasts with existing models for bacterial cell wall charging and metal binding, which usually include electrostatic correction terms (e.g., Fein et al., 1997; Daughney et al., 2001; Haas et al., 2001; Claessens et al., 2006a). For example, the cell wall charging of *S. putrefaciens* as a function of pH due to reactions 5.1-5.3 has been successfully reproduced using the constant capacitance model, with a capacitance of  $5 \text{ F m}^{-2}$ , a total cell wall functional group density of  $6.5 \times 10^{-16} \text{ mol cell}^{-1}$ , and a specific surface area of  $55 \text{ m}^2 \text{ g}^{-1}$  (Claessens et al., 2006a). The high value of the specific surface area used ( $55 \text{ m}^2 \text{ g}^{-1}$ , Haas et al., 2001) has recently been questioned, however. Based on a wet cell mass of  $2 \times 10^{-12} \text{ g cell}^{-1}$  for *S. putrefaciens*, a much lower value of  $2.7 \text{ m}^2 \text{ g}^{-1}$  appears more realistic (Claessens et al., 2006a). In order to reproduce the observed cell wall charge as a function of pH, a much higher capacitance ( $\geq 30 \text{ F m}^{-2}$ ) must then be applied (results not shown). Such high capacitance implies that electrostatic interactions in the cell wall are relatively weak. This agrees with the small effect of variations in salt concentrations on the charging behavior of isolated bacterial cell walls (Plette et al., 1995).

The affinity constants in Table 5.3 imply stronger binding of  $\text{Cu}^{2+}$  to the cell wall sites of *S. putrefaciens* compared to  $\text{Zn}^{2+}$ , as also observed for humic substances (Tipping et al., 2002; Weng et al., 2002). Enhanced binding of  $\text{Cu}^{2+}$  to the cell wall is consistent with the binding isotherms observed at pH 4 and 5.5 (Figs. 5.2A and B), and the competitive effects in two-metal systems (Figs. 5.7 and 5.8). At pH 4, and low dissolved metal concentrations ( $\leq 1 \mu\text{M}$ ), the data and model calculations indicate that almost all  $\text{Cu}^{2+}$  is bound to the cells, while a large fraction of  $\text{Zn}^{2+}$  remains in solution as free metal ions. This behavior is not unlike that

observed in surficial sediments of acidic lakes, where lower pore water Cu concentrations, relative to Zn, have been explained by stronger complexation of Cu to sediment organic matter (Tessier et al., 1996).

Despite the higher affinity constants of  $\text{Cu}^{2+}$  for cell wall functional groups, at neutral pH the binding isotherms of both metals to *S. putrefaciens* are similar, at least for dissolved metal concentrations up to 10  $\mu\text{M}$  (Fig. 5.2C), because of the efficient competition of dissolved organic and inorganic ligands for  $\text{Cu}^{2+}$  (Fig. 5.9). Thus, even in relatively simple experimental systems competing complexation reactions may lead to a complex pH dependence of metal binding to cells. In natural environments, the greater tendency of  $\text{Cu}^{2+}$  to associate with the cell walls of living microorganisms may further be offset by its affinity for binding to non-living particulate materials, especially detrital organic matter (Tessier et al., 1996; Tipping et al., 2002; Weng et al., 2002).

### **Acknowledgments**

Dr. T. Behrends and dr. M. Wolthers are acknowledged for discussions on metal binding and surface complexation modeling. E. van Vilsteren is acknowledged for performing ICP-MS analyses. This research was financially supported by the Netherlands Organization for Scientific Research (NWO-Pionier Award).

---

---

## References

- Agraz R., van der Wal A., van Leeuwen H.P. (1994) Voltammetric study of the interaction of cadmium with bacterial cells, *Bioelectrochem. Bioenerg.* **34**, 53-59.
- Andrews J.A., Schlesinger W.H. (2001) Soil CO<sub>2</sub> dynamics, acidification, and chemical weathering in a temperate forest with experimental CO<sub>2</sub> enrichment, *Global Biogeochem. Cycles* **15**, 149-162.
- Appenzeller B.M.R., Duval Y.B., Thomas F., Block J.-C. (2002) Influence of phosphate on bacterial adhesion onto iron oxyhydroxide in drinking water, *Environ. Sci. Technol.* **36**, 646-652.
- Avena M.J., Koopal L.K., van Riemsdijk W.H. (1999) Proton binding to humic acids: Electrostatic and intrinsic interactions, *J. Colloid Interface Sci.* **217**, 37-48.
- Bargar J.R., Brown Jr. G.E., Parks G.A. (1997) Surface complexation of Pb (II) at oxide-water interfaces: II XAFS and bond-valence determination of mononuclear Pb (II) sorption products and surface functional groups on iron oxides, *Geochim. Cosmochim. Acta* **61**, 2639-2652.
- Bell P.E., Mills A.L., Herman J.S. (1987) Biogeochemical conditions favoring magnetite formation during anaerobic iron reduction, *Appl. Environ. Microbiol.* **53**, 2610-2616.
- Benderitter M., Vincent-Genod L., Pouget J.P., Voisin P. (2003) The cell membrane as a biosensor of oxidative stress induced by radiation exposure: A multiparameter investigation, *Radiat. Res.* **159**, 471-483.
- Benedetti M.F., Milne C.J., Kinniburgh D.G., van Riemsdijk W.H., Koopal L.K. (1995) Metal ion binding to humic substances: Application of the non-ideal competitive adsorption model, *Environ. Sci. Technol.* **29**, 446-457.
- Bennett P.C., Rogers J.R., Choi W.J., Hiebert F.K. (2001) Silicates, silicate weathering, and microbial ecology, *Geomicrobiol. J.* **18**, 3-19.
- Bento F.M., Camargo F.A.O., Okeke B.C., Frankenberger W.T. (2005) Comparative bioremediation of soils contaminated with diesel oil by natural attenuation, biostimulation and bioaugmentation, *Bioresour. Technol.* **96**, 1049-1055.
- Beveridge T.J., Murray H.G.E. (1980) Sites of metal deposition in the cell wall of *Bacillus subtilis*, *J. Bacteriol.* **141**, 876-887.

- Borrok D.M., Fein J.B. (2005) The impact of ionic strength on the adsorption of protons, Pb, Cd, and Sr onto the surfaces of Gram negative bacteria: testing non-electrostatic, diffuse, and triple-layer models, *J. Colloid Interface Sci.* **286**, 110-126.
- Chou L., Garrels R.M., Wollast R. (1989) Comparative study of the kinetics and mechanisms of dissolution of carbonate minerals, *Chem. Geol.* **78**, 269-282.
- Claessens J., Behrends T., Van Cappellen P. (2004) What do acid-base titrations of live bacteria tell us? A preliminary assessment, *Aquat. Sci.* **66**, 19-26.
- Claessens J., van Lith Y., Laverman A.M., Van Cappellen P. (2006a) Acid-base activity of live bacteria: Implications for quantifying cell wall charge, *Geochim. Cosmochim. Acta* **70**, 267-276.
- Claessens J., Laverman A.M., van Lith Y., Van Cappellen P. (2006b) Response of *Shewanella putrefaciens* to pH stress and possible geochemical implications, submitted to *Geomicrobiol. J.*
- Clark D.P. (1989) The fermentation pathways of *Escherichia coli*, *FEMS Microbiol. Rev.* **63**, 223-234.
- Cox J.S., Smith D.S., Warren L.A., Ferris F.G. (1999) Characterizing heterogeneous bacterial surface functional groups using discrete affinity spectra for proton binding, *Environ. Sci. Technol.* **33**, 4514-4521.
- Cubillas P., Kohler S., Prieto M., Chairat C., Oelkers E.H. (2005) Experimental determination of the dissolution rates of calcite, aragonite, and bivalves, *Chem. Geol.* **216**, 59-77.
- Daughney C.J., Fein J.B. (1998) The effect of ionic strength on the adsorption of H<sup>+</sup>, Cd<sup>2+</sup>, Pb<sup>2+</sup> and Cu<sup>2+</sup> by *Bacillus subtilis* and *Bacillus licheniformis*: A surface complexation model, *J. Colloid Interface Sci.* **198**, 53-77.
- Daughney C.J., Fein J.B., Yee N. (1998) A comparison of the thermodynamics of metal adsorption onto two common bacteria, *Chem. Geol.* **144**, 161-176.
- Daughney C.J., Fowle D.A., Fortin D. (2001) The effect of growth phase on proton and metal adsorption by *Bacillus subtilis*, *Geochim. Cosmochim. Acta* **65**, 1025-1035.
- DiChristina T.J. (1989) Dissimilative iron (III) reduction by *Alteromonas putrefaciens* strain 200, PhD thesis. California Institute of Technology, Pasadena, CA, USA, 192 pp.
- Donlan R.M., Pipes W.O., Yohe T.L. (1994) Biofilm formation on cast iron substrata in water distribution systems, *Wat. Res.* **28**, 1497-1503.

- 
- Dzombak D.A., Morel F.M.M. (1990) *Surface Complexation Modeling. Hydrous Ferric Oxide*, Wiley & Sons, NY.
- Fein J.B., Daughney C.J., Yee N., Davis T.A. (1997) A chemical equilibrium model for metal adsorption onto bacterial surfaces, *Geochim. Cosmochim. Acta* **61**, 3319-3328.
- Fein J.B., Boily J.-F., Yee N., Gorman-Lewis D., Turner B.F. (2005) Potentiometric titrations of *Bacillus subtilis* cells to low pH and a comparison of modeling approaches, *Geochim Cosmochim Acta* **69**, 1123-1132.
- Fowle D.A., Fein J.B. (1999) Competitive adsorption of metal cations onto two gram positive bacteria: Testing the chemical equilibrium model, *Geochim. Cosmochim. Acta* **63**, 3059-3067.
- Fowle D.A., Fein J.B. (2000) Experimental measurements of the reversibility of metal-bacteria adsorption reactions, *Chem. Geol.* **168**, 27-36.
- Fowle D.A., Fein J.B., Martin A.M. (2000) Experimental study of uranyl adsorption onto *Bacillus subtilis*, *Environ. Sci. Technol.* **34**, 3737-3741.
- Gelabert A., Pokrovsky O.S., Schott J., Boudou A., Feurtet-Mazel A., Mielczarski J., Mielczarski E., Mesmer-Dudons N., Spalla O. (2004) Study of diatoms/aqueous solution interface. I. Acid-base equilibria and spectroscopic observation of freshwater and marine species, *Geochim Cosmochim Acta* **68**, 4039-4058.
- Goncalves M.L.S., Sigg L., Reutlinger M., Stumm W. (1987) Metal ion binding by biological surfaces: voltammetric assessment in the presence of bacteria, *Sci. Total Environ.* **60**, 105-119.
- Gonzalez-Davila M., Santana-Casiano J.M., Perez-Pena J., Millero F.J. (1995) Binding of Cu (II) to the surface and exudates of the alga *Dunaliella tertiolecta* in seawater, *Environ. Sci. Technol.* **29**, 289-301.
- Greenstock C.L. (1981) Redox processes in radiation biology and cancer, *Radiat. Res.* **86**, 196-211.
- Gurbuz F., Ciftci H., Akcil A., Karahan A.G. (2004) Microbial detoxification of cyanide solutions: a new biotechnological approach using algae, *Hydrometallurgy* **72**, 167-176.
- Gustafsson J.P., Pechova P., Berggren D. (2003) Modeling metal binding to soils: The role of natural organic matter, *Environ. Sci. Technol.* **37**, 2767-2774.
-

- Haas J.R., Dichristina T.J., Wade Jr. R. (2001) Thermodynamics of U (VI) sorption onto *Shewanella putrefaciens*, *Chem. Geol.* **180**, 33-54.
- Haas J.R. (2004) Effects of cultivation conditions on acid-base titration properties of *Shewanella putrefaciens*, *Chem. Geol.* **209**, 67-81.
- Hiebert F.K., Bennett P.C. (1992) Microbial control of silicate weathering in organic-rich ground water, *Nature* **258**, 278-281.
- Hiemstra T., van Riemsdijk W.H. (1996) A surface structural approach to ion adsorption: The charge distribution (CD) model, *J. Colloid Interface Sci.* **179**, 488-508.
- Jansson P.E. (1999) The chemistry of O-polysaccharide chains in bacterial lipopolysaccharides. In *Endotoxin in Health and Disease* (eds. H. Brade, S.M. Opal, S.N. Vogel, D.C. Morrison), Marcel Dekker, Inc., New York. pp. 155-178.
- Jourabchi P., Van Cappellen P., Regnier P. (2005) Quantitative interpretation of pH distributions in aquatic sediments: A reaction-transport modeling approach, *Amer. J. Sci.* **305**, 919-956.
- Kelly S.D., Kemner K.M., Fein J.B., Fowle D.A., Boyanov M.I., Bunker B.A., Yee N. (2002) X-ray absorption fine structure determination of pH-dependent U-bacterial cell wall interactions, *Geochim. Cosmochim. Acta* **66**, 3855-3871.
- Kim S.-J., Choi D.H., Sim D.S., Oh Y.-S. (2005) Evaluation of bioremediation effectiveness on crude oil-contaminated sand, *Chemosphere* **59**, 845-852.
- Kinniburgh D.G., Milne C.J., Benedetti M.F., Pinheiro J.P., Filius J., Koopal L.K., van Riemsdijk W.H. (1996) Metal ion binding by humic acid: Application of the NICA-Donnan model, *Environ. Sci. Technol.* **30**, 1687-1698.
- Leammler U.K. (1970) Cleavage of structural proteins during assembly of the head bacteriophage T4, *Nature* **227**, 680-685.
- Lin G., Bennett G.N., San K.-Y. (2005) Chemostat culture characterization of *Escherichia coli* mutant strains metabolically engineered for aerobic succinate production: A study of the modified metabolic network based on metabolite profile, enzyme activity, and gene expression profile, *Metabol. Eng.* **7**, 337-352.
- Liu C., Zachara J.M., Gorby Y.A., Szecsody J.E., Brown C.F. (2001) Microbial reduction of Fe (III) and sorption/precipitation of Fe (II) on *Shewanella putrefaciens* strain CN32, *Environ. Sci. Technol.* **35**, 1385-1393.

- 
- Lovley D.R., Phillips E.J.P. (1988) Novel mode of microbial energy metabolism: organic carbon oxidation coupled to dissimilatory reduction of iron or manganese, *Appl. Environ. Microbiol.* **54**, 1472-1480.
- Lovley D.R., Phillips E.J.P., Gorby Y.A., Landa E.R. (1991) Microbial reduction of uranium, *Nature* **350**, 413-416.
- Madigan T.M., Martinko J.M., Parker J. (1997) *Biology of Microorganisms* (ed. T.D. Brock), Prentice Hall International, Inc., New Jersey.
- Mirimanoff N., Wilkinson K.J. (2000) Regulation of Zn accumulation by a freshwater Gram-positive bacterium (*Rhodococcus opacus*), *Environ. Sci. Technol.* **34**, 616-622.
- Newman D.K., Banfield J.F. (2002) Geomicrobiology: How molecular-scale interactions underpin biogeochemical systems, *Science* **296**, 1071-1077.
- Obuekwe C.O., Westlake D.W.S. (1982) Effect of reducible compounds (potential electron acceptors) on reduction of ferric iron by *Pseudomonas* species, *Microbios Lett.* **19**, 57-62.
- Pinchuk I.V., Bressollier P., Sorokulova I.B., Verneuil B., Urdaci M.C. (2002) Amicoumacin antibiotic production and genetic diversity of *Bacillus subtilis* strains isolated from different habitats, *Res. Microbiol.* **153**, 269-276.
- Plette A.C.C., van Riemsdijk W.H., Benedetti M.F., van der Wal A. (1995) pH dependent charging behavior of isolated cell walls of a Gram-positive bacterium, *J. Colloid Interface Sci.* **173**, 354-363.
- Plette A.C.C., Benedetti M.F., van Riemsdijk W.H. (1996) Competitive binding of protons, calcium, cadmium, and zinc to isolated cell walls of a Gram-positive soil bacterium, *Environ. Sci. Technol.* **30**, 1902-1910.
- Prescott L.M., Harley J.P., Klein D.A. (1996) *Microbiology*, Wm. C. Brown Publishers.
- Quesnel D., Nakhla G. (2005) Optimization of the aerobic biological treatment of thermophilically treated refractory wastewater, *J. Hazard. Mater.* **B125**, 221-230.
- Rius N., Sole M., Loren J.G. (1998) Acid-base response of bacterial suspensions, *J. Ind. Microbiol. Biotech.* **21**, 65-74.
- Roden E.E., Zachara J.M. (1996) Microbial reduction of crystalline iron (III) oxides: Influence of oxide surface area and potential for cell growth, *Environ. Sci. Technol.* **30**, 1618-1628.
-

- Roden E.E., Wetzel R.G. (2002) Kinetics of microbial Fe (III) oxide reduction in freshwater wetland sediments, *Limnol. Oceanogr.* **47**, 198-211.
- Sanchez A.M., Bennett G.N., San K.-Y. (2005) Novel pathway engineering design of the anaerobic central metabolic pathway in *Escherichia coli* to increase succinate yield and productivity, *Metabol. Eng.* **7**, 229-239.
- Scanlan D.J., West N.J. (2002) Molecular ecology of the marine cyanobacterial genera *Prochlorococcus* and *Synechococcus*, *FEMS Microbiol. Ecol.* **40**, 1-12.
- Schlegel H.G. (1986) *General Microbiology*, Cambridge University Press, Cambridge.
- Schlesinger W.H. (1997) *Biogeochemistry: an analysis of global change*, Academic Press, San Diego, California.
- Schultze-Lam S., Fortin D., Davis B.S., Beveridge T.J. (1996) Mineralization of bacterial surfaces, *Chem. Geol.* **132**, 171-181.
- Semple K.M., Westlake D.W.S. (1987) Characterization of iron-reducing *Alteromonas putrefaciens* strains from oil field fluids, *Can. J. Microbiol.* **33**, 366-371.
- Sokolov I., Smith D.S., Henderson G.S., Gorby Y.A., Ferris F.G. (2001) Cell surface electrochemical heterogeneity of the Fe (III) reducing bacteria *Shewanella putrefaciens*, *Environ. Sci. Technol.* **35**, 341-347.
- Stumm W., Morgan J.J. (1996) *Aquatic Chemistry: Chemical equilibria and rates in natural waters*, John Wiley & Sons, New York.
- Tessier A., Fortin D., Belzile N., DeVitre R.R., Leppard G.G. (1996) Metal sorption to diagenetic iron and manganese oxyhydroxides and associated organic matter: Narrowing the gap between field and laboratory measurements, *Geochim. Cosmochim. Acta* **60**, 387-404.
- Thullner M., Van Cappellen P., Regnier P. (2005) Modeling the impact of microbial activity on redox dynamics in porous media, *Geochim. Cosmochim. Acta* **69**, 5005-5019.
- Tipping E., Rey-Castro C., Bryan S.E., Hamilton-Taylor J. (2002) Al (III) and Fe (III) binding by humic substances in freshwaters, and implications for trace metal speciation, *Geochim. Cosmochim. Acta* **66**, 3211-3224.
- Toner B., Manceau A., Webb S.M., Sposito G. (2006) Zinc sorption to biogenic hexagonal-birnessite particles within a hydrated bacterial biofilm, *Geochim. Cosmochim. Acta* **70**, 27-43.

- Tsai C.M., Frasch C.E. (1982) A sensitive silver stain for detecting lipopolysaccharides in polyacrylamide gels, *Anal. Biochem.* **119**, 115-119.
- Tziotzios G., Teliou M., Kaltsouni V., Lyberatos G., Vayenas D.V. (2005) Biological phenol removal using suspended growth and packed bed reactors, *Biochem. Eng. J.* **26**, 65-71.
- Urrutia Mera M., Kemper M., Doyle R., Beveridge T.J. (1992) The membrane-induced proton motive force influences the metal binding ability of *Bacillus subtilis* cell walls, *Appl. Environ. Microbiol.* **58**, 3837-3844.
- Van Cappellen P., Wang Y. (1996) Cycling of iron and manganese in surface sediments: A general theory for the coupled transport and reaction of carbon, oxygen, nitrogen, sulfur, iron and manganese, *Am. J. Sci.* **296**, 197-243.
- Van Cappellen P., Viollier E., Roychoudhury A.N., Clark L., Ingall E., Lowe K., DiChristina T. (1998) Biogeochemical cycles of manganese and iron at the oxic-anoxic transition of a stratified basin (Orca Basin, Gulf of Mexico), *Environ. Sci. Technol.* **32**, 2931-2939.
- Van der Wal A., Norde W., Zehnder A.J.B., Lyklema J. (1997a) Determination of the total charge in the cell walls of Gram-positive bacteria, *Colloids Surf. B Biointerfaces* **9**, 81-100.
- Van der Wal A., Minor M., Norde W., Zehnder A.J.B., Lyklema J. (1997b) Electrokinetic potential of bacterial cells, *Langmuir* **13**, 165-171.
- Vasconcelos M.T.S.D., Leal M.F.C., van den Berg C.M.G. (2002) Influence of the nature of the exudates released by different marine algae on the growth, trace metal uptake and exudation of *Emiliania huxleyi* in natural seawater, *Mar. Chem.* **77**, 187-210.
- Venkateswaran K., Moser D.P., Dollhopf M.E., Lies D.P., Saffarini D.A., MacGregor B.J., Ringelberg D.B., White D.C., Nishijima M., Sano H., Burghardt J., Stackebrandt E., Nealson K.H. (1999) Polyphasic taxonomy of the genus *Shewanella* and description of *Shewanella oneidensis* sp. Nov., *Int. J. Syst. Biol.* **49**, 705-724.
- Welch S.A., Ullman W.J. (1993) The effect of organic acids on plagioclase dissolution rates and stoichiometry, *Geochim. Cosmochim. Acta* **57**, 2725-2736.
- Weng L., Temminghoff E.J.M., Lofts S., Tipping E., van Riemsdijk W.H. (2002) Complexation with dissolved organic matter and solubility control of heavy metals in a sandy soil, *Environ. Sci. Technol.* **36**, 4804-4810.

- Winkler J., Cherry R.S., Schlesinger W.H. (1996) The  $Q_{10}$  relationship of microbial respiration in a temperate forest soil, *Soil Biol. Biochem.* **28**, 1067-1072.
- Xue H., Sigg L. (1990) Binding of Cu (II) to algae in a metal buffer, *Wat. Res.* **24**, 1129-1136.
- Xue H., Sigg L. (1999) Comparison of the complexation of Cu and Cd by humic or fulvic acids and by ligands observed in lake waters, *Aquat. Geochem.* **5**, 313-355.
- Yee N., Fein J. (2001) Cd adsorption onto bacterial surfaces: A universal adsorption edge? *Geochim. Cosmochim. Acta* **65**, 2037-2042.

---

# Summary

---

To gain insight into the surface chemistry of live microorganisms, pH stat experiments are combined with analyses of the time-dependent changes in solution chemistry using suspensions of live cells of *Shewanella putrefaciens*. The results of this study illustrate the complex response of the live cells to changes in pH of the aqueous medium. In particular, the observed acid-base activity of the organism cannot be attributed solely to the protonation or deprotonation reactions of functional groups in the cell wall. Time-dependent acid and base consumption curves by the bacterial cells are interpreted to consist of the following three contributions. (1) The near-instantaneous (time scale of minutes) buffering capacity associated with the functional groups present in the cell wall, (2) the short-term (< 1 hour) utilization of the intracellular buffering capacity, and (3), under basic conditions, the long-term (1-5 hours) release of (acidic) metabolic byproducts.

By measuring the initial acid or base consumption at different pH values, the buffering capacity associated with the functional groups in the cell wall can be determined as a function of the pH of the medium. The functional group concentrations and the pH dependent cell wall charges inferred from the pH stat experiments for *S. putrefaciens* and *B. subtilis* are in general agreement with those obtained in previous studies using continuous titrations. Lipopolysaccharides (LPS), the major constituent of the outermost layer of the cell wall of Gram-negative bacteria, contribute little to the buffering capacity of the intact cell wall. Comparing the buffering capacities of the cell walls of live cells to that of cell wall components show that, while LPS may be important in regulating cell adhesion of Gram-negative bacteria, they may not provide many anionic binding sites for metal cations. The latter must therefore migrate deeper inside the cell wall. The relatively minor buffering capacity associated with LPS may also explain the very similar cell wall charging behavior of *S. putrefaciens* and *B. subtilis*.

The main sources of acidity that explain the long-term base neutralizing capacity of live cells of *S. putrefaciens* are release of organic acids and dissolution of metabolically produced CO<sub>2</sub>. The redox, pH and temperature conditions regulate the type and rates of excreted metabolic products since each microorganism functions at an optimum pH and temperature. The observed release of acids under basic conditions may have important implications for the activity of live microorganisms in natural environments. For instance, by releasing protons, metal reducing bacteria, such as *S. putrefaciens*, may compensate for the

proton consumption due to metal reduction, thereby maintaining favorable conditions for metal reduction in their immediate vicinity. Protons and organic acids released by microorganisms may also significantly affect the weathering of silicate and carbonate minerals in soils and groundwater environments.

Combining the results of the initial part of the acid-base consumption curves in the pH stat experiments with  $Zn^{2+}$  and  $Cu^{2+}$  binding experiments provides information about the surface chemistry of the cell walls. Carboxylate and phosphate groups are identified as the major sites for metal binding to *S. putrefaciens*. The binding isotherms of  $Cu^{2+}$  are best explained by invoking the presence of a small percentage of high affinity carboxylate sites in the cell wall. Using a simple cell wall complexation model shows that metal binding to cell wall functional groups is sensitive to metal complexation reactions of organic acids in solution, as well as to the acidity of high affinity sites in the cell wall. Characterization of the affinity of the organic ligands, released by cellular activity, for metal ions is needed to better constrain the affinity constants of cell wall functional groups for metal ions. The modeling results also illustrate that the charging behavior of bacterial cell walls differs fundamentally from that of mineral surfaces. While electrostatic interactions play a key role in the surface chemistry of mineral surfaces, they are relatively small in bacterial cell walls.

From this study we can conclude that the acid-base behavior of live microorganisms involves both passive and active processes. Acid-base and metal binding properties of live microorganisms are affected by the cellular activity of the microorganisms. Using surface complexation models to derive affinity constants for proton and metal binding to cell wall functional groups should take into account (1) the release of organic ligands due to microbial activity, and (2) the fundamental differences between mineral and microbial surfaces, especially electrostatic interactions. The results of this study imply that microbial surfaces may have a large effect on metal ion mobility in natural waters. Furthermore, acid release by live microorganisms may significantly influence biogeochemical processes such as reductive and non-reductive mineral dissolution reactions.

---

---

# Samenvatting

---

Om inzicht te krijgen in de oppervlaktechemie van levende microorganismen zijn pH-stat experimenten uitgevoerd. Hierbij zijn de tijdsafhankelijke veranderingen in de chemie van waterige milieus bestudeerd. In dit onderzoek is gebruik gemaakt van levende cellen van *Shewanella putrefaciens*. De resultaten van deze studie illustreren de complexe reacties van levende cellen op veranderingen van de pH in waterige milieus. De waargenomen zuur-base activiteit van *S. putrefaciens* kan niet alleen worden toegeschreven aan protonerings- en deprotonerings-reacties van functionele groepen in de celwand. Tijdsafhankelijke zuur- en base-consumptiecurven van de levende cellen blijken te bestaan uit de volgende drie bijdragen. (1) De initiële buffercapaciteit van de celwand (tijdschaal van minuten). Deze is geassocieerd met de functionele groepen in de celwand. (2) Het korte-termijn (< 1 uur) gebruik van de intracellulaire buffercapaciteit. (3) Het lange-termijn (1-5 uur) uitscheiden van zure metabolische producten onder basische omstandigheden.

Door het meten van de initiële zuur- of base-consumptie bij verschillende pH-waarden, kan de buffercapaciteit die geassocieerd is met de functionele groepen in de celwand bepaald worden als functie van de pH van het waterige milieu. De concentratie van functionele groepen in de celwand en de pH-afhankelijke celwandlading zijn afgeleid van de pH-stat experimenten die zijn uitgevoerd met *S. putrefaciens* en *B. subtilis*. Deze komen over het algemeen overeen met wat is bepaald in eerdere studies waar gebruik is gemaakt van continue titraties. De lipopolysacchariden (LPS), die de belangrijkste component in de buitenste laag van de celwand van Gram-negatieve bacteriën zijn, dragen weinig bij aan de buffercapaciteit van de intacte celwand. Het vergelijken van de buffercapaciteiten van de celwanden van levende cellen en celwandcomponenten laat zien dat, hoewel LPS belangrijk kan zijn voor aanhechting van Gram-negatieve bacteriën aan oppervlakken, LPS niet veel bindingsplaatsen heeft voor metaal-ionen. Metaal-ionen moeten daarom dieper in de celwand migreren. De relatief kleine buffercapaciteit die geassocieerd is met de LPS kan ook het vergelijkbare celwandladingsgedrag van *S. putrefaciens* en *B. subtilis* verklaren.

De belangrijkste bron van zure componenten die de lange-termijn basische neutraliseringsreacties door levende cellen van *S. putrefaciens* kan verklaren is het uitscheiden van organische zuren en het oplossen van metabolisch geproduceerd CO<sub>2</sub>. De redox-, pH- en temperatuur-condities reguleren de snelheid van de metaboliseringsreacties en ook de aard van de uitgescheiden metabolische producten, omdat ieder organisme optimaal

functioneert bij een bepaalde pH en temperatuur. De waargenomen produktie van zuren onder basische omstandigheden zou belangrijke implicaties kunnen hebben voor de activiteit van levende microorganismen in natuurlijke milieus. Metaalreducerende bacteriën, zoals *S. putrefaciens* zouden bijvoorbeeld, door het uitscheiden van protonen, de protonconsumptie als gevolg van metaalreductie kunnen compenseren. Zij zouden daarbij de condities voor metaalreductie in hun directe omgeving gunstig kunnen beïnvloeden. Protonen en organische zuren die worden uitgescheiden door microorganismen kunnen ook een significant effect hebben op de verwerking van silicaat- en carbonaat-mineralen in bodems en grondwater milieus.

Door het combineren van de resultaten van het initiële deel van de zuur-base consumptiecurven in de pH-stat experimenten met  $Zn^{2+}$  en  $Cu^{2+}$  bindingsexperimenten kan informatie worden verkregen over de oppervlaktechemie van de celwanden. In deze studie zijn carboxylaat- en fosfaatgroepen geïdentificeerd als de belangrijkste bindingsplaatsen voor metaalbinding aan *S. putrefaciens*. De bindingsisothermen van  $Cu^{2+}$  kunnen worden verklaard door de aanwezigheid van een klein percentage carboxylaat-bindingsplaatsen met een hoge affiniteit voor metalen. Door gebruik te maken van een celwand-complexerings model kan aangetoond worden dat de metaalbinding aan functionele groepen in de celwand niet alleen gevoelig is voor metaalcomplexerings reacties met organische zuren in de oplossing, maar ook voor de protonering van hoge-affiniteit carboxylaat-bindingsplaatsen. Karakterisering van de affiniteit van de organische zuren, geproduceerd door celmetabolismen, voor metaalionen is dan ook noodzakelijk om de affiniteit van de functionele groepen in de celwand voor metaalionen nauwkeuriger te kunnen bepalen. De resultaten van de modelstudie laten ook zien dat het ladingsgedrag van de bacteriële celwanden fundamenteel anders is dan dat van mineraaloppervlakken. Waar de oppervlaktechemie van mineralen wordt bepaald door elektrostatische interacties aan het oppervlak, zijn deze relatief onbelangrijk in de celwanden van bacteriën.

Uit deze studie kunnen we concluderen dat actieve en passieve processen een rol spelen in het zuur-base gedrag van levende microorganismen. Zuur-base- en metaalbindings-eigenschappen van levende microorganismen worden beïnvloed door het metabolisme van de microorganismen. Bij het gebruik van oppervlakte-complexerings-modellen om affiniteitsconstanten af te leiden voor proton- en metaalbinding aan de celwand moet rekening

worden gehouden met (1) De produktie van organische zuren als een gevolg van microbiële activiteit. (2) De fundamentele verschillen tussen microbiële- en mineraaloppervlakken en in het bijzonder de elektrostatische interacties die hierbij een rol spelen. De resultaten van deze studie laten zien dat microbiële oppervlakken een groot effect kunnen hebben op metaalion-mobiliteit in natuurlijke waterige milieus. Tenslotte kan de zuurproduktie door levende microorganismen een significant effect hebben op biogeochemische processen zoals reductieve en niet-reductieve mineraal-oplossingsreacties.

## Dankwoord

Na ruim 4 jaar hard werken is er dan toch een einde gekomen aan mijn onderzoek. Met heel veel plezier heb ik gewerkt aan dit project waarvan ik zelf enorm veel heb geleerd. Veel mensen hebben op allerlei manieren bijgedragen aan het resultaat dat hier nu ligt en die zou ik graag willen bedanken.

First, I would like to thank my promotor Philippe Van Cappellen for giving me the opportunity to work on this project. Discussions with you were always very inspiring and motivating. After our discussions there were always plenty or even too many ideas to continue with my work.

Vervolgens zijn er veel mensen die meer betrokken zijn geweest bij de dagelijkse besommingen van mijn onderzoek. Als eerste zou ik graag Thilo Behrends willen bedanken die een belangrijke rol heeft gespeeld bij het opstarten van het project. Vervolgens wil ik Anniet Laverman en Yvonne van Lith hartelijk bedanken voor hun bijdrage aan de meer microbiologische aspecten van het onderzoek. Ook zou ik graag Mariette Wolthers willen bedanken voor de discussies in de laatste maanden van het onderzoek. Dit heeft me erg geholpen om ook nog het laatste hoofdstuk op tijd af te krijgen. I would also like to thank Pierre Regnier for helping me with the general introduction in the last weeks. Rick Canavan, Socratis Loucaides and Vasso Alexandratos are thanked for helping me with English writing over the last years. En als laatste wil ik graag Pieter Kleingeld hartelijk bedanken voor het corrigeren van de Nederlandse teksten in het boekje.

Bij het uitvoeren van de vele experimenten heb ik onmisbare hulp gehad van een aantal mensen. Ik wil Pieter Kleingeld, Dineke van der Meent, Gijs Nobbe, Berthil van Os en Helen de Waard graag hartelijk bedanken voor alle advies bij het uitvoeren van experimenten en het analyseren van de vele monsters. Er is een persoon die ik graag in het bijzonder wil bedanken, Erik van Vilsteren. Het zeer snel analyseren van de vele ICP-MS monsters in de laatste maanden van het onderzoek heeft me enorm geholpen om het boekje op tijd af te krijgen.

De vele collega's hebben het werken in Utrecht ook tot een erg gezellige tijd gemaakt. Ik wil graag al mijn collega's bedanken voor gezellige koffie en lunch pauzes en andere gezellige activiteiten en ik hoop dat ik niemand vergeet: Andreas, Andy, Anke, Anniet, Arnold, Caroline, Celine, Christelle, Christof, David, Debby, Dennis, Dineke, Elisabeth, Elise,

Gernot, Gert, Gert Jan, Gijs, Goulven, Guus, Helen, Iana, Jeffrey, Katja, Laurent, Marjolijn, Martin, Nicolaj, Niels, Parisa, Pien, Pierre, Pieter, Rick, Rinske, Sandra, Sanela, Shauna, Socratis, Steeve, Thilo, Tom, Vasso, Vincent, Yvonne.

Er zijn een aantal mensen die ik in het bijzonder wil bedanken: Anja, Diana en Mariette. Het altijd mijn hart kunnen luchten bij jullie over wat dan ook heeft me op de wat mindere momenten vaak erg geholpen. And I would like to thank Claudette for all the fun we had in and outside the university in the last years.

Verder wil ik graag mijn vrienden buiten de universiteit bedanken om juist ook eens wat heel anders te kunnen doen. In het bijzonder wil ik Ellen heel hartelijk bedanken voor alle hulp bij de vormgeving van het boekje. Het boekje had er van binnen en buiten nooit zo uitgezien zonder jouw hulp.

En als laatste wil ik graag mijn ouders, Suzanne en Wil, Danielle en Itai bedanken voor alle steun en interesse in de afgelopen jaren. Dankjewel voor het altijd voor mij klaar staan en alle vertrouwen die jullie in mij hebben.

## Curriculum Vitae

Jacqueline Claessens werd geboren op 19 januari 1976 in Geldrop. In 1995 behaalde zij haar gymnasiumdiploma aan de Scholengemeenschap Augustinianum in Eindhoven. In datzelfde jaar begon zij met haar studie Bodem, Water, Atmosfeer aan de Universiteit van Wageningen. In 2001 studeerde zij af bij de vakgroep Bodemscheikunde. Tijdens haar studie liep zij stages bij de groep Geotechniek van de Universiteit van Cambridge (Verenigd Koninkrijk) en bij het Departement Fysische Chemie van de Nationale Universiteit van Cordoba (Argentinië). Voor haar eerste afstudeervak deed zij onderzoek naar de adsorptie van arseniet aan goethiet bij de vakgroep Bodemscheikunde in Wageningen. Tijdens haar tweede afstudeervak in het Laboratorium van Fysische-Chemie en Kolloïdkunde in Wageningen heeft zij onderzoek gedaan naar het competitie-effect van oxyanionen op de binding van humuszuren aan ijzeroxiden. In oktober 2001 werd zij aangesteld als assistent in opleiding (AIO) bij de vakgroep Geochemie van de Faculteit Geowetenschappen aan de Universiteit van Utrecht. Tijdens deze periode deed zij onderzoek naar de oppervlaktechemie van microorganismen. In haar tweede jaar heeft zij meegedaan aan een 2 maanden durende zomercursus Geobiologie in het Wrigley Instituut op Catalina Island (Verenigde Staten). De belangrijkste resultaten van het promotie-onderzoek zijn weergegeven in dit proefschrift.